# Towards Understanding the Mechanisms of Lipid Sensitivity in Pentameric Ligand-Gated Ion Channels

Submitted to the Department of Biochemistry, Microbiology, and Immunology at the Uninversity of Ottawa in partial requirement for the completion of a Masters of Science

University of Ottawa
Ottawa, Ontario, Canada
September 2013

| ***Supervisor*** | ***Thesis Advisory Commitee*** | ***Jury*** |
|---|---|---|
| Dr. John E. Baenziger | Dr. Nathalie Goto | Dr. Nathalie Goto |
| | Dr. Jean-Francois Couture | Dr. Danielle Carrier |

© Jonathan Labriola, Ottawa, Canada, 2013

**Acknoledgments**

- First and foremost, I would like to thank my supervisor John Baenziger. Without your guidance and tutelage I would not be the scientist, or even person, that I am right now. Although not always easy, the time I spent in your lab and the things I learned were invaluable.
- Anna: without your love and support I would not have been able to get through this process with my sanity intact. Since you were going through the same process you were always there to lean on or give me perspective in the darker moments.
- My TAC members; Nathalie Goto and Jean-Francois Couture. You were as good a TAC as I think anyone could ask for. Your criticism, encouragement, and honesty helped me grow and navigate this process and I thank you for being there for guidance even though you were not my supervisor.
- Members of the Baenziger lab, past and present; Corrie, what can I say you were the one who trained me, your attention to detail and adherence to scientific rigor is something I hope to match throughout my career. Mich; always there with a pot of extra strong black tar at 7am. Casey; everyone needs someone to hate on undergrads with, thanks for being that someone, oh and boosting my car in -40 degree weather. Shuzi; we worked together on some successful projects so you definitely helped me achieve what I did. The others; Dan, Julian, Fred, Lopa, Peter, you were great people to work with, our discussions both scientific and personal made work fun and the science great!
- Andre, Hui, and Donna, the technicians of BMI. I can honestly say that the job you do is amazing, you somehow keep the equipment running despite a constant stream of trainees threatening to destroy every piece (myself included at one point).
- And last but not least my parents: it goes without saying but you have supported me in every way one person can support another, without you guys none of this would have been possible.

# Table of Contents

**List of Figures**

**Chapter 1**



**Chapter 2**



**Chapter 3**

**List of Abbreviations**

***$^2H_2O$*** – deuterated water

***5-$HT_3R$*** – 5-hydroxytryptamine receptor or serotonin receptor

***ACh*** – acetylcholine

***AChBP*** – acetylcholine binding protein

***aso*** – asolectin lipid extracts

***ATP*** – adenosine triphosphate

***$Ca^{2+}$*** - calcium ion

***Carb*** – carbamylcholine

***Chol*** – Cholesterol

***cryoEM*** – cryo-electron microscopy

***DAG*** – diacylglycerol

***DDM*** – n-dodecyl-β-D-maltopyranoside

***ECD*** – extracellular domain

***EcoLip*** – polar lipid extracts from *E. coli.* membranes

***ELIC*** – *Erwinia chrysanthemi* pentameric ligand-gated ion channel

***EthBr*** – ethidium bromide

***FTIR*** – Fourier transform infrared spectroscopy

***$GABA_A$*** – ionotropic γ-aminobutyric acid receptor

***GLIC*** – *Gloeobacter violacious* pentameric ligand-gated ion channel

***GluCl*** – glutamate receptor

***GlyR*** – Glycine receptor

***ICD*** – intracellular domain

***IPTG*** – isopropyl-β-D-thiogalactopyranoside

***$K^+$*** - potassium ion

***MBP*** – Maltose binding protein

***nAChR*** – nicotinic acetylcholine receptor

***$Na^+$*** - sodium ion

***$Na^+/K^+$ ATPase*** – sodium-potassium pump

***PA*** – phosphatidic acid

***PC*** – phosphatidylcholine

***PE*** – phospatidylethanolamine

***pET*** – plasmid for expression though T7 polymerase

***PI*** – phosphatidylinositol

***pLGIC*** – pentameric ligand-gated ion channels

***Post-M4*** – carboxy-terminal end of M4 transmembrane domain helix

***PS*** – phosphatidylserine

***TMD*** – transmembrane domain

**Abstract**

Pentameric ligand-gated ion channels (pLGICs) are membrane bound receptors found in the nervous system. They are responsible for detecting neurotransmitters released from neurons and subsequently mediating responses of the cells on which they are found. Thus, pLGICs play an invaluable role in communication between cells of the nervous system and understanding their function is pivotal to understanding how the nervous system works in general. One factor which is known to mediate pLGIC function is lipids found in the membrane environment in which pLGICs are embedded. This dissertation explores the various ways in which lipids interact with and modulate the function of pLGIC. Potential mechanisms and biological consequences of this modulation will be presented and discussed within the context of our current state of knowledge of pLGIC and nervous system function.

## 1.1 - The Nervous System

The ability of animals to obtain and properly respond to information from their surrounding environment rests within the nervous system. The nervous system is comprised of specialized cells called neurons which form complex circuits connecting sensory organs, such as eyes and ears, to other tissues in the body. The nervous system serves as the doorway between the outside world and the body and is responsible for what is perceived and how the body reacts to that perception. Thus, in order to understand how animals function in response to external forces, we must understand the underlying mechanisms of nervous system function.

The human nervous system is comprised of some 100 billion neurons forming many more connections between themselves and other cells. This vast network allows for complex processing of external information and results in the specialized behaviors and abilities observed in mammals. Thus, a fundamental characteristic of neurons is to pass information that is received from sensory cells along to other neurons and to tissues and organs which can then mount a response.

This thesis is focused on a family of proteins called the pentameric ligand-gated ion channels (pLGICs), which are integral membrane proteins that are fundamental to inter-cellular communication within the nervous system. Specifically, it examines the structural mechanisms by which the membrane lipids modulate their function. As will be discussed, factors which regulate pLGIC function have important consequences on inter-cellular communication and, by extension, brain function. Therefore, an understanding of the mechanisms of lipid-pLGIC modulation is fundamental to understanding how the nervous system functions.

The introduction to this dissertation describes electrical transmission along neurons and the role that pLGICs play in this process. Next, I briefly examine the current understanding of

pLGIC structure and function. Finally, I review the relevant literature which focuses on the effect of lipids on pLGIC function and their potential mechanisms of action. This discussion will not only provide a sense of the current understanding of lipid modulated pLGIC function, but will highlight the questions that still need to be addressed and provide a rationale for the work done in this study.

## 1.2 - Electrical Signalling in Neurons

### 1.2.1 - Ion Permeability of the Plasma Membrane

The cell plasma membrane serves as a barrier between the interior of a cell and its external environment and is made up primarily of phospholipids. These molecules have two distinct domains; one is comprised of two hydrocarbon chains that are typically 16 to 22 carbons in length and hydrophobic in nature, while the other consists of a polar region called the head group. As the name suggests, the head group contains a phosphate typically bound to some other polar moiety. The plasma membrane is comprised two layers, or leaflets, of laterally arranged phospholipids, with the hydrophobic acyl-chains from each leaflet pointing to the centre of the membrane and the polar head groups facing the solvent on either side. This gives the interior of the plasma membrane a hydrophobic nature that prevents movement of large polar or charged molecules across the membrane.

### 1.2.2 - The Resting Membrane Potential

Transmission of an electrical signal along neurons involves the movement of small ions such as $K^+$ and $Na^+$ across the neurons' plasma membrane. While the plasma membrane itself is impermeable to these ions, the presence of two types of integral membrane proteins, pumps and channels, render many cells permeable to specific ions. Channels facilitate passive diffusion of

ions across the membrane while pumps move ions across the plasma membrane against concentration and/or electric potential gradients using energy derived from ATP hydrolysis (Figure 1.01A).

At rest, the action of pumps and channels in the neuron leads to an imbalance of ions on either side of their plasma membrane. The $Na^+/K^+$ ATPase pumps three $Na^+$ ions out of the cell for every two $K^+$ ions pumped into the cell leading to a roughly ten times higher concentration of $Na^+$ outside compared to inside the cell, with the opposite being true for $K^+$ ions. Furthermore, neurons contain constitutively open leak channels, the most important of which is the $K^+$ leak channel, which renders the resting neuron membrane far more permeable to $K^+$ over any other ion. Since $K^+$ is more concentrated within the cell, it will diffuse out of the $K^+$ leak channels along its concentration gradient, which will cause negative charge to accumulate within the cell resulting in an electric potential difference across the membrane. At a certain point the diffusional force of $K^+$ moving out of the cell along its concentration gradient will match the force of the accumulating electric potential and the net flux of $K^+$ will cease. By convention, a more positive cell interior is indicated by a positive membrane potential. Neurons have a resting electric potential between -70 and -85 mV, since potassium efflux creates a more negative cell interior.

### 1.2.3 - The Action Potential

Neurons send and receive electrical signals in the form of fluctuations in their membrane electric potentials. These fluctuations originate at structures called dendrites, which are filament like projections extending from the neuron's cell body (Figure 1.01). Here, inputs from sensory cells and from other neurons leads to opening of cation-selective ion channels, resulting in

**Figure 1.01-** Cartoon representation of a neuron and synapse. Expanded images (A and B) show close up of an axon and synapse, respectively, with important features labelled. (A) The ATPase $K^+/Na^+$ pump, $Na^+$ channel, and $K^+$ channel are colored red, green, and purple, respectively. Sodium and potassium ions are colored green and purple, respectively. (B) Cartoon of a synapse. pLGICs are shown on the post-synaptic membrane in white. Neurotransmitter is shown as a blue circles and ions are shown as yellow crosses.

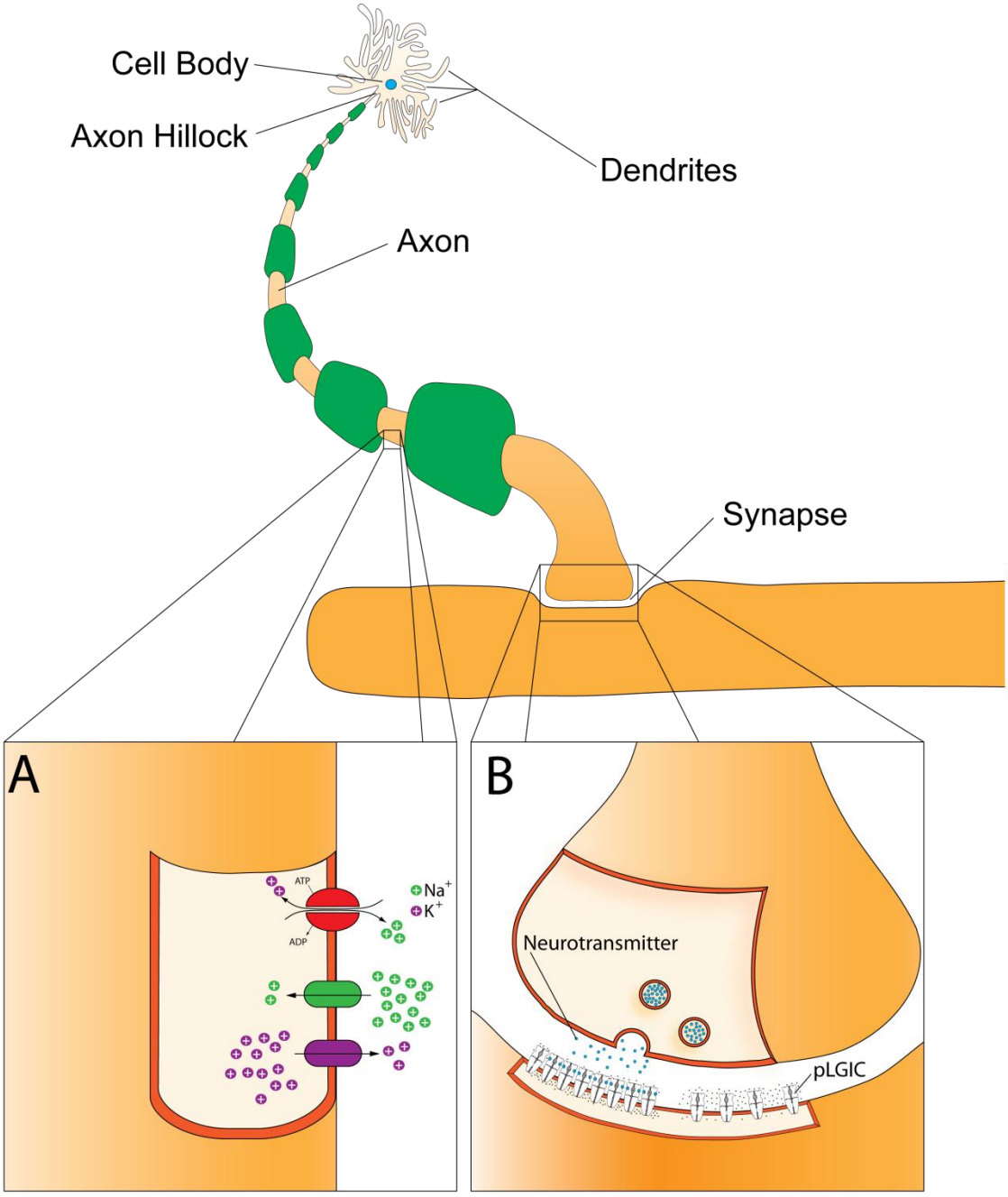
Cell Body
Axon Hillock
Dendrites
Axon
Synapse
A
ATP
ADP
$Na^+$
$K^+$
B
Neurotransmitter
pLGIC

sodium influx, moving the membrane electric potential closer to zero. This process is called as depolarization.

Next, in a process called passive spread, depolarization is propagated across the cell surface, as $Na^+$ which enters the cell will diffuse away from the entry point (i.e. the ion channel) toward the other structures of the neuron. While the change in membrane potential by passive spread attenuates rapidly across the cell surface there are many inputs on any given dendrite or cell body which originate from one source or multiple sources. Consequently, many signals are integrated and summated by the action of passive spread resulting in large changes in membrane potential over a significant area of the cell surface.

Under certain conditions, integration of inputs at dendrites by passive spread will result in membrane depolarization at the axon hillock above a value called the threshold potential, which is typically about -55mV. When this occurs it triggers opening of voltage gated $Na^+$ channels found in high concentrations at the axon hillock. This event renders the membrane highly permeable to $Na^+$, causing a rapid influx of $Na^+$ and thus a spike in the membrane potential to about +40mV after which the $Na^+$ channels shut and voltage gated $K^+$ channels open, restoring the resting membrane potential. The rapid spike in membrane potential is passively spread from the axon hillock to an elongated tubular structure called the axon which also contains a high concentration voltage gated $Na^+$ channels on its surface. Passive spread of the membrane potential spike down the axon sequentially opens $Na^+$ channels further and further down the length of the axon, effectively propagating the membrane potential spike down the entire length of the axon until it reaches the axon terminus. This wave of membrane potential fluctuation down the axon is called an action potential, and it is how neurons send signals they receive to other cells in the nervous system.

### 1.2.4 - The Synapse

Axons terminate at structures known as synapses, which are junction points between two cells in the nervous system that serve as the nodes of communication between them. Some synapses act as the inputs to the dendrites or cell bodies of other neurons, while others regulate the activity of other organs and tissues, such as muscle. In either case, the arrival of an action potential at the axon terminus leads to the release of a chemical neurotransmitter which diffuses across the synaptic cleft and binds receptors on the postsynaptic cell (Figure 1.01B).

There are many types of neurotransmitters which bind various types of receptors giving rise to the many responses observed in the cells of the nervous system. pLGICs are one such receptor which transiently open a membrane spanning ion channel in response to neurotransmitter binding, a process also known as "gating". Cation selective pLGICs allow the influx of $Na^+$, resulting in depolarization of the membrane and are thus excitatory. Anion selective channels facilitate the influx of $Cl^-$, making the cell interior more negative, or hyperpolarized. Since the latter channels move the membrane potential further from the threshold potential they have an inhibitory effect on activation. pLGICs thus play an essential role in rapid inter-neural communication by initiating or inhibiting responses, such as action potentials, in the postsynaptic cell.

Importantly, pLGICs are not simple on/off switches, their sensitivity to neurotransmitter is tuneable, and tuning of pLGICs will affect the strength of a synaptic connection, which can have profound effects on human biology. For example some diseases, such as myasthenic syndrome, are the result of minor alterations in pLGIC gating kinetics at the neuromuscular junction(1). Thus understanding factors which are able to tune pLGIC activity are essential toward a full understanding of nervous system function. This dissertation focuses on the mechanisms by

which lipids modulate pLGIC function. Before lipid-pLGIC interactions are discussed, the current understanding of pLGIC structure will be presented.

### 1.3 - pLGIC Subtypes and Structure

There are four known types of pLGIC's in vertebrates. Nicotinic acetylcholine receptors (nAChR) and serotonin receptors (5-$HT_3$R) are cation-selective, excitatory channels, while glycine receptors (GlyR), and γ-aminobutyric acid receptors ($GABA_A$R) are anion-selective, inhibitory channels (2). In invertebrates, glutamate receptors (GluCl) serve as the anionic inhibitory channels. These receptors are collectively known as 'Cys-loop receptors' owing to the presence of a highly conserved stretch of 13 residues flanked by disulphide-bridge forming cysteine residues. As discussed below, the eponymous Cys-loop is thought to play a key role in pLGIC function. More recently, prokaryotic homologues of the Cys-loop receptors have been discovered which are homologous in their secondary and tertiary fold, and quaternary arrangement, but lack the cysteine residues covalently linking the Cys-loop (3)(Figure 1.02B).

The nAChR was the first Cys-loop receptor discovered (4), and elucidation of its primary structure facilitated the discovery of the other Cys-loop receptors through sequence alignments (5,6). It was also found to be highly enriched in the electroplaque organ of the *Torpedo* electric ray (7). Because of this, the nAChR has served as the model for investigating Cys-loop receptor structure and function, and still remains the most well characterized pLGIC. In the past decade, however, the discovery of Cys-loop receptor homologues amenable to high resolution structural studies has expanded atomic level understanding of pLGIC structure and function (8).

The secondary, tertiary, and quaternary structure of all pLGICs is generally conserved. They are pentamers made up of identical or homologous subunits arranged pseudosymmetrically

**Figure 1.02 –** Low resolution schematic of the tertiary and quaternary arrangement of pLGICs. (A) A low-resolution representation of Cys-loop receptor tertiary structure (modified from Changeux, J.P., 'Chemical Signalling in the Brain' *Scientific American* (Nov. 1993) pp. 58 – 62. Each receptor is comprised of 5 identical or homologous subunits which arrange themselves around a central axis. There are three main domains, the extracellular domain (ECD), transmembrane domain (TMD), and intracellular domain (ICD – omitted from the schematic). The neurotransmitter binding site occurs at the interface between subunits in the ECD. The pore through which ions flow is located in the TMD. (B) Schematic of a single Cys-loop receptor subunit. Each subunits contains and ECD, TMD, and ICD domain. The left schematic shows a subunit from a vertebrate Cys-loop receptor. The conserved Cys-loop is in the ECD (coloured yellow). The TMD is comprised of 4 membrane spanning regions, and the ICD is formed from an extended loop between the M3 and M4 region. The right schematic shows a subunit from prokaryotic homologues lacking the Cys-loop and extended ICD.

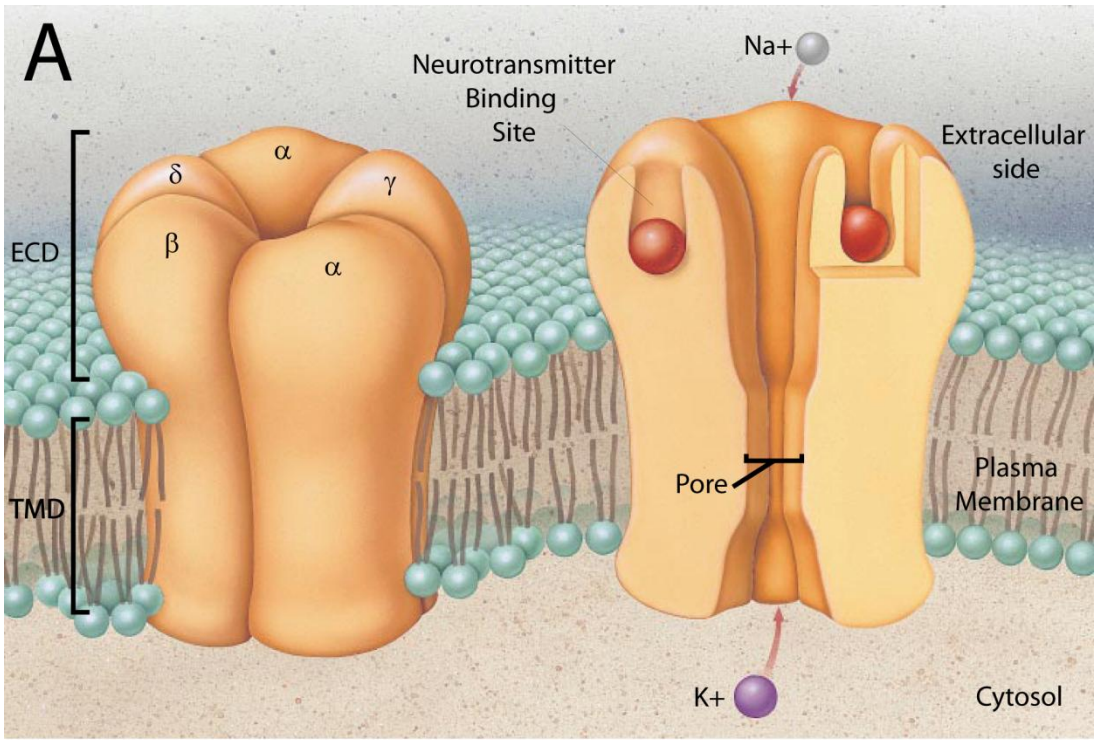
A
Neurotransmitter
Binding
Site
Na+
Extracellular
side
δ
α
γ
β
α
ECD
TMD
Pore
Plasma
Membrane
K+
Cytosol

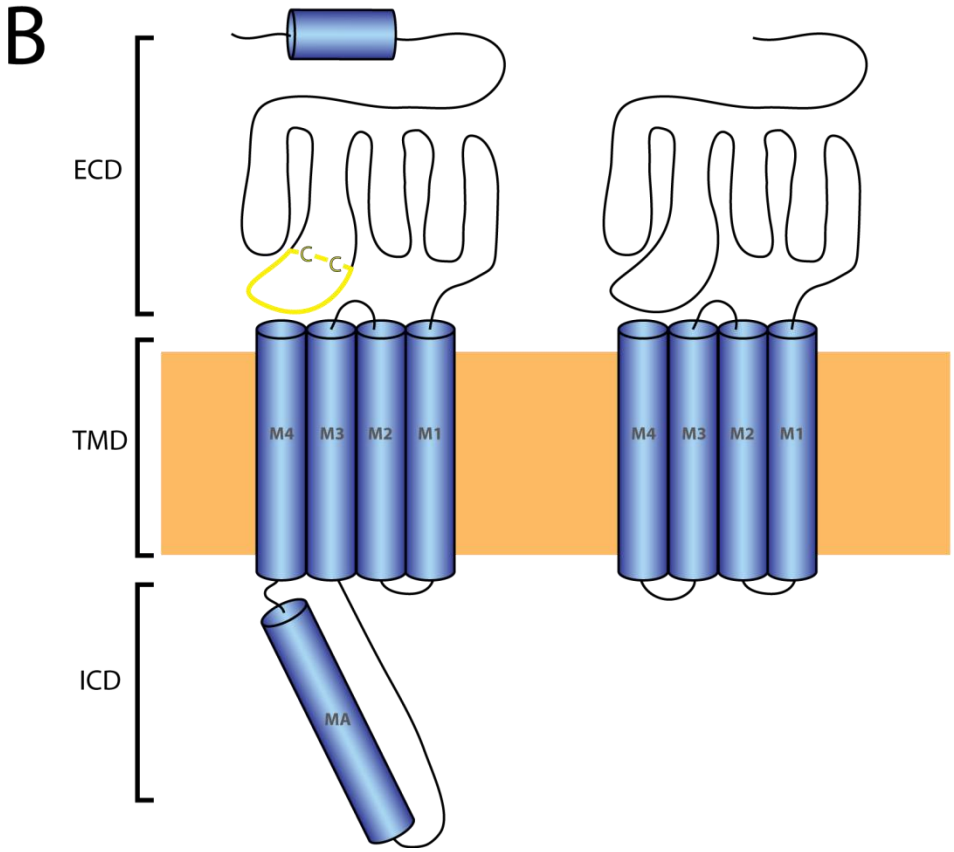
B
ECD
C
C
TMD
M4
M3
M2
M1
M4
M3
M2
M1
ICD
MA

around an axis normal to the membrane (Figure 1.02A). Each subunit contains an N-terminal extracellular domain (ECD), transmembrane domain (TMD), and, in the case of eukaryotic Cys-loop receptors, an intracellular domain (ICD). The ECD houses the neurotransmitter binding site, the TMD contains the ion channel pore, and ICD function is still somewhat elusive, although the absence of the latter in prokaryotic pLGICs indicates it has little role in ligand binding and ion flux functionalities (Figure 1.02B).

### 1.3.1 - Acetylcholine Binding Protein (AChBP) as a Model for pLGIC ECD

The extracellular domain of pLGICs is the location of the agonist binding site (Figure 1.02A). The first high-resolution insight into the structure of the pLGIC ECD came in the form of a crystal structure of the acetylcholine binding protein (AChBP) (9). The AChBP is a water soluble protein found in the snail nervous system which is released from glial cells into the synaptic cleft where it sequesters free ACh thereby mediating synaptic transmission (10). The AChBP is structurally homologous to the ECD of pLGICs, as was verified both by sequence alignments along with functional assays, the latter showing the AChBP binds a variety of agonists and antagonists common to the nAChR. The AChBP is a homopentamer arranged with five fold symmetry around a central pore (Figure 1.03). Each protomer is comprised of a 10 stranded twisted β-sandwich (Figure 1.04C). The N-terminal end, which would be at the top of the pLGIC, has a short α-helix, while the C-terminal end would lead right into the TMD. The β-sandwich has an inner and an outer β-sheet arranged in a ‘Greek key’ motif (Figure 1.04B). The two β-sandwich structures are held together by a hydrophobic core, while the exterior has many hydrophilic residues, making the entire protein water soluble. The interface between two protomers is mainly hydrophobic and serves as the location of the agonist binding site (9)(Figure 1.04A).

**Figure 1.03** - Crystal structure of snail AChBP (PDB: 1I9B). Top and side view of the protein. The entire tertiary and quaternary fold is homologous to the ECDs of currently solved Cys-loop receptors. The protein is comprised of 5 subunits or protomers which are identical. Each subunit is coloured differently for clarity.

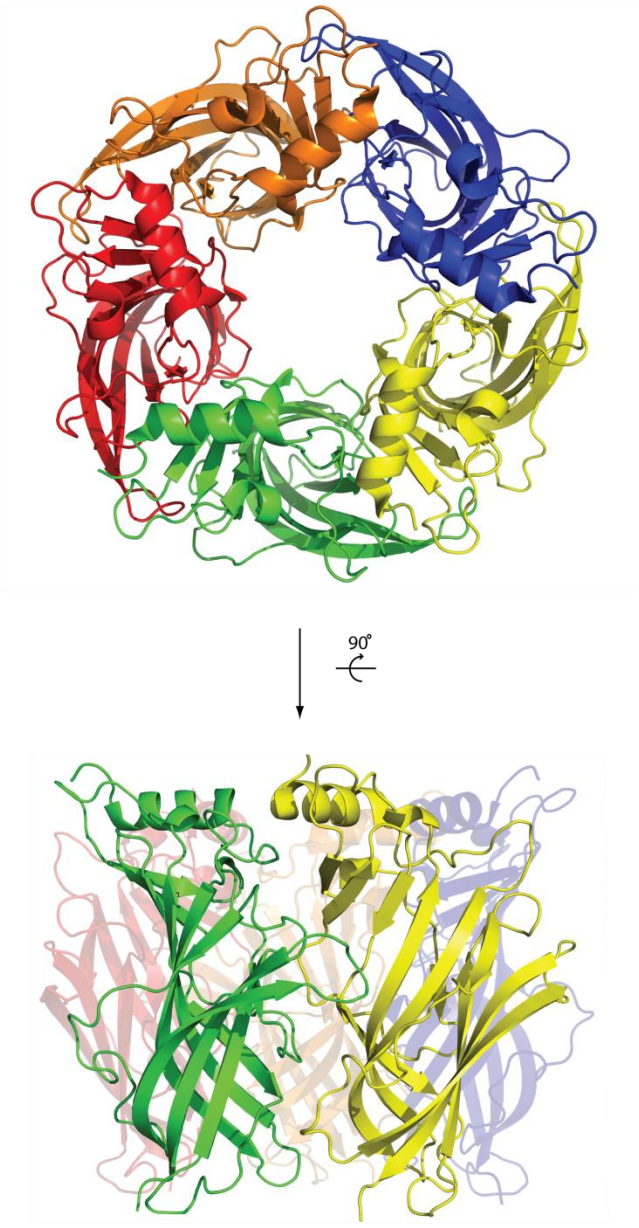
90°

**Figure 1.04 –** Features of the snail AChBP which are conserved among pLGIC ECDs. (A) Cartoon showing the location of the agonist binding site in the AChBP. The agonists bind at the interface between protomers. Residues involved in binding are found on Loops A, B, and C, which make up the + face, from one subunit, and Loops D, E, and F, which make up the – face, from another subunit. Since AChBP is a homopentamer there are 5 binding sites, the other 4 being omitted in this schematic. (B) Ribbon diagram of one protomer from the AChBP crystal structure. The Loops are colored the same as in (A) and the Cys-loop is colored yellow. The β-strands which make up the outer sheet are coloured red and the inner sheet are coloured blue. (C) schematic of an AChBP protomer. The β-strands and loop regions are colored the same as in (A) and (B). The disulphide bond of the Cys-loop is shown as a dashed line.

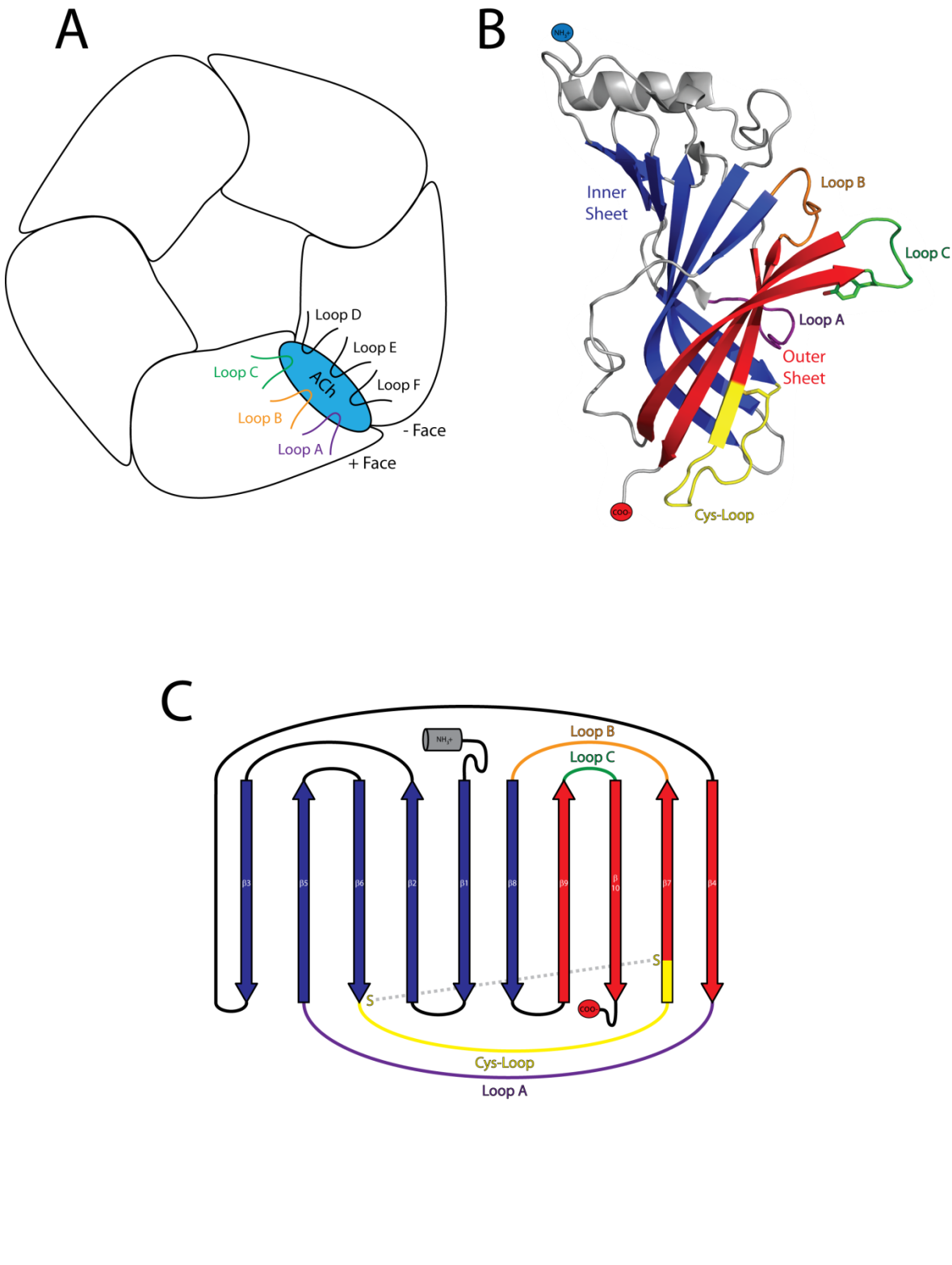
A
Loop D
Loop E
Loop C
ACh
Loop F
Loop B
- Face
Loop A
+ Face
B
Inner
Sheet
Loop B
Loop C
Loop A
Outer
Sheet
Cys-Loop
C
Loop B
Loop C
S
S
Cys-Loop
Loop A

Crystal structures of the AChBP bound to nicotine and carbamylcholine (Carb), an analogue of ACh (Figure 1.05), reveal the structural basis of agonist binding at high resolution (11). Residues involved in agonist binding are found on loops connecting the β-strands of the ECD from each of the two subunits surrounding the binding site (Figure 1.04A). One subunit provides the principal (or +) face of the binding site, consisting of loops A, B, and C, where highly conserved aromatic residues are found (12) (Figure 1.05). In the crystal structure these aromatic residues form cation-π interactions with the quaternary ammonium of the agonists (Figure 1.05A). The adjacent subunit provides the complementary (or -) face of the binding site and contains loops D, E, and F. Some residues in this region provide hydrophobic contacts with ligands while others provide polar contacts (9,13). The principal face is essential for agonist binding and channel activation. For example, the *Torpedo* nAChR is a heteropentamer with a subunit stoichiometry of $\alpha_2\beta\gamma\delta$, the + face being provided by the α-subunits. Consequently, the nAChR binds only two ACh molecules and requires the α-subunit for activity upon expression in heterologous expression systems (14). More recently crystal structures of the ECD of the nAChR α1 subunit (15) and a nAChR α7 ECD/AChBP chimera in complex with a nAChR agonist (16) confirm the overall pLGIC ECD fold and agonist interaction initially observed in the AChBP structures. Moreover, since all pLGIC agonists contain a positively charged region (Figure 1.05C), and pLGICs contain conserved aromatic residues in the A,B, and C (Figure 1.05B) loops that are implicated in agonist binding (12) (17) (18) (19), it is likely the mode of binding depicted in AChBP crystal structures is also conserved among pLGICs.

### 1.3.2 - The *Torpedo* nAChR

Unwin and colleagues made significant contributions to our understanding of the entire pLGIC structure through studies with the *Torpedo* nAChR using cryo-electron microscopy

**Figure 1.05 –** Ligand binding mode is conserved among the AChBP and ECDs of pLGICs. (A) Sequence alignments of the AChBP with the ECD of other members of the Cys-loop receptor family. Sequences shown are of the loops A, B, and C from the complementary face of the binding site. Residues in green boxes are highly conserved aromatic residues shown to form cation-π interactions with agonist through structural or biochemical studies. (B) Structure of the agonist binding site with carbamylcholine (Top) and nicotine (bottom). Highly conserved aromatic residues from the + face are shown as sticks. (C) Representation of the various Cys-loop receptor agonists. All chemicals are drawn at physiological pH (pH = 7). γ-aminobutyric acid (GABA) and Glycine are agonists for the anionic pLGICs $GABA_A$ and GlyR, respectively. Acetylcholine and serotonin (5-HT) are agonists for the cationic pLGICs nAChR and 5-HTR, respectively. Cystamine is the agonist for ELIC.

A

| | LoopA | LoopB | LoopC |
|---|---|---|---|
| GABA | FFHNGKKSV | GSYAYTR | GIVQSSTGEYV |
| GlyR | FFANEKGAH | ESFGYTM | CTKHYNTGKFT |
| 5-HT | LIN-EFVDV | TSWLHTI | EFSIDISNSYA |
| nAChR | VLYNNADGD | GIWTYDG | YYTCCPDTPYL |
| AChBP | AAYN-AISK | GSWTHHS | TYSCCP-EAYE |

B

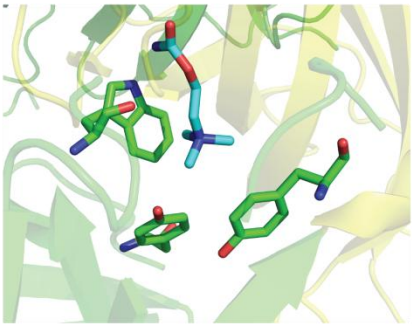

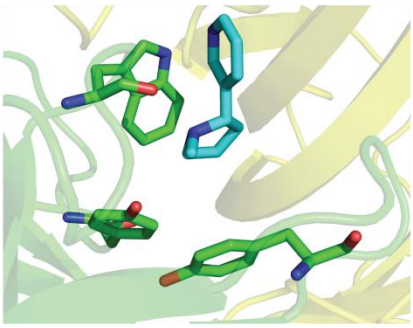

C

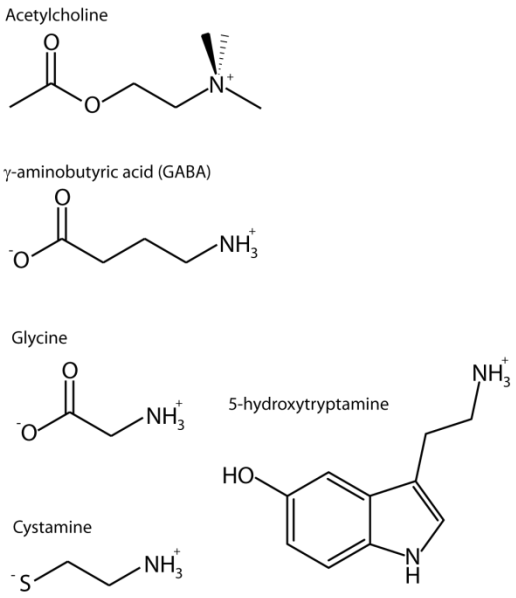

(cryoEM) (20-24). These studies began in 1984 where preliminary cryo-EM images of tubular crystals grown from *Torpedo* electroplaque native membranes allowed construction of a 30Å resolution EM map (25). Technical improvements coupled with the solution of the AChBP crystal structure culminated in a 4.0 Å resolution electron density map of the membrane embedded *Torpedo* nAChR in 2005 (Figure 1.06) which represents the first atomic scale model of any pLGIC (20). When viewed from the side, the entire protein is about 150Å long, with a 60 - 70 Å long ECD, and a 40Å long TMD and ICD. The overall fold and quaternary arrangement of the nAChR ECD is consistent with that observed in the AChBP crystal structure.

The TMD is comprised of 4 α-helices (M1 – M4) from each subunit (Figure 1.07), which traverse the membrane in an antiparallel fashion and are connected by short loops. The M2-M3 loop, which lies on the extracellular side of the TMD and makes contact with the ECD, is important for coupling of ligand binding to channel gating (see section *1.3.4*). The loop between transmembrane helices M3 and M4 is extended, and forms an α-helix (MA) which makes up the ICD in eukaryotic Cys-loop receptors. Owing to the five-fold pseudosymmetrical arrangement of the subunits, the helices of each subunit form concentric rings when looking down on the protein (Figure 1.07C). The M2 helices from each subunit form the inner ring and line the ion channel pore, the M1 and M3 helices form an outer ring and protect the M2 helices from the surrounding lipid environment, and the M4 helices extend out into the membrane lipid environment and are thus are the lipid exposed.

Following solution of the 4.0Å cryo-EM structure of the nAChR, the crystal structures of the prokaryotic pLGICs ELIC (26) and GLIC (27) were solved, and a few years later the invertebrate glutamate channel (GluCl) from *C. elegans* (28). These structures reveal the same tertiary fold and quaternary subunit arrangement as the nAChR. As mentioned, ELIC and GLIC

**Figure 1.06 - The structures of (A) GLIC (pdb code 3EAM) and B) the *Torpedo* nAChR (pdb code 2BG9).** Both structures are side views from within the plane of the membrane. Coloring highlights the domain structure: extracellular agonist-binding domain, red; transmembrane domain, blue; and cytoplasmic domain, green. Figure reproduced from (29)

-

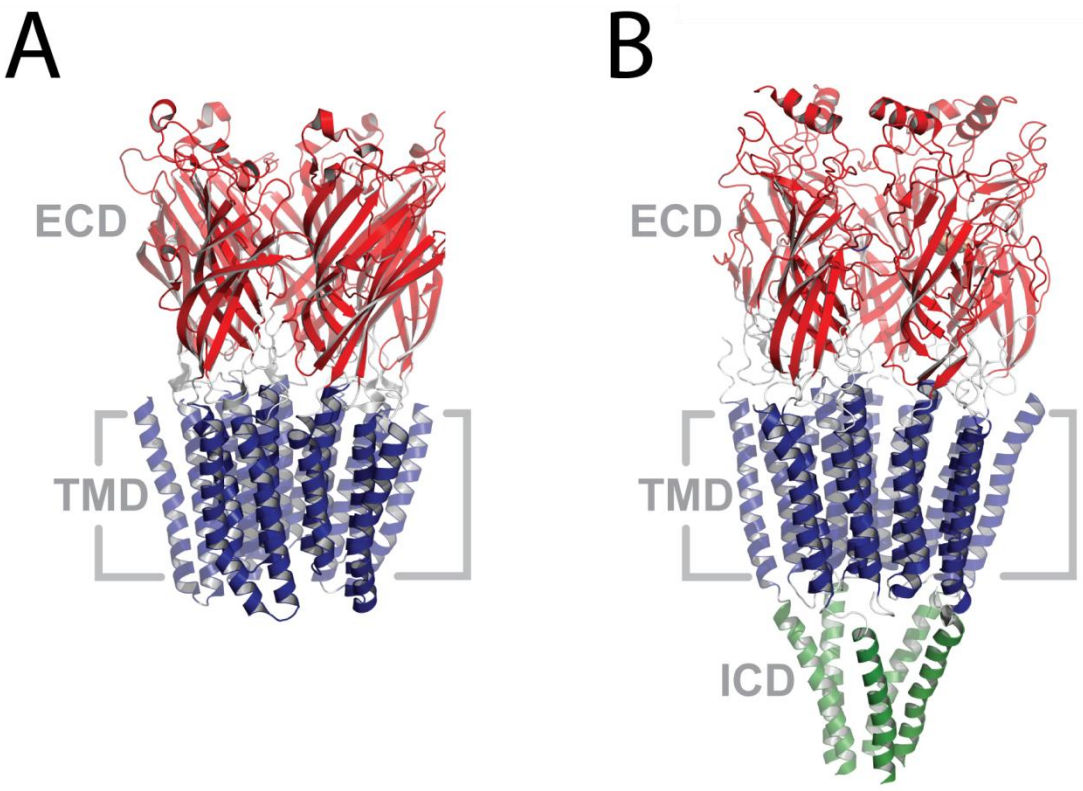
A
ECD
TMD
B
ECD
TMD
ICD

**Figure 1.07-** Architecture of the *Torpedo* nAChR pore at 4Å (PDB; 2BG9). (A) Cartoon representation of the nAChR TMD with each subunit being colored differently. (B) View of the TMD from the top. The left hand image is coloured as in (A) with each helix of the α-subunit labelled. The right hand figure depicts the concentric rings formed by helices from each subunit. The M2 helices form the pore and are coloured red. The M1 and M3 helices form the second ruing which shields the pore from the lipid environment. The M4 helices are highly lipid exposed.

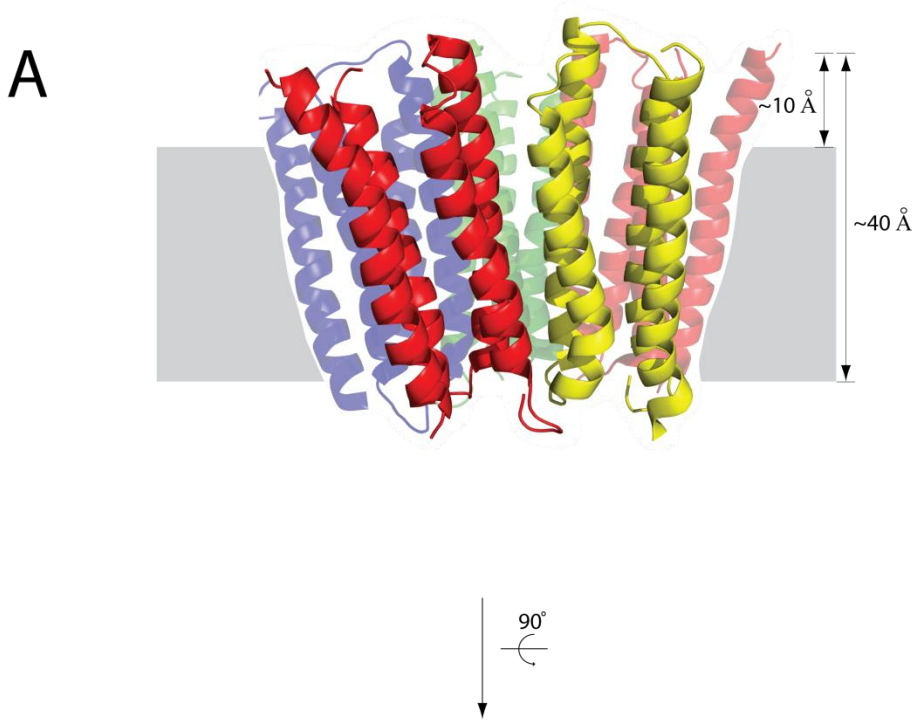
A
~10 Å
~40 Å
90˚
B
M2
M1
M3
M4
C

do not have an extended M3-M4 loop and thus lack a significant ICD. In each pLGIC structure, specific residues along the M2 helices of each subunit project into the pore lumen (Figure 1.08B). Pore facing residues from each subunit thus form rings along the wall of the pore of a specific chemical nature which have functional consequences. Accordingly, a numbering system was developed to compare residues along the M2 helix between different pLGICs, in which 0' is assigned to a highly conserved positively charged residue at the cytoplasmic end of M2 and increases by 1' moving up each residue toward the extracellular side.

### 1.3.3 - The Gate

The most narrow region of the ion channel pore in the *Torpedo* nAChR exists midway between the extracellular and intracellular bilayer surfaces (20). The residues in this region are hydrophobic, consisting of a leucine and a valine at position 9' and 13', respectively. There are conserved side-to-side interactions, adjacent to the pore facing residues, which bring the M2 helices together, forming a tight hydrophobic girdle that is roughly 6Å in diameter for an 8Å stretch along the channel beginning at position 9' (30). Sequence alignments show that bulky hydrophobic residues are conserved among pLGICs at the 9' and 13' positions (Figure 1.08A). In the crystal structures of GLIC, ELIC, and GluCl the residues at this position protrude into the pore lumen as well.

Functional studies have demonstrated that mutation of the 9' leucine residues to more polar side chains increases sensitivity to agonist and slows the rate of desensitization in $GABA_A$ receptors and the nAChR (31-33). Moreover, cryo-EM images of the membrane bound nAChR flash frozen in the open conformation shows widening of the M2 helices in the 9' region of the protein (34). Finally, mutations of M2 residues to cysteine followed by reaction with water

**Figure 1.08 –** Conserved pore linings residues in pLGICs. (A) Sequence alignments of the M2 pore forming helix from various members of the Cys-loop receptor family. The putative location of the gate is shown in yellow. (B) Cartoon representation on the left shows the functionally important positions along the pore forming M2 helices. The front two M2 helices are removed for clarity. Ribbon diagrams are, from left to right; GLIC and nAChR. Residues implicated in gating are coloured yellow.

A

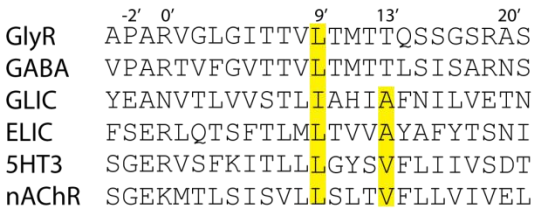
-2′ 0′ 9′ 13′ 20′
GlyR APARVGLGITTVLTMTTQSSGSRAS
GABA VPARTVFGVTTVLTMTTLSISARNS
GLIC YEANVTLVVSTLIAHIAFNILVETN
ELIC FSERLQTSFTLMLTVVAYAFYTSNI
5HT3 SGERVSFKITLLLGYSVFLIIVSDT
nAChR SGEKMTLSISVLLSLTVFLLVIVEL

B

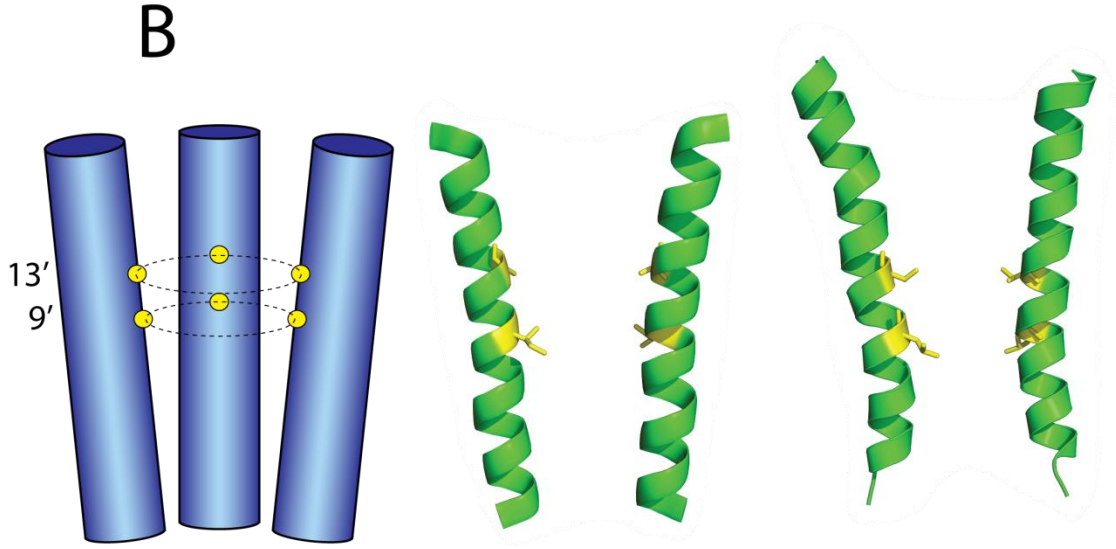
13′
9′

soluble thiol-modifying probes were also used to identify the location of the gate. Initially, when applied to the extracellular side, these probes were able to modify residues all the way down to the 2' position, suggesting the gate was at the extracellular end of M2 (35). Later on, investigators discovered that the thiol-modifying agents were partial pLGIC agonists which allowed them access to residues beyond the gate by opening the channel. Subsequent studies with non-competitive antagonists in conjunction with the thiol-modifying agents led to reassignment of the gate to the 9' – 13' region (36,37).

As there is no physical occlusion within the pore of the 4Å nAChR model, the gate must present an energetic barrier to ions. $Na^+$ and $K^+$ ions are about 2.5Å in diameter, and with their first hydration shell their diameter increases to about 8Å. Considering that the diameter of the pore is ~6Å, ions would not be able to pass through the closed gate without losing their first hydration shell. Since the rings at 9' and 13' are hydrophobic, dehydration of ions in this environment presents a steep energetic barrier and effectively reduces the rate of diffusion of a dehydrated ion through the closed channel pore to zero. Thus, opening of the gate must result in dilation of the hydrophobic girdle beyond 8Å to accommodate the hydrated ions.

### 1.3.4 - The ECD/TMD Coupling Interface

The coupling of ligand binding to channel opening rearrangements in all pLGICs requires a molecular link between the ECD and TMD. The interface between these domains is formed mainly of contacts between the loop regions from each domain. There are also residues in this region which are conserved or invariant across pLGICs (Figure 1.09A). Mutagenesis studies show that many of these residues are essential for pLGIC structural integrity as well maintenance of native gating kinetics (38) (39). These observations have led to the general conclusion that

proper ECD-TMD interface interactions are essential for maintaining communication between the ECD and TMD and, therefore, coupling of ligand binding and channel gating events.

The 4.0Å model of the ECD-TMD interface proposes the specific interactions between the residues of each respective domains loop region. The highly conserved Cys-loop (or β6-β7 loop) as well the β1-β2 loop, make close contact with the M2-M3 linker, which connects helices M2 and M3 in the TMD (Figure 1.09). Additionally, an invariant arginine (R209 in nAChR) located on the linker between the ECD β10 strand and TMD M1 α-helix projects into the interface and forms a salt bridge with a conserved aspartic acid (E45 in nAChR) of the β1-β2 loop (Figure 1.09). Mutation of either of these residues impairs channel gating in nAChR, and mutations which reverse the charge of either residue prevents expression on the surface of *Xenopus* oocytes (38). Structurally, the E45 and V46 of the β1-β2 loop straddle a conserved proline (P272) on the M1-M2 linker. Conserved hydrophobic residues found on the Cys-loop also form similar interactions with the M1-M2 linker as E45 and V46. Lastly, the end of the M4 (or post –M4) extends out of the membrane and forms interactions with the conserved F137 of the Cys-loop via its Q435 residue (40). The structural significance of this last interaction is illustrated by the fact that truncation of M4 abolishes receptor expression in heterologous systems (41). The functional relevance of post-M4 is demonstrated by its involvement in potentiation of α4β2 nAChRs by estradiol (42).

### 1.3.5 - pLGICs are Allosteric Proteins

pLGICs are allosteric proteins which exists in an equilibrium between their various functional states. In the absence of any ligand, inhibitor, or other allosteric effectors, the nAChR exists predominantly in a resting state, which is characterized by a low affinity for agonist in the ECD and a closed channel pore in the TMD (43). Upon exposure to agonist, the receptor

**Figure 1.09 –** Structural features of conserved ECD-TMD interface in pLGICs revealed by 4Å model of *Torpedo* nAChR. At the top of the figure there is a sequence alignment of the β1-β2 loop, M2-M3 loop, and Cys-loop regions of Cys-loop family members. Residues are colored according to the loops in which they are found and match the coloring in the cartoon below. The highly conserved R is shown in a black box. Conserved residues determined by functional studies to be important for ECD-TMD communication are also highlighted in black and shown in sticks in the diagram below.

| | β1–β2 | Cys-loop | | M2-M3 |
|---|---|---|---|---|
| GlyR | IAETTMD | ACPMDLKNFPMDVQTCI | ERQ | SYVKAID |
| GABA | VSDHDME | ECPMHLEDFPMDAHACP | KRK | AYATAMD |
| 5-HT3 | VDEKNQV | ACSLDIYNFPFDVQNCS | RRR | IGTPLIG |
| nAChR | VDEVNQI | YCEIIVTHFPFDQQNCT | QRI | SAVPLIG |

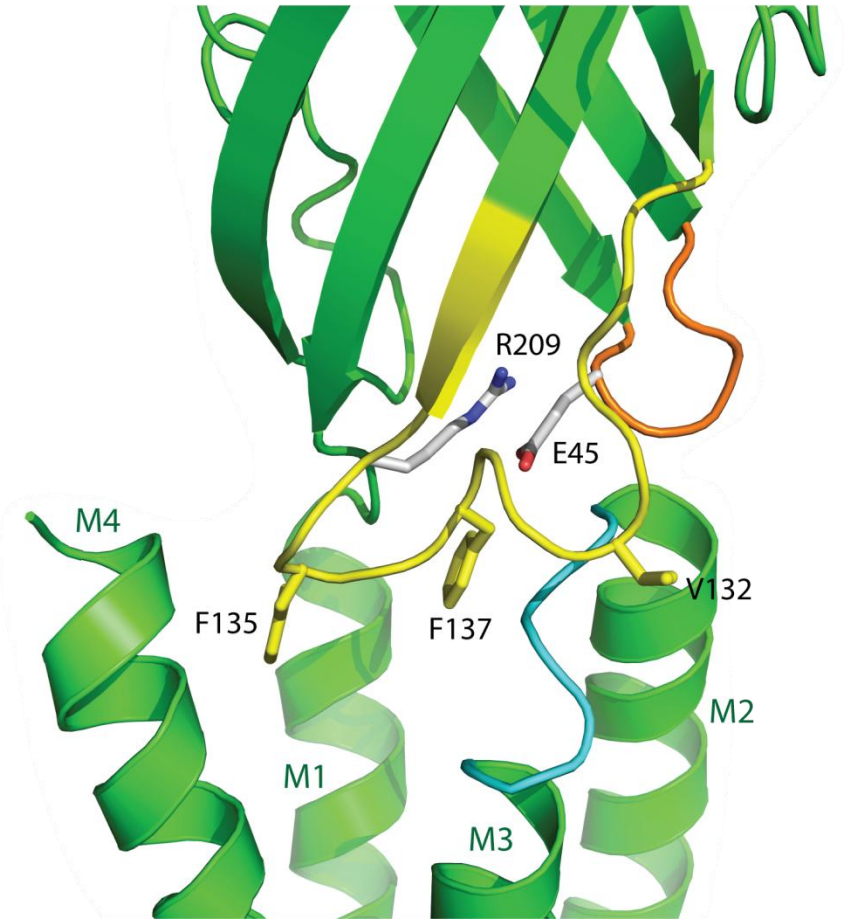

undergoes rapid transition between resting and open conformations over a millisecond timescale after which the receptor is stabilized in a desensitized conformation (44). While the binding affinity of the desensitized state is high the pore does not open in response to this binding. Dissociation of ACh from the nAChR results in reversion of the receptor back to the resting state.

### 1.4 - Lipid Dependant Modulation of nAChR Activity

Lipids are increasingly recognised as modulators of membrane protein function. In the context of pLGICs, the only receptor whose lipid sensitivity is well characterized is the *Torpedo* nAChR. This became apparent during the first attempts to purify the nAChR from its native source and reconstitute its function in synthetic lipid environments. The first successful reconstitution was achieved by Epstein and Racker, who found that solubilised lipids must be present throughout purification in order to restore the channel gating properties of the nAChR (45).

This observation sparked immediate interest into how and which lipids are required to stabilise nAChR function. One of the first steps taken to answer this question was to determine the lipid content of the *Torpedo* electroplaque membrane. One major component is cholesterol, which comprises about 45% (mol) of the total lipid content (46). The polar lipid content was examined by Gonzales-Ros *et al.* who found that the major types of polar lipids were the zwitterionic lipids phospatidylcholine (PC: ~39%), and phosphatidylethanolamine (PE: ~40%). Anionic lipids such as phosphatidylserine (PS), cardiolipin, and phosphatidic acid (PA) comprise the majority of the remaining polar lipids (46). The predominance of anionic lipids in the latter fraction of the lipids gives the electroplaque membranes a slightly negative charge.

Extensive studies have shown that the nAChR reconstituted into membranes lacking any neutral or anionic lipid (historically meaning membranes comprised solely of PC) does not gate or undergo conformational transitions in the presence of agonist (47-49). Addition of neutral and/or anionic lipids, however, shifts receptors to an activatable conformation (50-53). For example, it is generally accepted that a 3:1:1 (mol:mol:mol) mixture of PC, PA, and cholesterol provides an environment which recovers optimal nAChR function. PA and cholesterol, however, are not the only lipids which stabilize functional nAChRs (54). It has been demonstrated that many anionic lipids such as phosphatidylinositol (PI), phosphatidylserine (PS), and cardiolipin, as well as many neutral lipids, such as squalene, steroids, and diacylglycerol (DAG), are also able to stabilize nAChR function when present in reconstituted membranes (52). Thus, it appears as though neutral and anionic lipids are able to stabilize functional receptors in a non specific manner, with combinations of both being necessary to reconstitute a fully-functional nAChR sample.

Other work attempted to elucidate the mechanism of lipid-dependant modulation of nAChR function. The observation that there is a nonspecific lipid requirement for stabilizing nAChR function lead to the idea that lipids exert their effects on the nAChR by altering the bulk fluidity of the plasma membrane (51). This notion is consistent with the observation that PA and cholesterol are the most effective at stabilizing functional nAChRs, since both lipids tend to make membranes more rigid (55). Indeed, investigators were able to show a correlation between nAChR function and the fluidity of the membrane where it is embedded (51). Moreover, the presence of the nAChR in membranes capable of stabilising nAChR function renders the membranes themselves more rigid (55). Evidently, lipid ordering is tightly coupled to nAChR

function, although whether membrane rigidity confers function onto the nAChR or it is merely a symptom of placing the nAChR into the membrane remains to be determined.

Spectroscopic studies of reconstituted nAChR systems have lead to alternate theories of lipid modulated nAChR function. Electron paramagnetic studies show that the presence of nAChR in synthetic lipid membranes causes immobilization of different types of phospholipids which correlates with the phospholipids ability to stabilize functional receptors. Lipid immobilisation is interpreted as binding to 'annular' sites on the TMD surface (56). Further studies using brominated cholesterol suggest that there are sites between nAChR TMD helices where cholesterol binds, which have come to be known as 'non-annular' sites (57). The presence of lipid binding sites on the TMD of pLGICs has gained recent support with the crystal structure of GLIC and the cryoEM model of the nAChR. In the nAChR model, electron density between the α-helices is more similar to the surrounding lipid environment than to the water filled channel, suggesting these areas are occupied by lipid (58). In the GLIC crystal structure, there is electron density at the interface between M4 and M3+M1 helices which is modelled as a co-purified lipid molecule (27). Finally, docking studies and molecular dynamics simulations show that the purported non-annular sites can support cholesterol binding with high affinity resulting in structural stabilization of the nAChR (58). While these studies provide compelling evidence for the presence of these binding sites, their existence has not yet been proven.

### 1.4.1 - Lipid-Dependant nAChR Uncoupling and the Lipid Sensor Model

Recently, it was demonstrated that the observed inactivity of the nAChR in PC membranes stems from the fact that the nAChR adopts a novel conformation in these membranes known as the uncoupled state. This state is characterized by loss of allosteric coupling between agonist binding and channel gating events, although the uncoupled receptor still binds agonist

with resting state affinity. Structural characterization of the uncoupled nAChR by Fourier transform infrared spectroscopy (FTIR) reveals that its secondary structure remains intact, and has a similar thermal stability to the resting or desensitized receptor, although the co-operativity of unfolding is slightly reduced. On the other hand, the uncoupled nAChR exhibits more extensive exchange of backbone amide hydrogens for deuterium upon exposure to $^{2}H_2O$ compared to resting or desensitized nAChR, suggesting there is exposure of previously buried protein regions to aqueous solvent upon uncoupling (40).

Based on these observations, a model of lipid dependant nAChR uncoupling was proposed. In this model, the presence of neutral or anionic lipid within the plasma membrane drives the association of the lipid-exposed M4 helix with the rest of the TMD. This association causes the C-terminal end of M4 (post-M4) to interact with the Cys-loop to promote proper interactions between the Cys-loop and other loop regions which, as previously discussed, are essential for communicating agonist binding to channel gating (see section 1.3.4). In the absence of activating lipids, M4 dissociates from the rest of the TMD, resulting in increased physical separation between the ECD and TMD thus weakening essential interactions between the ECD and TMD loop regions. In this way M4 acts as a 'lipid sensor'; its interaction with the rest of the TMD is driven by lipids and promotes 'post-M4'-Cys-loop interactions which in turn promote essential TMD-ECD interface interactions (40).

### 1.4.2 - Is There a Biological Role for Lipid Dependant pLGIC Uncoupling?

While the lipid dependant nAChR uncoupling sufficiently explains the biophysical and biochemical behaviour of nAChR reconstituted into membranes lacking activating lipids and is consistent with the current understanding of nAChR biochemistry and function, one will invariably question whether lipid dependant uncoupling is a biologically relevant phenomenon or

simply an artefact of reconstitution into non-biologically relevant membranes. Several anecdotal observations suggest pLGIC uncoupling may have broader biological significance. For example, heterologous expression of α4β2 receptors in HEK cells results in a large fraction (~90%) of the surface receptors being able to bind agonist yet unable to undergo subsequent gating (59), essentially mimicking the functional profile of the lipid-dependant uncoupled nAChR. The activation of previously non-activatable neuronal α4β2 is also implicated in prolonged nicotine exposure (60). The latter observation suggests shuttling of nAChRs between active and inactive uncoupled conformations may serve physiological roles.

Although speculative, one mechanism by which nAChRs could be shuttled between uncoupled and coupled conformations is through association/disassociation with lipid rafts. The involvement of lipid rafts in pLGIC structure and function is well documented. For example, lipid rafts are involved in nAChR trafficking to the plasma membrane (61) and clustering on the cell surface (62). Since active pLGICs on post-synaptic cells have been shown to cluster (63), the association of nAChRs to lipid rafts may be related to shifting the pool of activatable receptors via lipid dependant uncoupling. The involvement of lipid rafts in nAChR trafficking suggests that lipid uncoupling may also be a mechanism which ensures receptors do not gate before they reach the post-synaptic membrane.

It is also interesting to note that the nAChR has an ordering effect on its surrounding lipid environment through concentration of protons and cations at the membrane surface (64). nAChRs have also been shown to interact uniquely with the headgroup of PS, likely through recruitment of a calcium ion (54). Finally, as will be demonstrated in this thesis, the *Torpedo* nAChR co-purifies with a PA-specific phospholipase activity, meaning that nAChR may be able to convert PA to DAG *in vivo* (65). The plethora of effects and interactions between the nAChR

and its surrounding lipid environment presents several mechanisms by which nAChRs may regulate their own activity.

### 1.4.4 - Does Uncoupling Occur in pLGIC Crystal Structures?

Recent structural studies of pLGICs in the presence of different agonists and inhibitors have attempted to shed light on their gating mechanism. Despite these efforts, this mechanism is still obscure. One of the reasons for this ambiguity is difficulty in assigning the various crystal structures to the putative resting, open, and desensitized conformations, which would demonstrate the structural changes that occur between state transitions. This difficulty potentially stems from several factors. The first is that a detailed functional understanding of some of the pLGICs used in these studies, namely ELIC and GLIC, is still in its infancy. Another is that the time scale for data acquisition in crystallography far exceeds the rate at which these receptors transition between their various functional states, making it difficult to isolate a given conformation long enough to collect diffraction data. Finally, while the function of these receptors has been studied in reconstituted and heterologous expression systems, it is not known whether or not they maintain function in the detergent solubilised state, being the environment in which membrane protein crystals are grown. Therefore, it is possible that ELIC and GLIC are non functional in the detergent solubilised state, and even represent a conformation that is more akin to the uncoupled state.

Careful scrutiny of the ECD-TMD coupling interface in ELIC, and to a lesser extent GLIC, crystal structures compared to that of the *Torpedo* nAChR ECD-TMD interface suggests that the former may serve as a structural model for uncoupling. In the nAChR 4.0 Å model L132 and F137 of the Cys-loop forms tight interactions with P272 of the M2-M3 linker (20) (Figure 1.10A). These residues are known to be energetically coupled within the context of nAChR

**Figure 1.10 –** Scrutiny of ECD-TMD interface of GLIC and ELIC crystal structures reveal predicted features consistent with lipid-dependant uncoupling. Close up view of the ECD-TMD interface of (A) nAChR, (B), GLIC, (C) ELIC. For each structure the M2-M3 linker is colored cyan and the β6-β7 loop (Cys-loop) is coloured yellow. In the nAChR, the functionally significant S269 and P272 on the M1-M2 linker are shown as transparent spheres, as are the conserved pheylalanines and valine on the Cys-loop, and residues at the end of M4. In GLIC and ELIC, conserved M2-M3 linker, β6-β7, and post-M4 residues are similarly depicted.

A

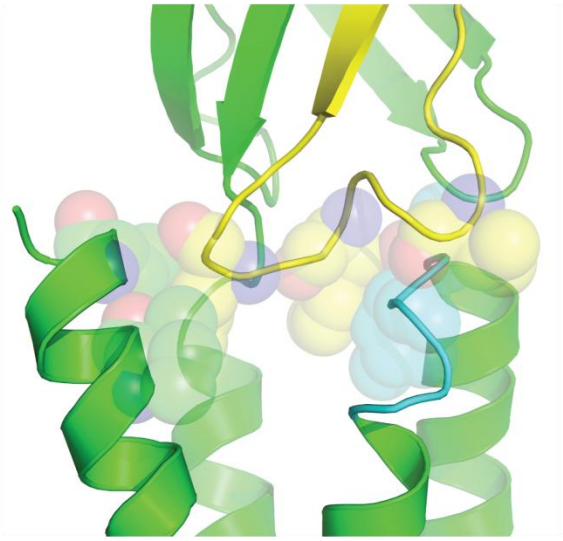

B

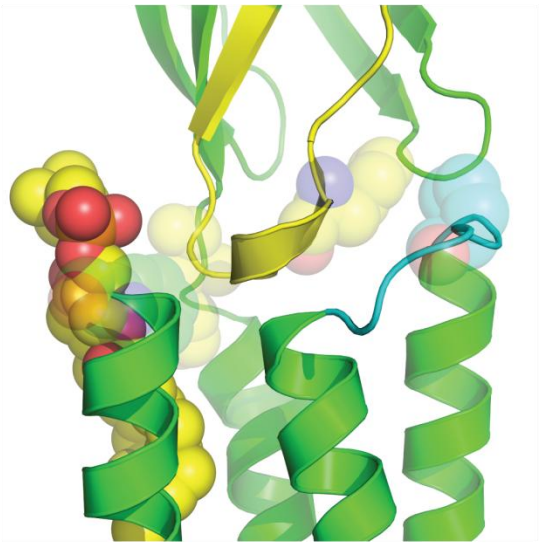

C

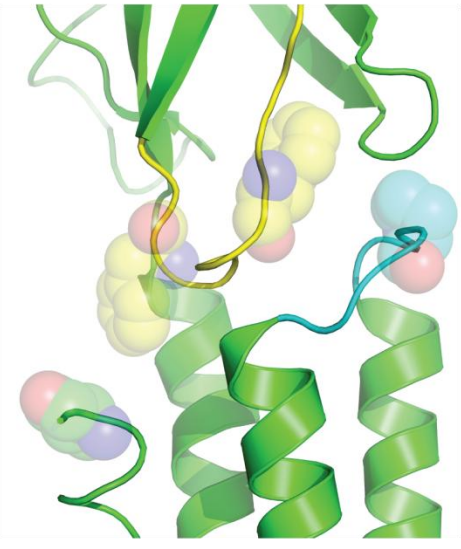

gating and form part of the so called 'principal pathway' linking ligand binding to channel gating (38). On the other hand, the ELIC crystal structure shows unravelling of post-M4 concomitant with a loss of interaction between the conserved residues of the β6-β7 loop and the invariant proline of the M2-M3 linker. In the GLIC crystal structure, interactions occur between the end of M4 and the Cys-loop via a bridging, presumably co-purified, lipid molecule (Figure 1.10B), the β6-β7 residues are still detached from the proline of the M2-M3 linker as observed in the ELIC crystal structure (Figure 1.10B) (27). Moreover, since the end of M4 is essential for proper assembly and function in some pLGICs (66), it is reasonable to suggest the ELIC crystal structure represents an inactive state, given that the end of M4 is completely disordered, albeit the functional consequences of M4 truncation in ELIC is unknown. Finally, note that the detachment of M4 followed by disruption of the interactions between the Cys-loops (β6-β7 loop) and the M2-M3 linker is predicted by the M4 lipid sensor model. While it has been suggested that the subtle structural differences between the loop regions of ELIC and GLIC represent conformational changes between closed and open/desensitized states, it is difficult to explain why nAChR would show such vastly different ECD-TMD interactions from either, since the latter is known to be in a closed, functional state.

Attempts to resolve functional studies with nAChR, ELIC and GLIC models also suggest their crystal structures may not represent native functional states of the receptor. For example, the diameter of the GLIC pore in the apparently open conformation is similar to the closed pore observed in the 4.0 Å nAChR model (27). Moreover, the conformation of the GLIC TMD does not change appreciably when its crystal structure is solved in the presence of functional inhibitors. Also, these inhibitors do not seem to bind to solubilised GLIC with near as high affinity, as judged by the weak electron density in the putative inhibitor binding site in (67).

Finally, in an attempt to address these concerns, a structural characterization of an ELIC mutant which does not desensitize and gates stably, as opposed to transiently, shows no change in the TMD of its crystal structure in both the presence and absence of agonist (68). While some of these observations can be explained in light of recent data (69), others are more difficult to reconcile. These functional inconsistencies in conjunction with observed lack of interactions present in the ECD-TMD interface of GLIC and ELIC crystal structures suggests the possibility that one or both of these structures represent an inactive conformation that is structurally similar to the uncoupled conformation.

If it is true that GLIC and ELIC exists in an uncoupled conformation in their crystal structures, and thus in a detergent solubilised state, then understanding pLGIC lipid dependant uncoupling is important not only from a biological standpoint, but a technological one as well. Since most high resolution techniques require removal of membrane proteins from the lipid membrane by detergent solubilisation, it is essential that the loss of the plasma membrane environment is compensated for in the detergent solubilised state, either by creating mutants or designing small molecules which will stabilise the protein structure. Understanding the mechanisms by which lipids stabilise pLGIC structure and function will guide in the strategic design of mutants or molecules that allow pLGICs to remain functional in the detergent solubilised state.

### 1.5 - Summary and Statement of Objective

The above discussion shows that there are complex interactions between the nAChR and its lipid environment which may have important implications for human biology and investigations into structure/function relationships of pLGICs in general. The ultimate goal of this project was to understand the molecular basis of nAChR lipid sensitivity. The nAChR

would be the ideal candidate for understanding this mechanism due to extensive functional and biophysical characterization in different lipid environments and the plethora of well characterized probes capable of monitoring its function. Unfortunately, the relevant nAChR mutants cannot be expressed at sufficient quantities suitable for these studies.

The recent discovery of the prokaryotic homologues GLIC and ELIC present an opportunity to investigate these mechanisms due to their homology to vertebrate pLGICs and amenability to high level expression and crystallographic studies. Unlike the nAChR however, their biophysical and functional properties in different lipid environments have not been characterized. Moreover, at the onset of this study there was no reliable protocol for reconstitution of ELIC or GLIC into model lipid systems available. Thus, an essential first step toward using GLIC or ELIC as a model for the above stated intentions required the development of a reconstitution protocol and characterization in different lipid systems.

Chapter 3 of this dissertation focuses on a project which I helped complete upon my arrival in Dr. Baenziger's lab dealing with the characterization of phospholipase activity observed in nAChR preparations. The results of this study were published in the *Journal of Biological Chemistry* (65). Chapter 4 describes the main body of work done throughout my M.Sc. thesis which focuses on the expression, purification, and reconstitution of GLIC as well as characterization of this reconstituted sample. These findings were recently published in the *Journal of Biological Chemistry* in a separate article (29). Note that initially there were problems expressing GLIC at suitable quantities and details of the purification had to be worked out. The details of these optimization experiments are presented in Appendix I.

## Chapter 2

# Phospholipase C activity affinity purifies with the *Torpedo* nicotinic acetylcholine receptor

Jonathan M. Labriola[1], Corrie J.B. daCosta[1†], Shuzhi Wang[1], R. Michel Sturgeon[1], Jeffrey C. Smith[2] and John E. Baenziger[1]*

## 2.1 - Preface

This project was already underway upon my arrival in Dr. John Baenziger's laboratory. The goal was to identify and characterize the source of a 'contaminant' that was observed in lipid extracts from nAChR reconstituted in to synthetic membranes containing PA. In time, the 'contaminant' in these lipid extracts was identified as diacylglycerol (DAG). The fact that 1) DAG is a product of the removal of the phosphate headgroup from PA, 2) This product is only observed in nAChR-reconstituted lipid systems with PA present, and 3) that this was occurring in reconstituted systems containing highly purified nAChR, lead to the hypothesis that nAChR exhibits phospholipase C specific activity.

My role in the project was to conduct control experiments which showed that the phospholipase C activity must originate from the nAChR itself or from some very tightly bound species that is not detectable by SDS-PAGE (Figure 2.03), as well as purify and reconstitute nAChR into DAG containing membranes and perform the functional experiments on these samples (Figure 2.05, panel *iii*). Finally, I prepared all the figures. Shuzi Wang conducted the initial experiments characterizing the phospholipase activity in nAChR containing reconstitutions and its inhibition by sodium orthovanadate. Dr. Corrie daCosta and Michel Sturgeon isolated the unknown product from TLC plates and performed initial characterization by FTIR. Jeffrey Smith from Dr. Daniel Figeys lab conducted mass spectrometry experiments which conclusively identified the unknown lipid product as DAG. Within the context of this dissertation, this project deepened our understanding of nAChR-lipid interactions and provided a potential mechanism of how nAChRs may modulate their own function *in vivo* through lipid-dependant uncoupling.

## 2.2 - Abstract

**Nicotinic acetylcholine receptors mediate fast synaptic transmission by fluxing ions across the membrane in response to neurotransmitter binding. We show here that during affinity-purification of the nicotinic acetylcholine receptor from *Torpedo*, phosphatidic acid, but not other anionic or zwitterionic phospholipids, is hydrolysed to diacylglycerol. The phospholipase C activity elutes with the acetylcholine receptor and is inhibited by a lipid phosphate phosphohydrolase inhibitor, sodium vanadate, but not a phosphatidate phosphohydrolase inhibitor, N-ethylmaleimide. Further, the hydrolysis product of phosphatidic acid, diacylglycerol, enhances the functional capabilities of the acetylcholine receptor in the presence of anionic lipids. We conclude that a phospholipase C activity, which appears to be specific for phosphatidic acid, is associated with the nicotinic acetylcholine receptor. The acetylcholine receptor may directly or indirectly influence lipid metabolism in a manner that enhances its own function.**

## 2.3 - Introduction

Cys-loop receptors mediate fast transmission at chemical synapses by transiently opening an ion channel across the cell membrane in response to neurotransmitter binding (2,70-74). The resultant influx of ions into the cell alters the membrane potential, leading to the generation or in some cases the inhibition of an action potential. Many endogenous and exogenous compounds influence the ability of Cys-loop receptors to flux ions, altering the efficiency of synaptic transmission. Cys-loop receptors play a dynamic role in communication within the nervous system.

The ability of Cys-loop receptors to flux ions is sensitive to membrane lipid composition (40,48,51,75,76). The effects of lipids on the function of the prototypical Cys-loop receptor, the *Torpedo* nicotinic acetylcholine receptor (nAChR), have been intensely studied, particularly in reconstituted membranes of "well-defined" lipid compositions. A mixture of both anionic and neutral lipids is optimal for the nAChR to adopt an agonist-activatable conformation (40). Of the many anionic lipids, phosphatidic acid (PA) is particularly effective at stabilizing a large proportion of agonist-activatable resting nAChRs (77).

Correlations between lipids and nAChR function are based on the assumption that the lipid composition of a reconstituted membrane is defined by the exogenous lipids supplied during affinity purification. Although this assumption holds in most cases, we show here that nAChR-reconstituted PC/PA membranes contain the unexpected lipid, diacylglycerol (DAG). DAG appears during affinity purification of the nAChR as a result of the hydrolysis of PA. PA-specific phospholipase C activity co-purifies with the nAChR and is inhibited by vanadate, but not N-ethylmaleimide. Also, the presence of DAG in a reconstituted membrane influences the ability of the nAChR to undergo agonist-induced conformational transitions. Our results support the novel hypothesis that nicotinic acetylcholine receptors influence cellular events by mechanisms that do not involve the flux of ions into the cell **(78-82)**. The nAChR may be able to alter the lipid composition of its surrounding microenvironment in a manner that enhances its own function.

### 2.4 - Experimental Procedures

*Materials.* Frozen *Torpedo californica* electroplax tissue was obtained from Aquatic Research Consultants (San Pedro, CA). 1-palmitoyl-2-oleoyl-*sn*-glycero-3-phosphocholine (PC), 1-palmitoyl-2-oleoyl-*sn*-glycero-3-phosphoglycerol (PG), 1-palmitoyl-2-oleoyl-*sn*-

glycero-3-phosphoserine (PS) and 1,2-dioleoyl-*sn*-glycerol (DAG) were from Avanti Polar lipids, Inc. (Alabaster, AL). (EthBr) and carbamylcholine chloride (Carb) were from Sigma (St. Louis, MO).

*nAChR Purification and Reconstitution.* The nAChR was affinity purified on a bromoacetylcholine bromide-derivatized Affi-Gel 102 column (Bio-Rad; Richmond, CA) as described elsewhere (54,55). The column bound nAChR was washed extensively with successive solutions of dialysis buffer (100 mM NaCl, 10 mM Tris-HCl, 0.1 mM EDTA, 0.02% w/v $NaN_3$, pH 7.8) containing 1% cholate supplemented with 1.3 mM, 3.2 mM (referred to as the lipid A wash), and 0.13 mM of the desired lipid. The nAChR was then eluted from the column with a 0.13 mM lipid solution in 250 mM NaCl, 0.1 mM EDTA, 0.02% $NaN_3$, 5 mM phosphate, pH 7.8 with 0.5% cholate and 10 mM Carb. After elution from the column, the nAChR was dialyzed five times against 2 litres of dialysis buffer with buffer change approximately once every 12 hours. The reconstituted membranes typically have lipid-protein ratios in the 150-300 mol:mol range, as estimated by FTIR (83) and enzymatic assays (77).

The origin of the phospholipase activity was examined in more detail by running columns, as described above, except that the nAChR fractions were extracted either immediately or one week after elution from the affinity column. The one-week samples were maintained under $N_2$ at 4 $^oC$ prior to extraction. The data in Figs. 2.03 and 2.04 were from columns eluted in 0.39 mM as opposed to 0.13 mM lipids.

*Thin Layer Chromatography.* Lipids were extracted using a modified Bligh & Dyer extraction protocol (84). Aliquots containing 500 μg of PC (Phospholipids C assay; Wako Chemicals USA; Richmond, VA) were diluted to 1.6 ml with dialysis buffer and mixed with 6

ml of $CHCl_3$:$CH_3OH$ 1:2 (v:v). After shaking vigorously, an additional 2 ml of both $CHCl_3$ and dialysis buffer were added (final ratio $CHCl_3$:$CH_3OH$:dialysis buffer 1:1:0.9 (v:v:v)) and the extraction tubes centrifuged at 500 X *g* for 10 minutes. The bottom organic phase (~4 ml) was removed and the extraction sometimes repeated by adding an additional 4 ml of $CHCl_3$. The pooled organic phases were evaporated under $N_2$ and dissolved in a small volume of $CHCl_3$.

TLCs were performed as described (40) using high performance silica gel plates (60 Å, 4.5 μm particle size; Whatman), except in 3.02 where silica gel 60 $WF_{254}$8 plates (EM Science) were used. TLC plates were typically developed using chloroform:methanol:formic acid:$H_2O$ (50:37.5:3.5:2, vol/vol) as a solvent system, except in Fig. 2.01B and 2.01D, where benzene:2-propanol:ethylacetate:formic acid (72.5:3.5:22:2) was used.

*Ethidium Fluorescence Measurements.* All fluorescence experiments were performed on a Cary Eclipse fluorescence spectrophotometer equipped with the Cary Eclipse v1.1 software package (Varian, Inc.). The fluorescence emission intensity at 590 nm was monitored as a function of time (2.0 s sampling time) while ethidium bromide was continuously excited at 530 nm excitation. Excitation and emission slits were 5 nm and 20 nm, respectively. For each experiment, 1.8 ml of 0.3 μM ($1xK_D$) ethidium bromide in TRB was equilibrated at 22.5°C inside the spectrophotometer. At the indicated times, 30 μg of nAChR suspended in 200 μl TRB was added, followed by 10 μl of 100 mM carbamylcholine and then 20 μl of 100 mM dibucaine (i.e. ~500 μM and 1 mM final concentrations, respectively for the two ligands).

**2.5 - Results**

*nAChR-reconstituted PC/PA membranes contain DAG.* Protocols are well-established for the affinity purification and reconstitution of the nAChR into membranes with a defined lipid

composition (54-56,85). Typically, the nAChR is solubilized with cholate and bound to an affinity column, where it is washed extensively with cholate-solubilized lipids to both remove non-specifically bound protein and replace the natural *Torpedo* lipids with the "lipids-of-interest". The nAChR is then eluted in the presence of the same cholate-solubilized lipids, and reconstituted into membrane vesicles by cholate dialysis.

We have examined the lipid compositions of numerous reconstituted nAChR membranes, as shown in Fig. 2.01A for the nAChR reconstituted into membranes composed of PC (PC-nAChR), PC/phosphatidylglycerol (PC/PG-nAChR), PC/phosphatidylserine (PC/PS-nAChR) and PC/PA (PC/PA-nAChR). This TLC, developed using the solvent system, chloroform:methanol:formic acid:$H_2O$ (referred to as the "polar solvent system"), shows that in all but one case, the lipid composition of the resulting membrane matches that of the exogenous lipids used to wash and elute the nAChR from the affinity column. For example, lipid extracts from PC-nAChR contain one lipid that runs adjacent to the PC standard. Lipid extracts from PC/PG-nAChR, PC/PS-nAChR, and PC/PA-nAChR each contain two lipids corresponding to PC and the expected anionic lipid, both at or very close to the expected PC/anionic lipid ratio. The lipid extracts from PC/PA-nAChR, however, contain a relatively intensely-staining band that runs slightly below the effective solvent front. The migration distance of this band suggests a neutral, as opposed to a phospho-lipid.

The unexpected neutral lipid observed in the lipid extracts from PC/PA-nAChR is resolved from the solvent front on a TLC plate developed using the solvent system, benzene:2-propanol:ethylacetate:formic acid (Fig. 2.01B)(referred to as the "non-polar solvent system"). The relative migration of the neutral lipid does not match that of cholesterol, cholesterol-ester or free fatty acid (Fig. 2.01C). The lipid runs slightly above the 1, 2-dipalmitoyl form of dipalmitin

**Figure 2.01 - Characterization of lipids in reconstituted nAChR membranes.** Thin-layer chromatography shows that the lipid compositions of most nAChR reconstitutions are as expected based on the lipids supplied during affinity purification of the nAChR, except that some of the PA in PC/PA-nAChR is hydrolyzed to DAG. (A) Lanes 1,3, 5, and 7 are lipid standards. Lanes 2, 4, 6, and 8 are lipid extracts from PC-nAChR, PC/PG-nAChR, PC/PS-nAChR, and PC/PA-nAChR. The TLC plate was developed using a chloroform:methanol:formic acid:$H_2O$ (50:37.5:3.5:2, vol/vol) solvent system. (B) The same as (A) except that the TLC plate was developed using a less polar solvent system (benzene:2-propanol:ethylacetate:formic acid (72.5:3.5:22:2)) that resolves neutral lipids while phospholipids remain at the origin. (C) *Lane 2*, dipalmitin (a mixture of 1,2DAG and 1,3 DAG with palmitoyl acyl chains); *Lane 3*, 1-palmitoyl-2-oleoyl-DAG; *Lane 4*, PC/PA-nAChR; *Lane 5*, cholesterol; *Lane 6*, cholesterol ester, *Lane 7*, oleic acid. Same solvent system as (B). (D) Representative SDS PAGE from two nAChR reconstitutions; *Lane 1*, Standards, *Lane 2*, PC-nAChR, *Lane 3*, PC/PA-nAChR. The SDS-PAGE samples were from the purifications used for the lipid extractions in Figs. 2.01A-C.

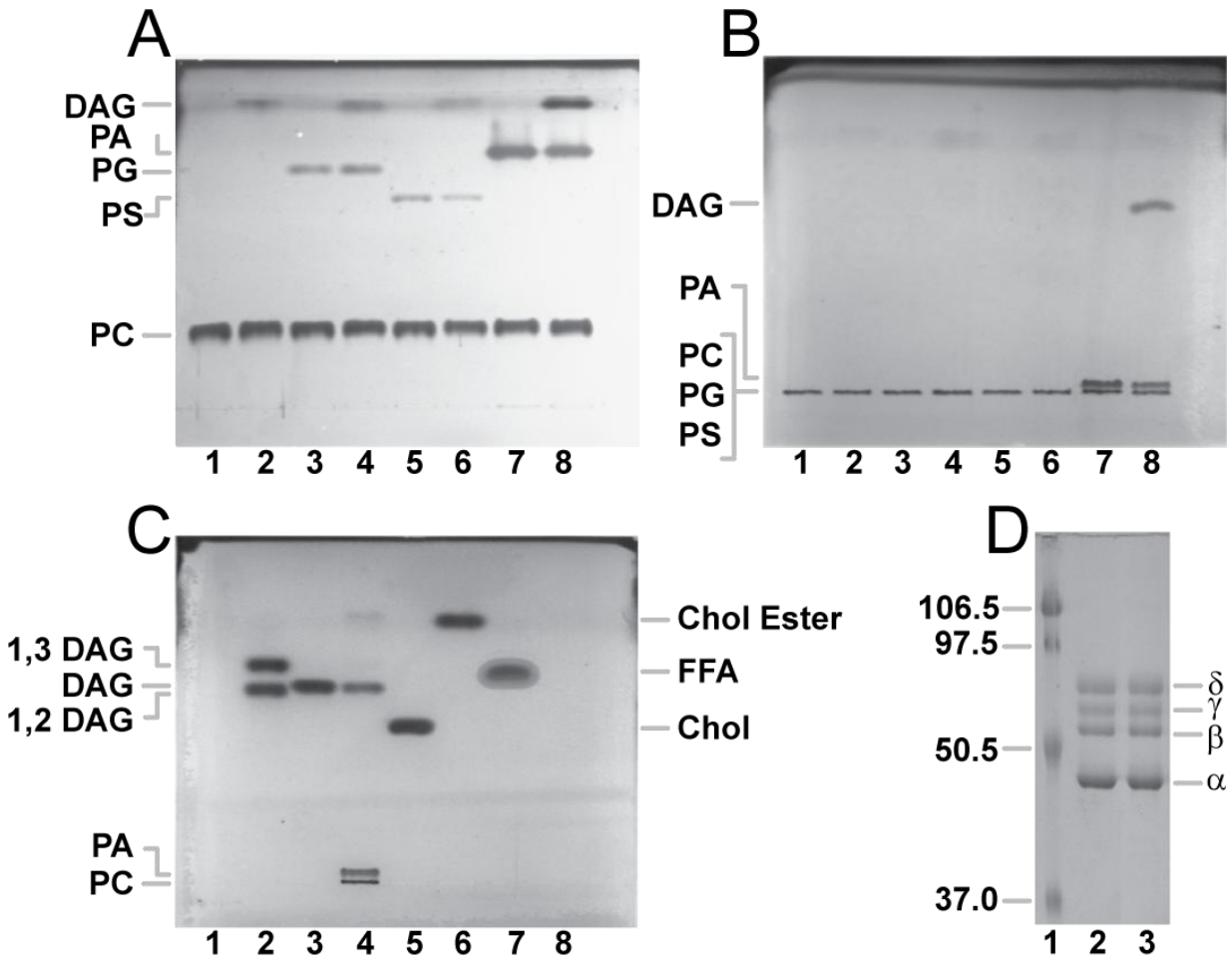
A
DAG
PA
PG
PS
PC
1 2 3 4 5 6 7 8
B
DAG
PA
PC
PG
PS
1 2 3 4 5 6 7 8
C
1,3 DAG
DAG
1,2 DAG
PA
PC
Chol Ester
FFA
Chol
1 2 3 4 5 6 7 8
D
106.5
97.5
50.5
37.0
δ
γ
β
α
1 2 3

(a mixture of 1,2-dipalmitoylglycerol and 1,3-dipalmitoylglycerol) and corresponds precisely to the 1-palmitoyl-2-oleoylglycerol (referred to here as DAG) standard. Analysis of the neutral lipid extracted from the TLC by mass spectrometry confirms that it is the palmitoyl-oleoyl form of DAG (data not shown). DAG stains intensely with Coomassie Blue even though control TLCs suggest that it represents less than 10 mol% of the total lipid in PC/PA-nAChR (data not shown).

The TLC developed with the non-polar solvent system (Fig. 2.01B) shows that DAG is not present in PC-nAChR, PC/PG-nAChR, or PC/PS-nAChR, although on TLCs overloaded with lipid, A very faint band due to DAG can be observed in the reconstitutions containing PG and PS. Further, DAG is not evident in reconstitutions containing the anionic lipids phosphatidylinositol or cardiolipin, and the zwitterionic lipid, phosphatidylethanolamine (data not shown). Given that DAG is only prominent in lipid extracts from PC/PA-nAChR and that only the 1-palmitoyl-2-oleoyl isomer of DAG is present, it seems likely that DAG appears as a result of hydrolysis of PA during affinity purification of the nAChR.

Note also that each of the lipid extractions (Fig. 2.01A, lanes 2, 4, 6, and 8) contains an additional faint band that runs at the solvent front slightly above DAG on TLCs developed using the polar solvent system (Fig. 2.01A, lanes 2, 4, 6, and 8). Surprisingly, no distinct band with equivalent staining intensity is observed on TLC plates developed using the non-polar solvent system (Fig. 2.01B, lanes 2, 4, 6, and 8). In our experience, trace organic contaminants that arise during lipid extraction/storage concentrate at the solvent front on TLC plates developed using the polar solvent system. These contaminants and DAG both stain intensely with Coomassie blue. The identity of this(these) trace compound(s) was not studied further – the important point being

that DAG is prominent in PC/PA-nAChR, but is essentially lacking in PC-nAChR, PC/PG-nAChR, and PC/PS-nAChR, i.e. those reconstitutions lacking PA.

*DAG forms via hydrolysis of PA.* We next determined the origin of DAG in our nAChR-reconstituted PC/PA membranes by examining the affinity-purification protocol. Affinity columns were run in the presence of either cholate-solubilized PC or PC/PA. In each case, the lipid compositions of the stock cholate-solubilized lipid solution (lipid A; see Experimental Procedures) was examined both before and after passing the lipids through the affinity column – the latter passed through the affinity column both before (data not shown) and while the solubilized nAChR was bound to the resin (Figs. 2.02A and B, panels *i* and *ii*, Controls *1* and *2*). In all cases, these control lipid solutions contained only PC or PC/PA. None of the incubation conditions led to the formation of DAG. This result shows that DAG formation is not the result of an inherent instability of PC or PA prior to, or after contact with the affinity resin (see also below).

Fractions of the detergent-solubilized nAChR eluted from the affinity column in the presence of PC were essentially free of DAG, with only a faint band running near the solvent in fractions containing substantial amounts of the nAChR (Fig. 2.02A, panel *i*, Fractions 1-9). As noted above, this band may be due to trace organic contaminants or possibly some neutral lipid(s) that co-purifies and/or co-extracts with the nAChR. Significantly, prolonged incubation of the fractions at 4 $^{o}$C for several days did not change the intensities of this weakly staining band and did not lead to the appearance of DAG. This result confirms that PC is not hydrolyzed to DAG in the presence of the nAChR (Fig. 2.02A, panel *ii*, Fractions 1-9).

In contrast, fractions of the affinity-purified nAChR eluted in the presence of PC/PA exhibit more intense staining of DAG (Fig. 2.02B, panel *i*, Fractions 1-9). The amount of DAG varied proportionally to the amount of the nAChR eluted in each fraction (Fig. 3.02B, panel *iv*). Of enormous significance, further incubation of the nAChR-containing fractions at 4 $^{o}$C under nitrogen led to loss of PA with the concomitant formation of DAG (Fig. 2.02B, panel *ii*, Fractions 1-9). In fact, prolonged incubation at 4$^{o}$C led to complete hydrolysis of PA to DAG in most fractions. As noted above, DAG was not formed in control lipid A solutions that were incubated under identical conditions (but lacking the nAChR) (Fig. 2.02B, panel *i* and *ii*, Controls 1 and 2). In addition, the hydrolysis of PA to DAG was less in those fractions containing minimal eluted affinity-purified nAChR (Fig. 2.02B, panel *i* and *ii*, Fractions 1, 8, and 9). These results show unequivocally that DAG is formed via hydrolysis of PA. Although it is not yet possible to precisely quantify the phospholipase C activity, densitometric analysis of the DAG production in Fig. 2.02B, panel *i* suggests a close correlation between the phospholipase C activity elution profile and that of the nAChR (Fig. 2.02B, panel *iv*). These correlations suggest that either the phospholipase activity is intrinsic to the nAChR itself or due a tightly nAChR-associated protein. An alternative interpretation, however, is that the phospholipase C activity is a distinct protein that exhibits a high affinity for the acetylcholine affinity resin. A distinct protein with high affinity for the acetylcholine affinity resin could co-elute with the nAChR upon the addition of Carb.

*The PA-specific phospholipase C activity is associated with the affinity-purified nAChR.* To test the possibility that a distinct protein with phospholipase C activity exhibits an intrinsic affinity for the acetylcholine-affinity resin, we ran parallel affinity columns in the presence of

\

**Figure 2.02 - PA-specific phospholipase activity elutes with the nAChR from the bromoacetylcholine-affinity column. (A)** Affinity purification of the nAChR in the presence of PC, **(B)** affinity purification of the nAChR in the presence of PC and PA. *Panels i and ii* are TLCs developed in chloroform:methanol:formic acid:$H_2O$ (50:37.5:3.5:2, vol/vol) of lipid extracts from the control lipid solutions and the detergent-solubilized nAChR fractions eluted from the affinity column. In each case, Control 1 is an extract of the stock lipid A solution. Control 2 is an extract of the same lipid A solution after it has been washed through the affinity column with while the nAChR is bound to the column. Fractions 1-9 were collected upon elution of the solubilized nAChR from each affinity column with Carb. *Panel i*, the lipid extractions were performed immediately after eluting the nAChR from the column. *Panel ii*, the lipid extractions were performed one week later (samples maintained at 4 $^{o}$C under $N_2$). *Panel iii* are SDS PAGE of each of the collected nAChR fractions. *Panel iv*, the $A_{280}$ of each of the eluted nAChR fractions. (B) *panel iv* also shows a densitometric analysis of the DAG bands observed on the TLC in (B) *panel i*.

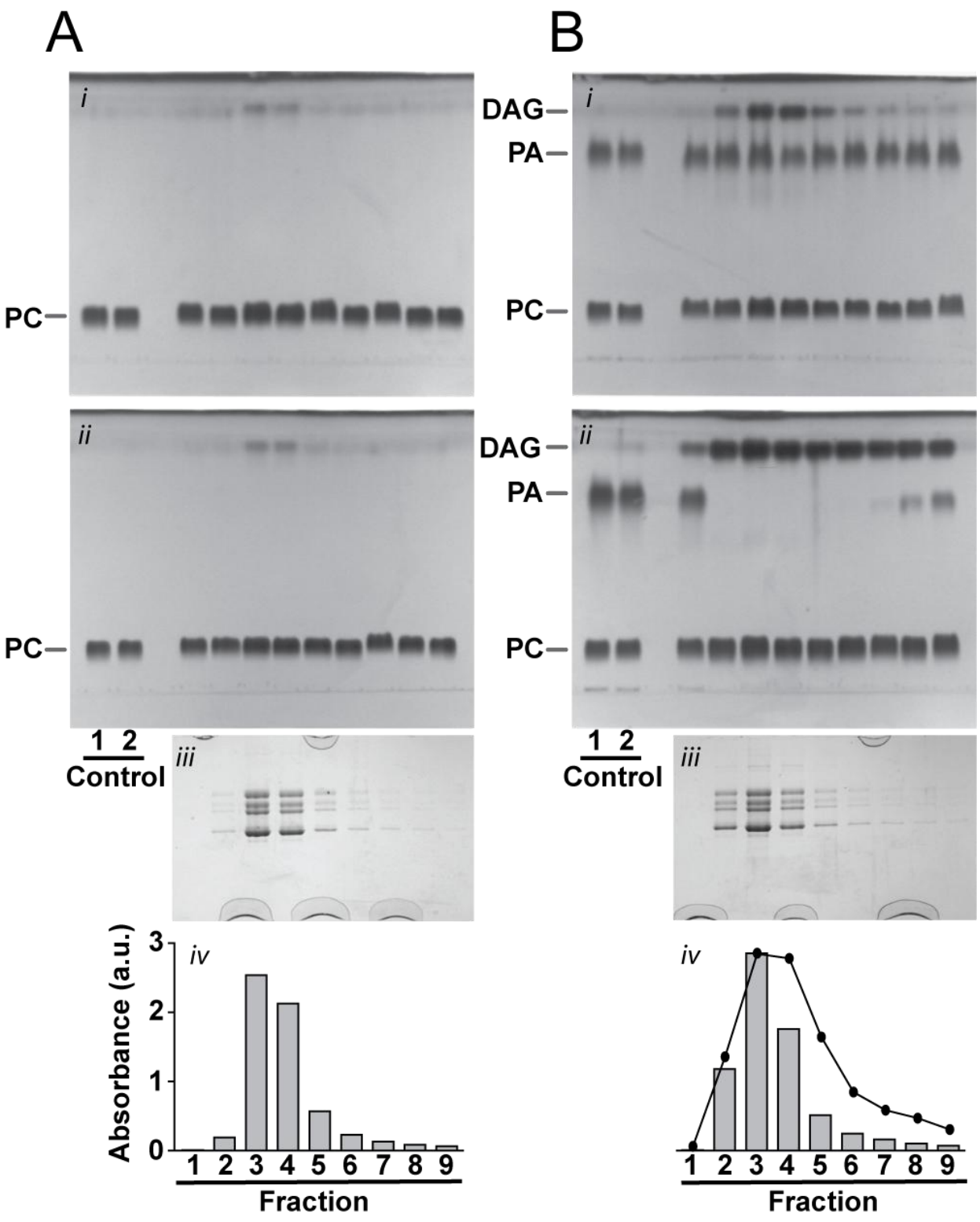
A
B
i
ii
iii
iv
DAG
PA
PC
1 2
Control
Absorbance (a.u.)
0
1
2
3
1 2 3 4 5 6 7 8 9
Fraction

PC/PA as in Fig. 2.02B, except that one of the solubilized nAChR samples was treated with α-bungarotoxin prior to application to the affinity column. α-Bungarotoxin is a competitive antagonist that binds to *Torpedo* nAChR with high affinity. α-Bungarotoxin treatment is sufficient to eliminate or at least greatly reduce the level of nAChR binding to the acetylcholine-affinity resin. Consequently, minimal if any protein elutes from the affinity resin upon exposure to Carb (Fig. 2.03B, panel *iii*).

Significantly, the Carb eluates from the column run after α-bungarotoxin-treatment show minimal if any PA-specific phospholipase activity. This control experiment shows unequivocally that the PA-specific phospholipase activity is not due to a distinct protein that associates independently with the acetylcholine-affinity resin. Our results show that for the phospholipase activity to associate with the affinity resin, the nAChR must also be bound. The phospholipase C activity is therefore either intrinsic to the nAChR itself or it resides in a protein that associates tightly with the nAChR.

*The PA-specific phospholipase C activity is vanadate-inhibitable.* Two different PA-specific phospholipases have been identified in mammalian tissues. Cytosolic phosphatidate phosphatases are sensitive to N-ethylmaleimide (86,87). Membrane bound lipid phosphate phosphohydrolases are inhibited by sodium vanadate (88). We repeated the nAChR affinity purifications with PC/PA in the presence of either N-ethylmaleimide or 1 mM vanadate. N-ethylmaleimide had no inhibitory effect on the observed phospholipase activity (Fig. 2.04B). In contrast, vanadate inhibits the hydrolysis of PA, even after prolonged incubation of the nAChR with the cholate-solulibilized lipid (Fig. 2.04C). The affinity purified nAChR phospholipase C

**Figure 2.03 - PA-specific phospholipase activity is associated with the nAChR.** Affinity purification of the nAChR in the presence of PC and PA either without **(A)** or with **(B)** prior treatment of the solubilized nAChR with ~8 μM α-bungarotoxin, the latter to diminish nAChR binding to the affinity resin. *Panels i and ii* are TLCs developed in chloroform:methanol:formic acid:$H_2O$ (50:37.5:3.5:2, vol/vol) of lipid extracts from the control lipid solutions and the detergent-solubilized nAChR fractions eluted from the affinity column. The control lipids are extracts of the stock lipid A solution, as described in Fig. 2.02. Fractions 1-6 were collected upon elution of the solubilized nAChR from each affinity column with Carb. *Panel i*, the lipid extractions were performed immediately after running the column. *Panel ii*, the lipid extractions were performed one week later (samples maintained at 4 $^{o}$C under $N_2$). *Panel iii*, SDS PAGE of each of the collected nAChR fractions. *Panel iv*, $A_{280}$ of each of the eluted nAChR fractions.

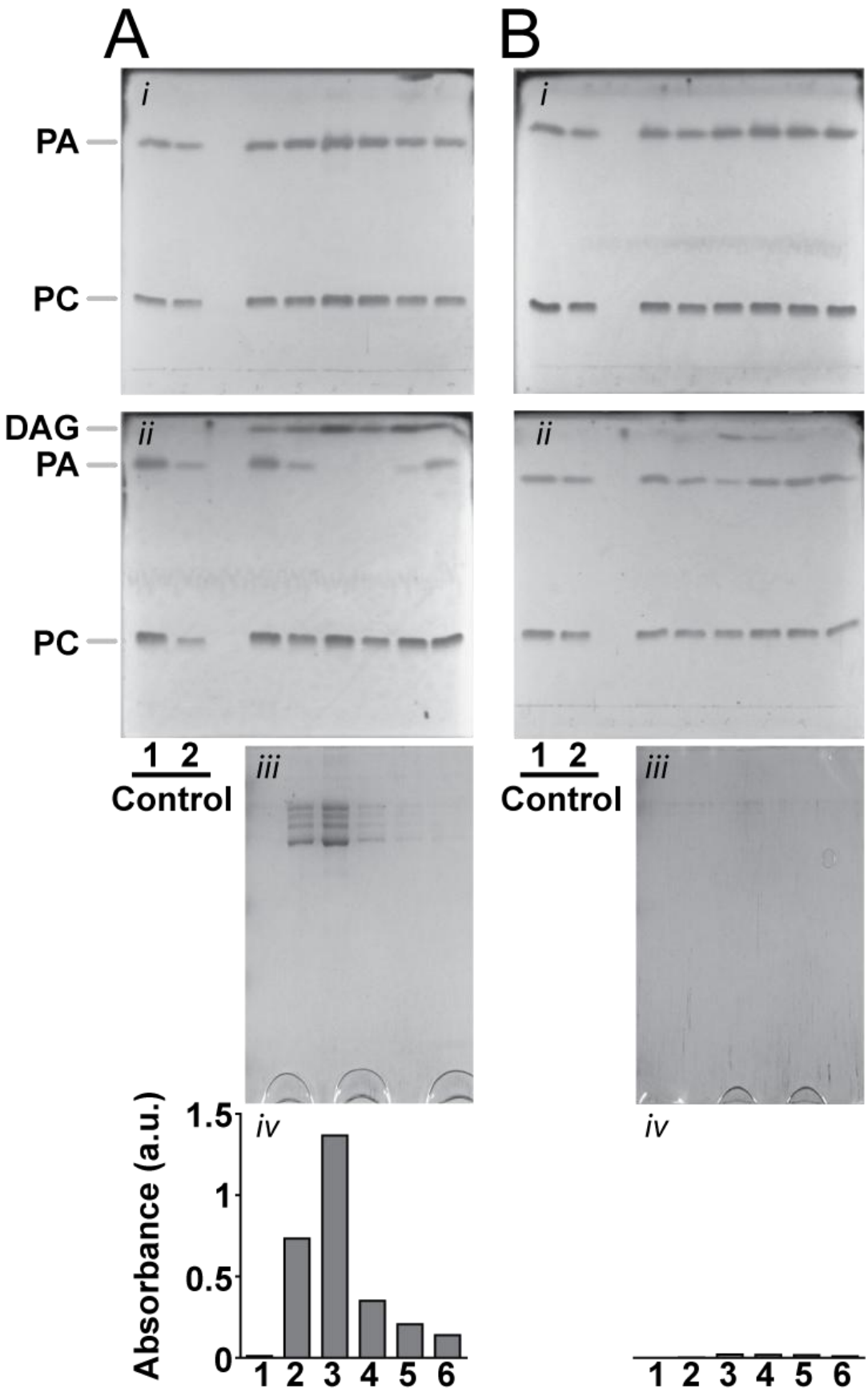
A
B
i
PA
PC
ii
DAG
PA
PC
1 2
Control
iii
iv
Absorbance (a.u.)
1.5
1
0.5
0
1 2 3 4 5 6

**Figure 2.04 - The effects of N-ethylmaleimide and vanadate on the nAChR-associated phospholipase activity.** Affinity purification of the nAChR in the presence PC and PA in the absence of inhibitor (A) or in the presence of (B) 4.2 mM N-ethylmaleimide or (C) 1 mM sodium vanadate. *Panel i and ii* are TLCs developed in chloroform:methanol:formic acid:$H_2O$ (50:37.5:3.5:2, vol/vol) of lipid extracts from the control lipid solutions and the detergent-solubilized nAChR fractions eluted from the affinity column. In each case, Control 1 is an extract of the stock lipid A solution. Control 2 is an extract of the same lipid A solution after it has been washed through the affinity column with the column-bound nAChR. Fractions 1-6 were collected upon elution of the solubilized nAChR from each affinity column with Carb. *Panel i*, lipid extractions performed immediately after running the column. *Panel ii*, lipid extractions performed one week later (samples maintained at 4 $^{o}$C under $N_2$). *Panel iii* are SDS PAGE of each of the collected nAChR fractions. *Panel iv,* the $A_{280}$ of each of the eluted nAChR fractions. Note that sodium vanadate absorbs strongly at 280 nm making the absolute $A_{280}$ readings somewhat unreliable.

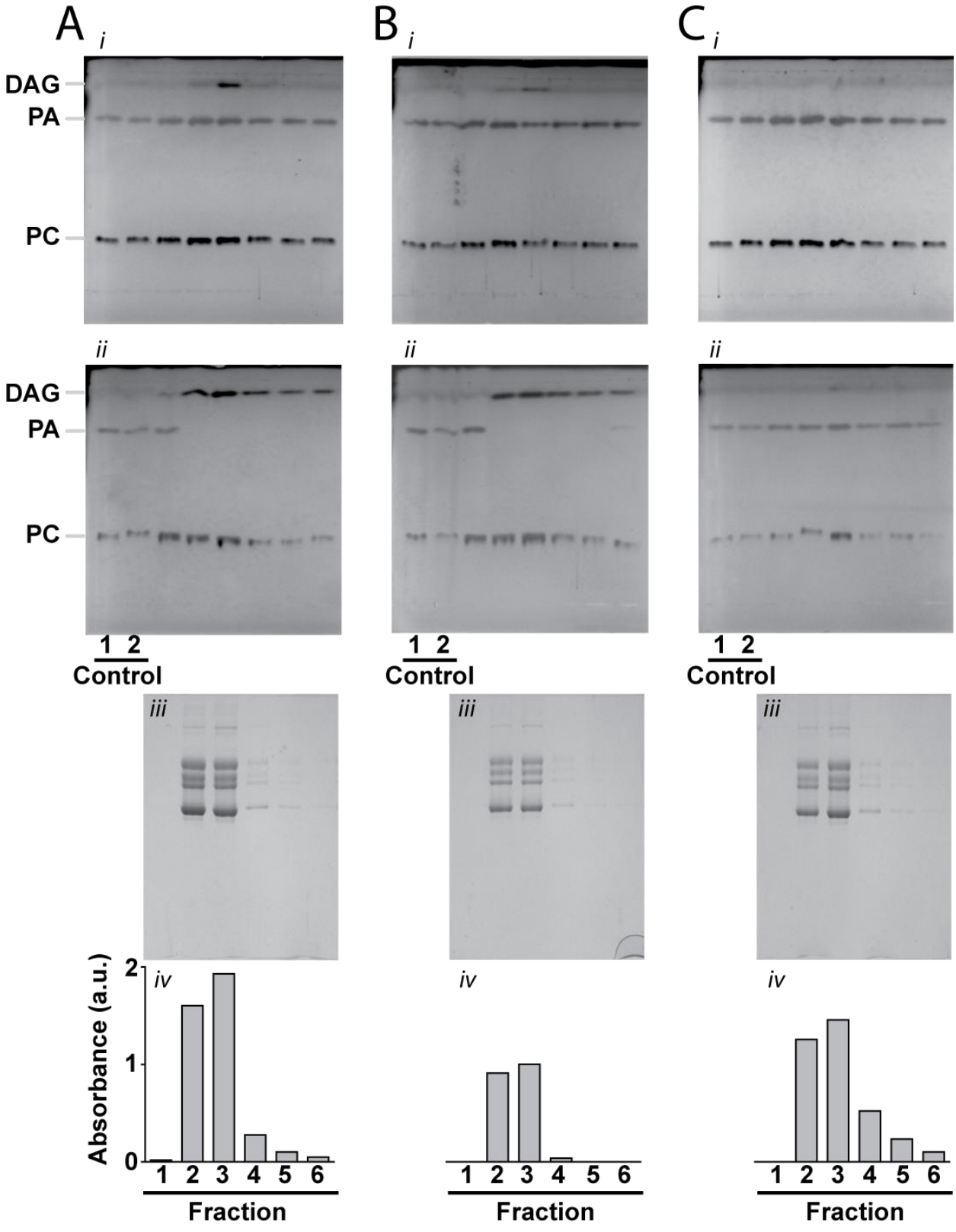
A
B
C
i
DAG
PA
PC
ii
1 2
Control
iii
iv
Absorbance (a.u.)
0
1
2
1 2 3 4 5 6
Fraction

activity is thus vanadate inhibitable. The phospholipase activity is similar to that of membrane bound lipid phosphate phosphohydrolase.

*DAG influences the ability of the nAChR to undergo agonist-induced conformational transitions.* Given that the PA-specific phospholipase activity purifies with the nAChR, we next tested whether the hydrolysis product of PA (i.e. DAG) influences nAChR activity. We

examined whether DAG influences the ability of the nAChR to undergo agonist-induced conformational transitions using the conformationally sensitive probe, ethidium bromide (Fig. 2.05). Ethidium is an open channel blocker that binds with high affinity to a hydrophobic site within the ion channel pore of the desensitized ($K_D \cong 0.3$ μM), but not the resting ($K_D \cong 1$ mM) nAChR (89). Relative to aqueous ethidium, nAChR-bound ethidium exhibits a greater fluorescence emission intensity, and its emission maximum shifts from 605 (aqueous solution) to 590 nm (nAChR-bound). The lipid-dependent uncoupled conformation of the nAChR in PC membranes also binds ethidium with low affinity (40).

Addition of PC/DAG-nAChR to a 0.3 μM aqueous solution of ethidium leads to a small increase in dibucaine-displaceable fluorescence (Fig. 2.05A, trace *ii*) similar to that observed upon the addition of PC/PA-nAChR, but not PC-nAChR. At this concentration (~$K_D$ for the desensitized state), the slow increase in fluorescence is due to the slow binding of ethidium to the ion pore of the desensitized nAChR. As noted, PC-nAChR does not bind ethidium because it adopts a low-affinity ethidium-binding conformation referred to as the lipid-dependent uncoupled state (40).

Addition of 500 μM Carb to PC/PA-nAChR leads to a rapid and further increase in dibucaine-displaceable ethidium fluorescence (Fig. 2.05A, trace *i*). The Carb-induced increase

**Figure 2.05 - DAG influences the ability of the nAChR to undergo Carb-induced conformational transitions.** The fluorescence emission of ethidium at 590 nm was monitored in the presence of the nAChR reconstituted into ***(i)*** 3:2 PC/PA, ***(ii)*** PC, **(*iii*)** 3:2 PC/DAG, ***(iv)*** 3:2 PC/PS, and ***(v)*** 3:1:1 PC/PS/DAG membranes. **(A)** At the indicated times ~50 nM nAChR, 500 µM Carb, and 500 µM dibucaine were added to a 0.3 µM ethidium solution. The sharp spikes in each fluorescence emission trace reflect the scattering of light upon insertion of the pipette into the cuvette. Note that the large increase in fluore **(B)** Dibucaine-displaceable ethidium fluorescence emission intensity at 590 nm in the presence (+) or absence (-) of Carb. Error bars are the standard error.

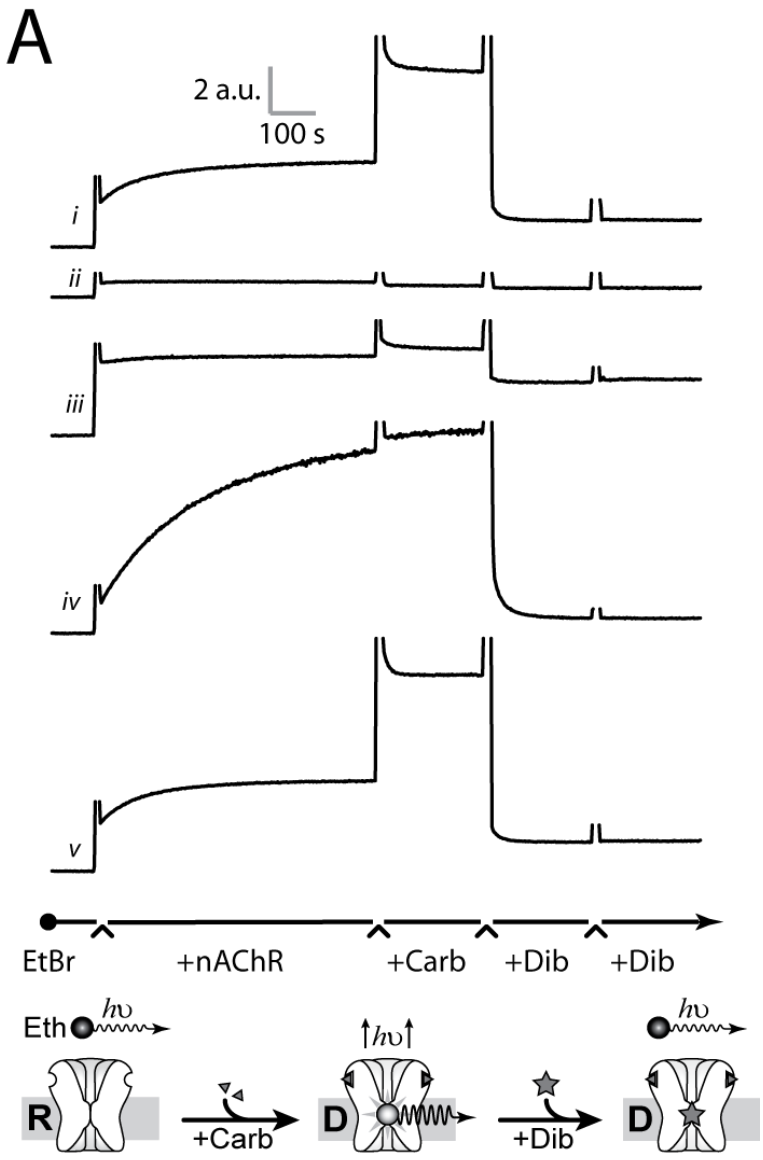
A
2 a.u.
100 s
i
ii
iii
iv
v
EtBr
+nAChR
+Carb
+Dib
+Dib
Eth
hυ
R
+Carb
D
hυ
+Dib
D
hυ

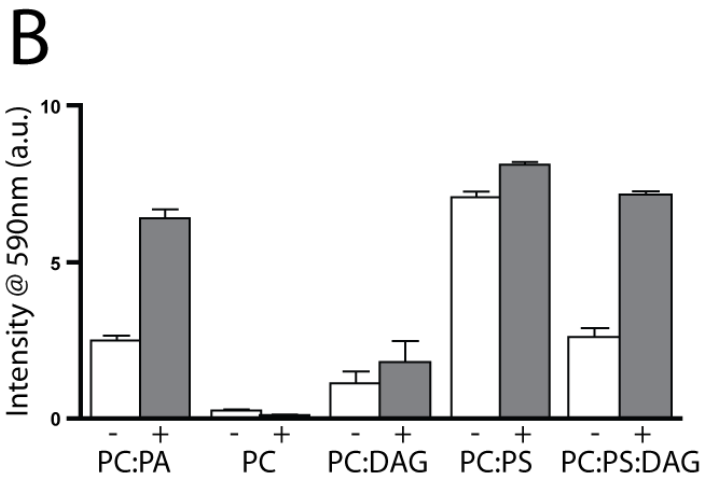
B
Intensity @ 590nm (a.u.)
10
5
0
- +
PC:PA
- +
PC
- +
PC:DAG
- +
PC:PS
- +
PC:PS:DAG

in fluorescence intensity is due to increased ethidium binding to the newly desensitized nAChR. The rapid rate of Carb-induced ethidium binding is likely due to increased accessibility to the ion pore as the nAChR transitions from the resting to the open and then the desensitized states (77). In contrast, DAG alone in a PC membrane is not sufficient to stabilize an agonist-responsive resting nAChR. Although the inclusion of DAG in a PC membrane shifts some receptors into the desensitized conformation, DAG alone is not sufficient to impart on the nAChR a strong ability to undergo agonist-induced conformational transitions.

The effects of DAG on membranes containing anionic lipids, however, are substantial. Membranes composed of PC/PS are relatively ineffective at stabilizing an agonist-responsive nAChR. Consistent with this finding, the addition of PC/PS-nAChR to 0.3 μM ethidium leads to the slow binding of ethidium to a large population of pre-existing desensitized nAChRs (Fig. 2.05A, trace *iv*). Carb has little effect on ethidium fluorescence. PC/PS-nAChR likely stabilizes primarily desensitized and uncoupled conformations (77).

Relative to PC/PS-nAChR, the addition of PC/PS/DAG-nAChR to 0.3 μM ethidium leads to a less intense increase in fluorescence due to ethidium binding to nAChRs pre-existing in the desensitized conformation (Fig. 2.05A, trace v). The addition of DAG therefore decreases the proportion of desensitized nAChRs in a PC/PS membrane. There is also a large and rapid increase in fluorescence upon the addition of Carb. The presence of DAG in a PC/PS membrane thus leads to the stabilization of a large proportion of resting nAChRs that likely undergo both channel gating and desensitization upon Carb-binding.

These simple studies show that the effects of DAG on nAChR function are complex and depend upon the lipid environment surrounding the nAChR. In the presence of PS, DAG

increases substantially the proportion of agonist-responsive nAChRs. Although the levels of DAG studied here are higher than the levels of PA or DAG expected *in vivo*, the effects of DAG on nAChR function observed here are also much larger than required to have a profound influence on synaptic transmission *in vivo*. Even subtle changes in nAChR gating open times in human muscle nAChRs have profound pathological consequences (73). It is possible that even small amounts of DAG, particularly if concentrated in an nAChR-associated raft or on one leaflet of the bilayer, could alter gating kinetics in manner that influence synaptic communication. Further studies are required to fully elucidate the potential effects of DAG on nAChR function *in vivo*.

Finally, it should be noted that the kinetics of ethidium displacement from the nAChR observed here and elsewhere (40) are much faster than those observed upon displacement of ethidium from the nAChR using either the local anesthetic phencyclidine and other cations (28). We also observe much slower ethidium displacement with the local anesthetic, proadifen (data not shown). The displacement of ethidium from the nAChR by dibucaine may thus involve complex mechanisms.

**2.6 - Discussion**

It is well-established that nAChRs influence cellular activity by fluxing ions across the membrane in response to neurotransmitter-binding. Increasing evidence suggests, however, that some nicotinic receptors play additional roles in cellular function not related to the flux of ions (78,79). Homomeric $\alpha$7 nAChRs function in non-excitable cells, such as endothelial cells, keratinocytes, and T cells. (80) Microglial $\alpha$7 nAChRs couple with phospholipase C activation and $Ca^{2+}$ mobilization from $IP_3$-sensitive $Ca^{2+}$ stores leading to the suppression of

neuroinflammation (81). Nicotinic agonists exert anti-inflammatory effects on macrophages that can be countered by α7 nAChR-selective antagonists. Also, α3, α4, and α5 nAChR subunits associate with PI3K in monocytes and macrophages leading to the stimulation of phospholipase C activity (82).

We report here the novel finding that phospholipase C activity co-purifies with "affinity purified nAChR from *Torpedo*. This phospholipase activity is specific for PA over other anionic (PS, PG, PI, and cardiolipin) and zwitterionic (PC) phospholipids. The phospholipase activity is inhibited by sodium vanadate, but not N-ethylmaleimide. The phospholipase activity elutes from an acetylcholine-linked nAChR affinity column with the same profile as the nAChR. SDS-PAGE shows that the eluted fractions contain 4 subunits corresponding to the α, β, γ, and δ subunits of the nAChR. No species corresponding in molecular weight to either cytosolic phosphatidate phosphatases (~100 kDa) or membrane bound lipid phosphate phosphohydrolases (~35 kDa) are observed (86-88)(Figs. 2.01-2.03), although we cannot rule out the existence of trace amounts of these proteins. We therefore conclude that either the nAChR-itself or a protein that closely associates with the nAChR and that binds tightly with the nAChR on the affinity resin exhibits phospholipase C activity.

The finding that either the nAChR itself or a tightly associated protein exhibits phospholipase activity provides further evidence that the nAChR can influence cellular function via mechanisms that do not involve the flux of ions. This phospholipase activity could generate DAG to influence cellular metabolism. The presence of DAG in the lipid micro-environment surrounding the nAChR could also directly influence nAChR function. It is interesting to note that discharge of *Torpedo* electric organ leads to the turnover of PA (90), possibly due to PA hydrolysis to DAG. The possibility that the nAChR can alter its lipid micro-environment in a

manner that influences nAChR function with important biological consequences requires further investigation.

**Acknowledgments**

This work was supported by a grant from the Canadian Institutes of Health Research to JEB. We thank Dr. Martin Pelchat for the use of his fluorescence spectrometer. We also thank Dr.'s David Brindley and Zemin Yao for their insightful comments.

# Chapter 3

## Structural sensitivity of a prokaryotic pentameric ligand-gated ion channel to its membrane environment*

Jonathan M. Labriola[1], Akash Pandhare[2], Michaela Jansen[3], Michael P. Blanton[2], Pierre-Jean Corringer[4], and John E. Baenziger[1]

## 3.1 - Preface

This project comprises the bulk of the work I performed as my time as a Masters student in Dr. John Baenziger's laboratory. The work began while Dr. Baenziger was on sabbatical in Dr. Pierre-Jean Corringer's laboratory (Pasteur-Institut – France) working with the prokaryotic pLGIC GLIC. Dr. Corringer had previously expressed, functionally characterized, and solved the crystal structure of GLIC and thus already had a working knowledge of the protein and materials required to study it.

The long term goal of this project is to use GLIC as a model for studying protein-lipid interactions in the context of pLGICs and to understand the structural and functional consequences of these interactions, as outlined in the introduction. For my part, I began expression and purification of GLIC back in Ottawa in the summer of 2010 using constructs Dr. Baenziger had sent from France, with the ultimate goal of developing an expression and reconstitution protocol along with a preliminary characterization of GLICs lipid sensitivity. These studies ultimately lead to the results presented below which were published in the *Journal of Biological Chemistry*. All experiments in this article were designed by Dr. Baenziger and myself. I conducted all experiments, with the exception of the α-BTX binding experiments (Figure 4B). All the data was analyzed by myself under the tutelage of Dr. Baenziger. I prepared all of the figures and Dr. Baenziger and I wrote the manuscript.

## 3.2 - Abstract

**Although the activity of the nicotinic acetylcholine receptor (nAChR) is exquisitely sensitive to its membrane environment, the underlying mechanisms remain poorly defined. The homologous prokaryotic pentameric ligand gated ion channel, GLIC, represents an excellent model for probing the molecular basis of nAChR sensitivity due to its high structural homology, ease of expression, and amenability to crystallographic analysis. We show here that membrane-reconstituted GLIC exhibits structural and biophysical properties similar to those of the membrane-reconstituted nAChR, although GLIC is substantially more thermally stable. GLIC, however, does not possess the same exquisite lipid sensitivity. In particular, GLIC does not exhibit the same propensity to adopt an uncoupled conformation where agonist binding is uncoupled from channel gating. Structural comparisons provide insight into the chemical features that may predispose the nAChR to the formation of an uncoupled state.**

## 3.3 - Introduction

Cys-loop receptors mediate rapid chemical communication between cells in the nervous system by opening a transmembrane ion channel across the synaptic membrane in response to neurotransmitter binding. Channel opening leads to the flow of either cations or anions down their electrochemical gradient into the cell, resulting in either an excitatory or an inhibitory response, respectively. Cys-loop receptors play a central role in brain function, are implicated in a variety of neurological disorders, and are the targets of both endogenous and exogenous modulators (2,8,91-93).

Early attempts at purifying and reconstituting the prototypic Cys-loop receptor, the *Torpedo* nicotinic acetylcholine receptor (nAChR)[5], in lipid bilayers revealed the importance of

lipids in Cys-loop receptor function (94). In the presence of both cholesterol and anionic lipids, the nAChR is stabilized predominantly in an activatable resting conformation (49,51,75,76). In their absence, the nAChR adopts an "uncoupled" conformation, where agonist binding fails to elicit channel gating (40). Understanding the mechanisms by which lipids influence the coupling of binding and gating remains central to understanding lipid-nAChR interactions. Uncoupled nAChRs may also have broader significance in that neuronal nAChRs that are functionally uncoupled have been observed in heterologous expression systems and may play a role in the physiological response to nicotine (see (95)). Unfortunately, detailed insight into the mechanisms of lipid-dependent uncoupling remains elusive (40,58). A major bottleneck is the inability to reliably express large quantities of Cys-loop receptors with site-directed mutations designed to test potential models of lipid-nAChR interactions.

Several prokaryotic pentameric ligand-gated ion channels (pLGICs) homologous to the eukaryotic Cys-loop receptors have recently been identified, and crystal structures of two of these, GLIC and ELIC, solved at high resolution (26,27,96,97). Prokaryotic pLGICs provide an opportunity for probing the mechanisms of Cys-loop receptor-lipid interactions at a molecular level owing to their high structural homology (Fig. 1.06), their ease of expression in bacterial systems, and their amenability to crystallographic analysis. While a recent study suggested that cholesterol depletion may influence GLIC gating kinetics (98), the broader effects of lipids on prokaryotic pLGIC structure and function remain to be studied. In fact, a reliable protocol for reconstituting prokaryotic pLGICs in membranes at lipid to protein ratios that are amenable to spectroscopic studies, particularly in the context of probing the electrophysiologically silent uncoupled state, has yet to be developed.

Here, we compare the structural and biophysical properties of membrane-reconstituted GLIC to those of its highly lipid-sensitive eukaryotic homolog, the *Torpedo* nAChR. These comparisons were performed in membranes that both support GLIC/nAChR function and those that promote formation of the uncoupled nAChR. Our results suggest that while the gating properties of GLIC are sensitive to its lipid environment, GLIC does not possess the exquisite lipid-sensitivity of its eukaryotic homolog. In particular, GLIC does not exhibit the same propensity to adopt an uncoupled conformation where agonist binding is uncoupled from channel gating. Structural comparisons provide insight into the chemical features that may predispose Cys-loop receptors to the formation of an uncoupled state

**3.4 - Experimental Procedures**

*Materials.* Soybean asolectin (L-α-phosphatidylcholine, type II-S), sodium cholate, carbamylcholine (Carb), and amantadine were from Sigma (St. Louis, MO). *E. coli* polar lipid extracts and 1-palmotyl-2-oleoyl-*sn*-glycero-3-phosphocholine were from Avanti (Alabaster, AL). *Torpedo californica* electroplaque organ was from Aquatic Research Consultants (San Pedro, CA). Dodecylmaltoside (DDM) was from Affymetrix (Santa Clara, CA). [$^{125}$I]-α-Bungarotoxin (107 Ci/mmol) was obtained from PerkinElmer Life Sciences (Boston, MA). Non-radioactive α-Bungarotoxin was from Biotium, Inc (Hayward, CA)

*GLIC expression and purification.* GLIC was expressed in the C43 strain of *E. coli* transformed with a pET-20b(+) vector containing the DNA sequence for the maltose binding protein fused to the N-terminus of GLIC through a thrombin-sensitive peptide linker (96). Briefly, 2 litre cultures of the transformed C43 cells were grown in 2YT media containing 50μg/mL ampicillin at 37˚C to an $OD_{600}$ of ~1.2 a.u, and the cultures induced overnight at 30˚C with 100μM IPTG. Cells were harvested, resuspended in Buffer A (250mM NaCl, 25mM Tris,

pH7.2) in the presence of Roche Complete™ antiprotease tablets (Branford, CT), and lysed with an Avestin Emulsiflex-C5 homogenizer (Ottawa, Canada). Membrane fractions were solubilised in 1% DDM in Buffer A and the GLIC fusion protein bound to an amylose affinity resin. After treatment with plasminogen-free thrombin from Calbiochem (Gibbstown, NJ), GLIC was eluted in 0.02% DDM and further purified on Superpose 6 10/300 gel-filtration column (GE Healthcare; Little Chafont, UK). The highly purified GLIC was passed quickly through 1ml of amylose resin to remove small amounts of an endogenous amylose binding protein that co-elutes with GLIC from the size exclusion column.

*Membrane reconstitution of GLIC.* The purified GLIC in 0.02% DDM in buffer A was slowly diluted at least 1:4 with lipids solubilised in 0.625% cholate in Buffer A to give the desired final lipid-to-protein ratio, in this case 2:1 (w/w) (99,100). After gently mixing for ~30 minutes, the protein/detergent/lipid mixture was dialyzed five times at 4˚C against 2L of Buffer A leading to a turbid solution of proteoliposomes, which were harvested by ultracentrifugation at 100,000g for 2h. The pelleted membranes were re-suspended and layered onto a discontinuous sucrose-density gradient. After ultracentrifugation at 100,000g for 20h in a Beckman SW41 swinging bucket rotor, sequential 400µL aliquots were removed and assayed for both protein (BCA$^{TM}$ assay from Thermo-Pierce; Rockford, IL) and lipid (Phospholipid C/Choline assay from Wako Chemicals; Richmond, VA). Appropriate fractions were pooled and either dialyzed a further 5 times or subjected to several centrifugation resuspension cycles to remove sucrose.

*Reconstituted nAChR membranes.* nAChR purification and reconstitution was performed as described (40,101). The nAChR was solubilised from *Torpedo* electroplaques with 1% sodium cholate and purified on a bromoacetylcholine affinity column in the presence of lipid.

Protein was eluted with 10 mM carbamylcholine (Carb) and then membrane reconstituted by dialysis.

*Fourier transform infrared spectroscopy.* Hydrogen/deuterium infrared spectra (Fig. 3.01a) were recorded on a Digilab (now Agilent Technologies; Santa Clara, CA) FTS40 spectrometer using a Golden-Gate™ attenuated total internal reflection accessory (SpecAc; Oprington, Kent, U.K.). 10 μl of the membrane-reconstituted GLIC (~1 mg/ml) in 2mM phosphate buffer (pH 7.0) were dried down onto the accessory under a gentle stream of $N_2$ gas. After collecting a 64 scan spectrum at 4 $cm^{-1}$ resolution, 10 μl of buffer A in $^2H_2O$ was added and another 64 scan spectrum collected.

For the more detailed amide I band analyses (Fig. 3.01b) and for thermal stability measurements, the membrane reconstituted GLIC was exchanged into 2mM phosphate $^2H_2O$ buffer, pH 7.0 for precisely 72 hours at 4˚C and then stored at -80 $^oC$ until use. Approximately 125μg of GLIC was deposited on a $CaF_2$ window with a gentle stream of $N_2$ gas followed by rehydration with 8μL of Buffer A in $^2H_2O$, pH 7.0. A 4000 scan spectrum was collected at 2 $cm^{-1}$ resolution and 22.5 $^oC$ on a Digilab (now Agilent Technologies; Santa Clara, CA) FTS7000 spectrometer. 128 scan spectra were then acquired at 1˚C intervals from 35 $^oC$ – 90 $^oC$ with a 20 minute equilibration period between each temperature jump.

Spectra were analyzed using GRAMS/AI software (Thermo Scientific; Waltham, MA). Residual water vapor was subtracted using the method of Reid et al (102). Resolution enhancement was performed between 1900 $cm^{-1}$ and 1300 $cm^{-1}$ using a $\gamma = 7$ and a Bessel smoothing function set to 70%. Thermal denaturation was measured as the change in intensity at 1681 $cm^{-1}$ and was evaluated using Graphpad Prism (La Jolla, CA) (40).

*Electrophysiology.* Electrophysiology was performed using a two electrode voltage clamp apparatus (OC-725C oocyte clamp; Holliston, MA) or as described elsewhere (103). Except where noted, oocytes were injected with 100ng of membrane-reconstituted GLIC or nAChR, or 6.6ng of GLIC mRNA and allowed to incubate for 1-2 days at 16˚C in ND96+ buffer (5mM HEPES, 96mM NaCl, 2mM KCl, 1mM $MgCl_2$, 1mM $CaCl_2$, and 2mM Pyruvate). Injected oocytes were placed in a RC-1Z oocyte chamber (Harvard Apparatus; Hamden, CT) containing MES buffer (140mM NaCl, 2.8mM KCl, 2mM $MgCl_2$, and 10mM MES, pH7.0). Currents through the plasma membrane in response to pH jumps were measured with the transmembrane voltage clamped at between -20mV or -60mV. The oocytes chamber was perfused with MES buffer at a rate of ~5mL/min.

*α-Bungarotoxin binding assays.* Individual oocytes were incubated with 2.58 nM [$^{125}$I]-α-bungarotoxin for 2 h at room temperature. Oocytes were washed 3 times with 1 mL of ice-cold buffer containing 1% BSA and then binding was quantified by gamma-counting. Nonspecific binding was determined with oocytes from the same batch incubated with 5 μM non-labeled α-bungarotoxin.

**3.5 - Results**

*Membrane reconstitution of GLIC.* GLIC was reconstituted into membranes at a lipid-to-protein ratio of 2:1 (wt:wt), as this ratio is ideal for spectroscopic studies, such as those used previously to characterize the uncoupled nAChR (see Discussion)(40). To reconstitute into model membranes, DDM-solubilized GLIC (see Supplemental Information, Fig. 3.S01) was diluted below the critical micellar concentration for DDM with a cholate-solubilized lipid

**Figure 3.S01** - Purification and reconstitution of GLIC. (A) The elution profiles of MBP-GLIC (top set of traces) or GLIC (bottom traces) from an SEC column. In both cases, MBP-GLIC was affinity purified on an amylose affinity resin. The MBP-GLIC was eluted using maltose, while GLIC was eluted after cleavage of the MBP-GLIC linker with thrombin. The affinity purified proteins were concentrated and then passed through the SEC column leading to the elution profiles shown in black. In the top set of traces, the red trace ~13 mls corresponds to purified MBP-GLIC, the purple trace at ~15 mls corresponds to an endogenous *E. coli* protein that binds to the amylose resin, and the purple trace at ~17 mls corresponds to MBP. In the bottom set of traces, the red trace at ~15 mls corresponds to purified GLIC. Individual traces are arbitrarily scaled for presentation purposes. (B) SDS PAGE gels of the eluted fractions from the SEC. Top gel *Lane 1*, concentrated MBP-GLIC plus endogenous *E. coli* protein eluted from the amylose affinity resin; *Lane* 2, MBP-GLIC; *Lane 3*, unknown *E. coli* protein; *Lane 4*, MBP. Bottom gel *Lane 1*, purified GLIC. (C) Sucrose density gradient purification of reconstituted aso-GLIC showing complete incorporation of GLIC into the asolectin membranes. The lipid assay measures choline content, and thus underestimates the lipid content of the reconstituted membranes.

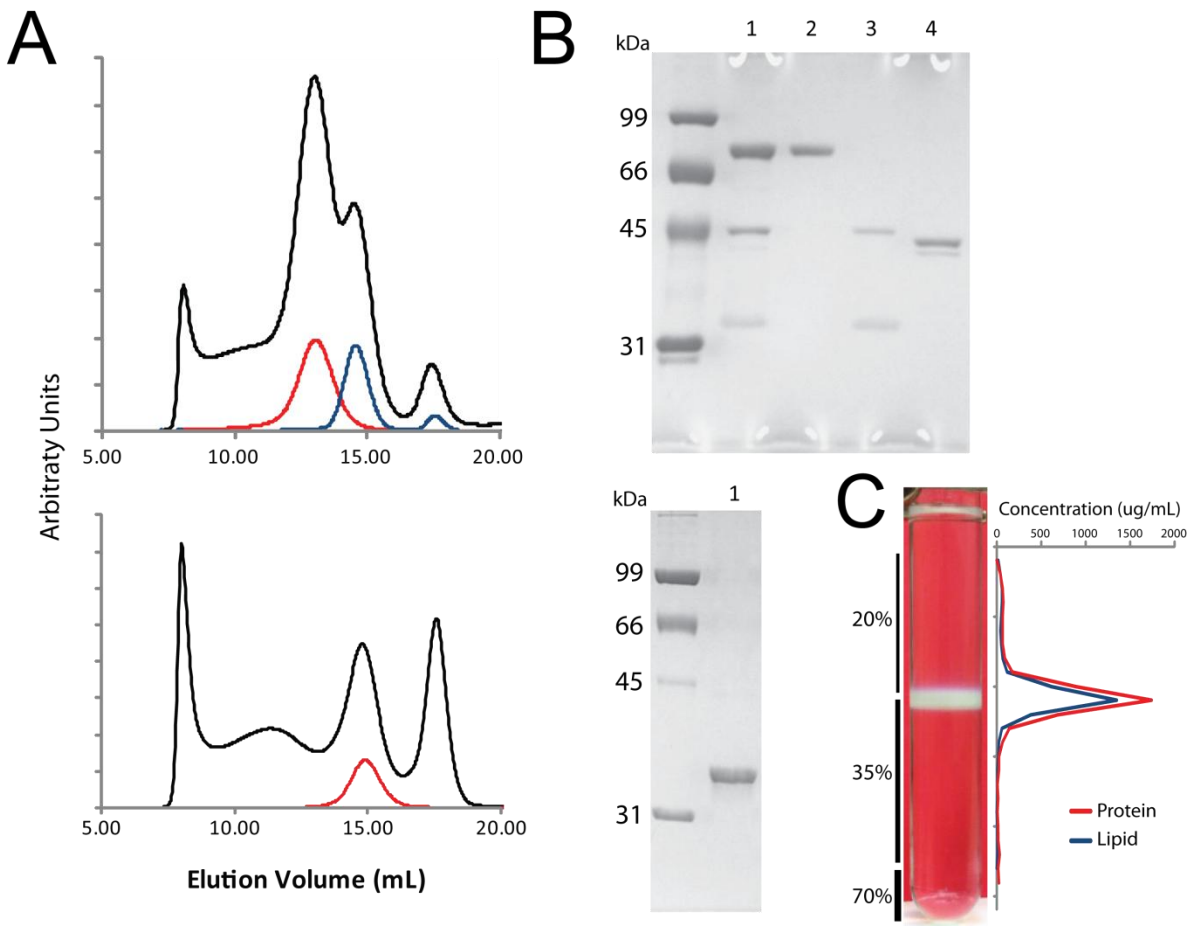
A
Arbitraty Units
5.00
10.00
15.00
20.00
5.00
10.00
15.00
20.00
Elution Volume (mL)
B
kDa
1
2
3
4
99
66
45
31
kDa
1
99
66
45
31
C
Concentration (ug/mL)
0
500
1000
1500
2000
20%
35%
70%
Protein
Lipid

solution, and the protein/detergent/lipid mixture dialyzed extensively to remove residual DDM and cholate. Sucrose density gradients showed that GLIC efficiently incorporates into model membranes. Neither residual DDM nor cholate could be detected in the reconstituted membranes using an infrared based assay for detergent (83). GLIC was initially reconstituted into membranes composed of either asolectin lipids (aso-GLIC) or *E. coli* polar lipid extracts (EcoLip-GLIC). These membranes were chosen because asolectin lipids (as well as defined membranes composed of PC/PA/Chol 3:1:1 (molar ratios)) stabilize the nAChR in a functional resting conformation and minimize GLIC aggregation (98), while *E. coli* polar lipid extracts likely resemble GLIC's natural lipid environment. We expected both membranes to stabilize an activatable "resting" conformation.

*Structure of membrane-reconstituted GLIC.* Infrared spectra of both aso-GLIC and EcoLip-GLIC gently dried from $^{1}H_2O$ buffer (to eliminate the intense overlapping vibrations of bulk water) exhibit two relatively intense protein bands, the amide I band between 1700 and 1600 $cm^{-1}$ and the amide II band centered near 1547 $cm^{-1}$ (Fig. 3.01a). The amide I band is due primarily to peptide backbone C=O stretching and is sensitive to protein secondary structure. The amide II band, due primarily to peptide backbone C-N stretching coupled to N-$^{1}$H bending, is also sensitive to secondary structure, but is used primarily to monitor the exchange of peptide N-$^{1}$H to N-$^{2}$H. The amide II band shifts down in frequency from 1547 $cm^{-1}$ to near 1450 $cm^{-1}$ in $^{2}H_2O$ - the downshifted vibration often referred to as the amide II' band.

The GLIC amide I contour observed in spectra dried from $^{1}H_2O$ exhibits a peak maximum near 1655 $cm^{-1}$, due to the overlapping vibrations of α-helix and loop/random secondary structures, and a prominent broad shoulder between 1640 and 1625 $cm^{-1}$, due

**Figure 3.01 -** Structural comparisons of membrane-reconstituted GLIC and the nAChR as probed by infrared spectroscopy. (A) Infrared spectra of aso-GLIC recorded after gentle drying from $^{1}H_2O$ buffer (solid black line) and immediately after addition of $^{2}H_2O$ (dashed grey line). Note the immediate changes in amide I band shape (1700 – 1600 $cm^{-1}$) and the immediate decrease in amide II band intensity (1547 $cm^{-1}$), both indicative of the rapid peptide N-$^{1}$H/N-$^{2}$H exchange of solvent exposed peptide hydrogens. Similar spectral effects are observed for other Cys-loop receptors (Fig. S02). (B) Infrared spectra recorded after 72 hours equilibration in $^{2}H_2O$ at 4 $^{o}$C from (i) aso-GLIC, (ii) EcoLip-GLIC, (iii) PC-GLIC, (iv) aso-nAChR, and (v) PC-nAChR. The left column shows the secondary structure sensitive amide I band both before (grey traces) and after resolution enhancement (black traces)(intensity scaling arbitrary). The right column shows the amide II band in each spectrum. The relative intensity of the amide II vibration is best assessed relative to the intensity of the adjacent broad peak between 1560 and 1600 $cm^{-1}$, due to aspartic and glutamic acid residues. All presented spectra are the average of several spectra recorded from at least two different purification/reconstitutions.

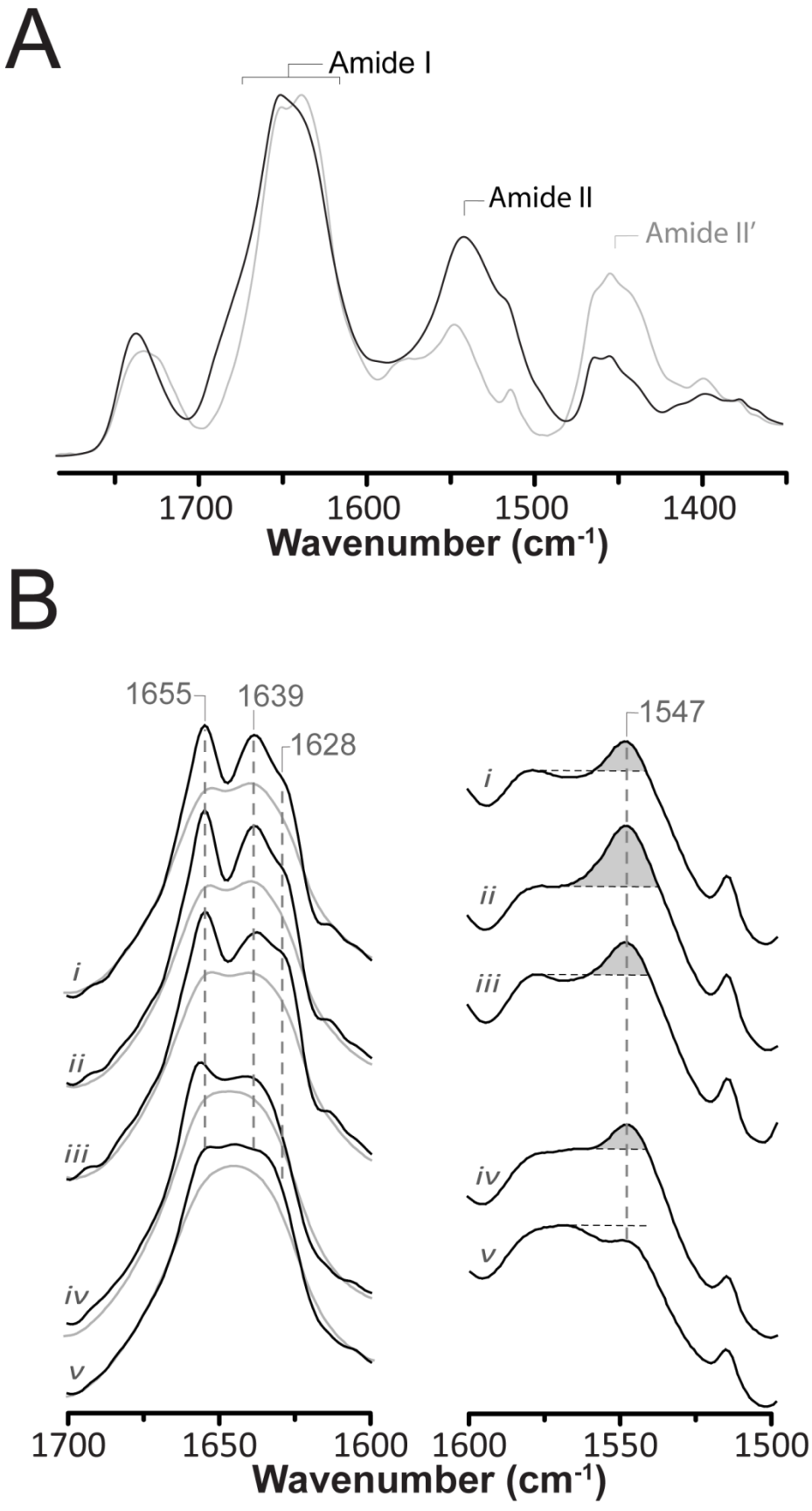
A
Amide I
Amide II
Amide II'
1700
1600
1500
1400
Wavenumber (cm-1)
B
1655
1639
1628
1547
i
ii
iii
iv
v
1700
1650
1600
1600
1550
1500
Wavenumber (cm-1)

primarily to the vibrations of β-sheet. The amide I band shape is similar to that observed for functional membrane-reconstituted *Torpedo* nAChRs (Fig. 3.S02) suggesting a similar mixed α-helix/β-sheet secondary structure. The slightly increased intensity between 1640 and 1620 $cm^{-1}$ indicates a slightly higher β-sheet content in GLIC. The mixed α-helix/β-sheet secondary structure of the reconstituted GLIC was confirmed by recording spectra in $^2H_2O$ buffer, where there is no overlap of the solvent vibrations with the amide I band (Fig. 3.01b). The resulting amide I contour still exhibits features at frequencies characteristic of both α-helix (1655 $cm^{-1}$) and β-sheet (1640-1625 $cm^{-1}$), as shown clearly by resolution enhancement. Curve fitting (Fig. 3.S03) suggests roughly 35% α-helix and 40% β-sheet (Fig. 3.S03), estimates that compare well with the crystal structure (roughly 35% α-helices with >5 residues and 30% β-sheet). The slight overestimate of β-sheet content could reflect difficulties precisely defining the start and end point of each β-strand in the crystal structure. In addition, spectra of the α-helical protein myoglobin (no β-sheet) exhibit weak intensity between 1640 and 1620 $cm^{-1}$ demonstrating that some none β-sheet structures contribute weak amide I intensity to regions of the spectra typically assigned to β-sheet (104).

Note that we recorded spectra both immediately after exposure to (Fig. 3.01a) and after prolonged equilibration with $^2H_2O$ buffer (72 hours, 4 $^oC$) (Fig. 3.01b). Spectra recorded immediately after exposure exhibit changes in band shape that result from the down shifts in frequency of solvent exposed regions of the peptide backbone. Subtle down shifts in the frequencies of amide I component bands due to turn (1700-1670 $cm^{-1}$ region, see supplemental information), loop/random and/or α-helical structures (1655 $cm^{-1}$ down to ~1645 $cm^{-1}$), and β-sheet (primarily 1640 - 1620 $cm^{-1}$ region) are detected (105). These rapid amide I band shifts are accompanied by a drop in amide II band intensity further demonstrating the rapid exchange of

**Figure 3.S02 - Infrared spectra recorded from (A) GLIC, (B) the nAChR, and (C) the α4β2 neuronal nAChR recorded after gentle drying to remove bulk solvent from $^{1}H_2O$ buffer (solid black line) and immediately after addition of $^{2}H_2O$ (dashed grey line).** Note the immediate changes in amide I band shape (1700 – 1600 $cm^{-1}$) and the immediate decrease in amide II band intensity (1547 $cm^{-1}$), both indicative of the rapid peptide N-$^{1}$H/N-$^{2}$H exchange of solvent exposed regions of the polypeptide backbone. (data from daCosta et al. (2011) *Biochem Biophy. Res Commun* **407**, 456-460)

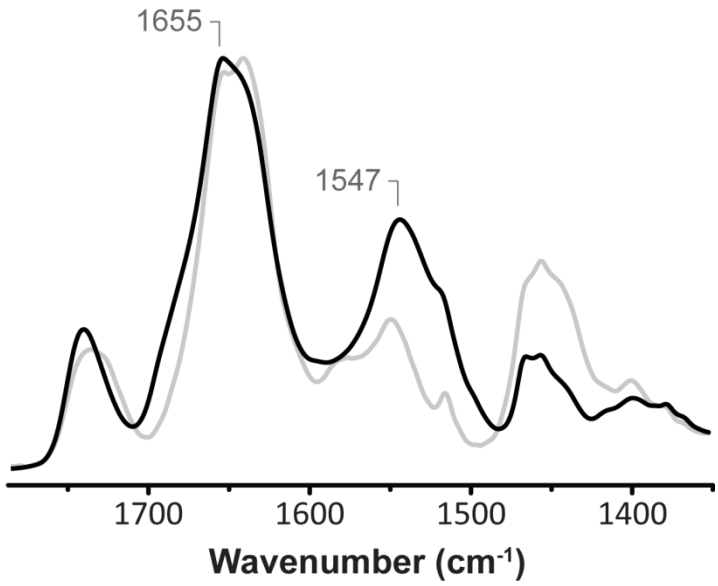
1655
1547
1700
1600
1500
1400
Wavenumber (cm-1)

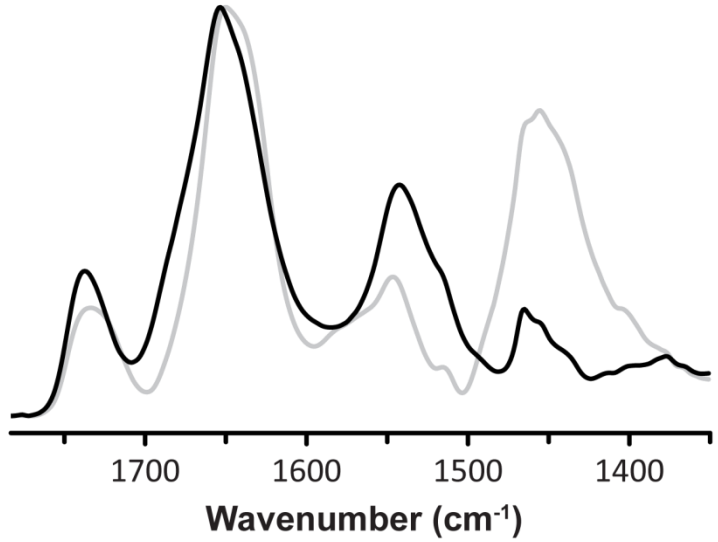
1700
1600
1500
1400
Wavenumber (cm-1)

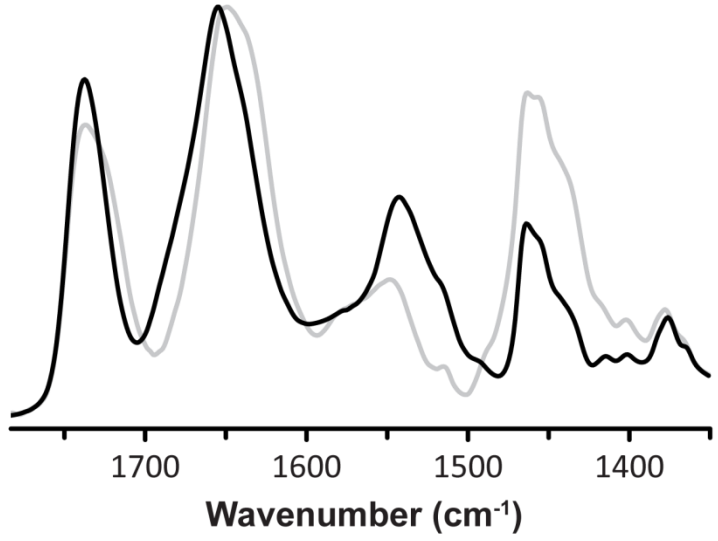
1700
1600
1500
1400
Wavenumber (cm-1)

**Figure 3.S03** - Representative curve fits of the amide I bands from (A) aso-GLIC, (B) EcoLip-GLIC, and (C) PC-GLIC. In each case, the left set of spectra include the experimental amide I absorbance contour (black line), the superimposed curve fit (open circles), and the individual component peaks summed to curve fit amide I contour. The two spectra on the right correspond to the the deconvolved experimental spectrum (top) and the deconvolved curve fit spectrum (bottom). (D) The resulting curve fit estimates and band assignments.

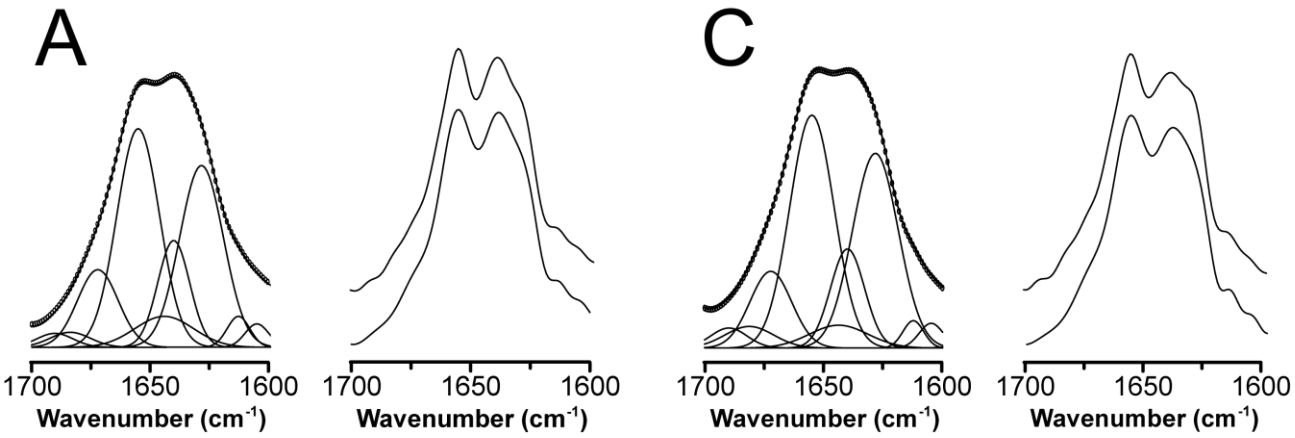


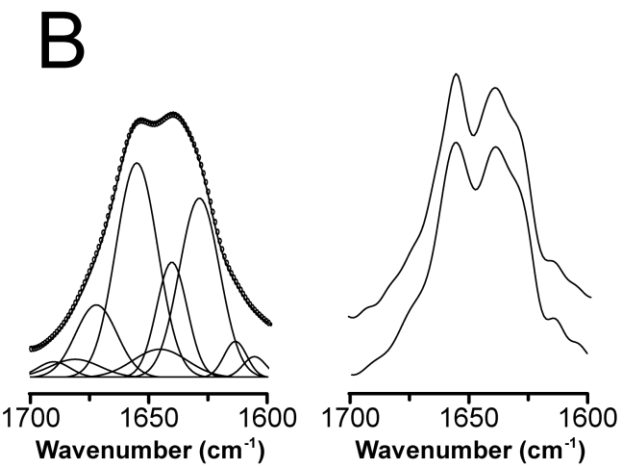


D

GLIC Secondary Structure in reconstituted membranes

| Band frequency ($cm^{-1}$) | Band Assignment[a] | aso-GLIC | *E.coli*-GLIC | PC-GLIC | nAChR[b] |
|---|---|---|---|---|---|
| 1691 | T | 2 | 2 | 2 | 1 |
| 1683 | T | 2 | 4 | 4 | 1 |
| 1676 | T+β | 12 | 12 | 11 | 9 |
| 1656 | α | 35 | 35 | 36 | 37 |
| 1644 | loop/random | 7 | 6 | 4 | 19 |
| 1633 | β | 13 | 13 | 12 | 24 |
| 1624 | β | 29 | 28 | 31 | 9 |

[a] *T = Turn, β = β sheet, α = α helix, loop/random = unstructured peptides likely forming loopa between secondary structures*

[b] *Values from Methot et al.(1994) (1)*

peptide N-$^{1}$H to N-$^{2}$H. The spectral changes are all similar to those observed immediately upon exposure of other Cys-loop receptors to $^{2}H_2O$ (Fig. 3.S02)(106), but differ from those typically observed for proteins with different tertiary folds (105). The results emphasize the existence of a substantial population of solvent exposed secondary structures, consistent with the large solvent exposed extramembranous agonist-binding domain in GLIC (27,97).

One particularly notable feature of the GLIC spectra is that the relatively intense 1655 $cm^{-1}$ amide I component band, which is due to the vibrations of protiated, and thus solvent shielded, α-helical and loop/random structures, is still observed in spectra recorded after prolonged exposure of GLIC to $^{2}H_2O$. This suggests the existence of a large population of exchange-resistant and likely transmembrane α-helices, as has been characterized for the nAChR (104,107). A large population of solvent shielded peptide hydrogens is also suggested by the residual amide II band intensity (Fig. 3.01b). The proportion of exchange-resistant peptide hydrogens in both aso-GLIC and EcoLip-GLIC is slightly higher than in aso-nAChR, although aso-GLIC exchanges to a greater extent than EcoLip-GLIC (see Discussion). The proportion of exchange resistant peptide hydrogens in aso-nAChR was estimated to be ~40%, sufficient to account for the peptide hydrogens located in the transmembrane domain (40,108). The greater proportion of exchange resistant peptide hydrogens in GLIC is likely due to the lack of an intracellular domain - the exchange-resistant transmembrane domain of GLIC makes up a greater proportion of the total protein structure (Fig. 1.06).

The one notable difference between the deconvolved amide I contours of GLIC and the nAChR is the existence in the latter of a more intense band centered near 1645 $cm^{-1}$ due to downshifted and thus peptide N-$^{1}$H to N-$^{2}$H exchanged α-helical and loop/random structures. This band appears immediately after exposure of the nAChR to $^{2}H_2O$ suggesting that the affected

structures are solvent exposed (107). Solvent exposed α-helical and loop/random structures exist in the intracellular domain of the nAChR. The lack of a similarly intense band centered near 1645 $cm^{-1}$ in the GLIC spectra is consistent with the absence of an intracellular domain in GLIC.

Finally, the thermal stabilities of both aso-GLIC and EcoLip-GLIC were examined by recording infrared spectra as a function of temperature. In both cases, increasing temperature led to changes in amide I band shape characteristic of protein denaturation (Fig. 3.S04), confirming that the reconstituted GLIC adopts a folded structure. It is noteworthy that the previously "exchange-resistant-peptide hydrogens" in the transmembrane domain of GLIC undergoes complete N-$^{1}$H to N-$^{2}$H exchange concomitant with unfolding. This behavior is similar to that observed for the nAChR, but differs from that of proteins, such as LacY, which undergoes complete N-$^{1}$H to N-$^{2}$H exchange at elevated temperatures, but prior to unfolding (100). The latter property of LacY has been attributed to a temperature induced increase in the conformational dynamics of the transmembrane domain, whereas as the transmembrane domain of GLIC may be conformationally "static" in the absence of bound agonist. The transmembrane domain of GLIC is also not expected to undergo such large conformational transitions (27,97,109). Both aso-GLIC and EcoLip-GLIC have higher thermal stabilities of 68.8±1.5 and 73.7±1.4 $^{o}$C, respectively, than that of the nAChR ~55 $^{o}$C (Fig. 3.03, Table 3.1). The higher thermal stability of GLIC is consistent with its enhanced suitability for crystallization (110).

*Gating properties of the membrane-reconstituted GLIC.* Although reconstituted membranes at a lipid-to-protein ratio of 2:1 (wt:wt) are ideal for spectroscopic studies, they are not useful for direct measurements of channel activity using electrophysiological approaches. Instead, we indirectly probed the activity of membrane-reconstituted GLIC by injecting the reconstituted GLIC membranes into *Xenopus laevis* oocytes and then monitoring the appearance

**Figure 3.S04** - Stacked plot of spectra collected for thermal stability characterization of (A) aso-GLIC and (B) aso-nAChR. Representative traces are shown from 35 $^{o}$C to 85 $^{o}$C, front to back. Spectra were collected at 1˚C increments.

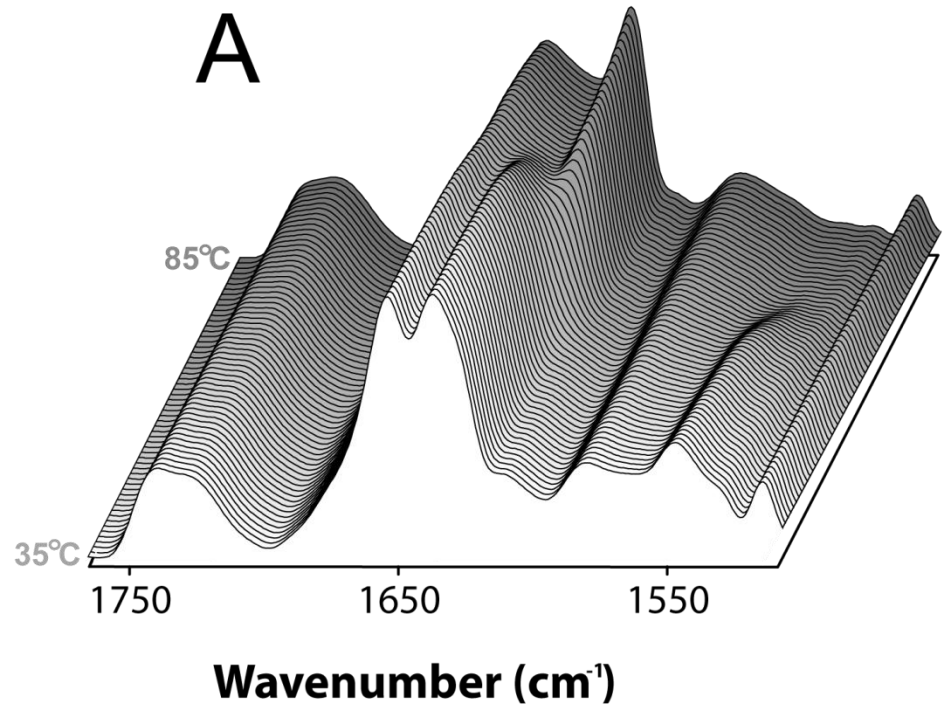
A
85℃
35℃
1750
1650
1550
Wavenumber (cm-1)

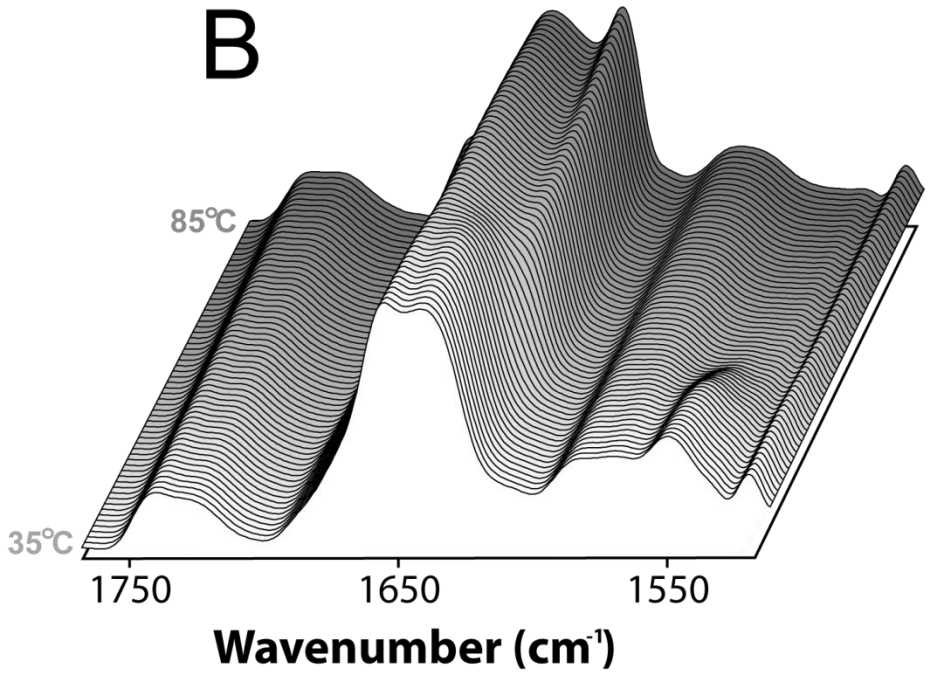
B
85℃
35℃
1750
1650
1550
Wavenumber (cm-1)

**Figure 3.02** - Representative thermal denaturation curves for GLIC (black lines) and the nAChR (grey lines) in different membranes. Denaturation curves are for aso-GLIC (▲), EcoLip-GLIC (●), PC-GLIC (□), aso-nAChR (△), PC/PA/Chol-nAChR (♦), and PC-nAChR (■). Each curve was fit with a Boltzmann sigmoid from which $T_d$ and Boltzmann slope were calculated using GraphPad Prism software (Table 1)(see supplemental information of (40)). The Boltzmann slope decreases with increasing cooperativity of unfolding.

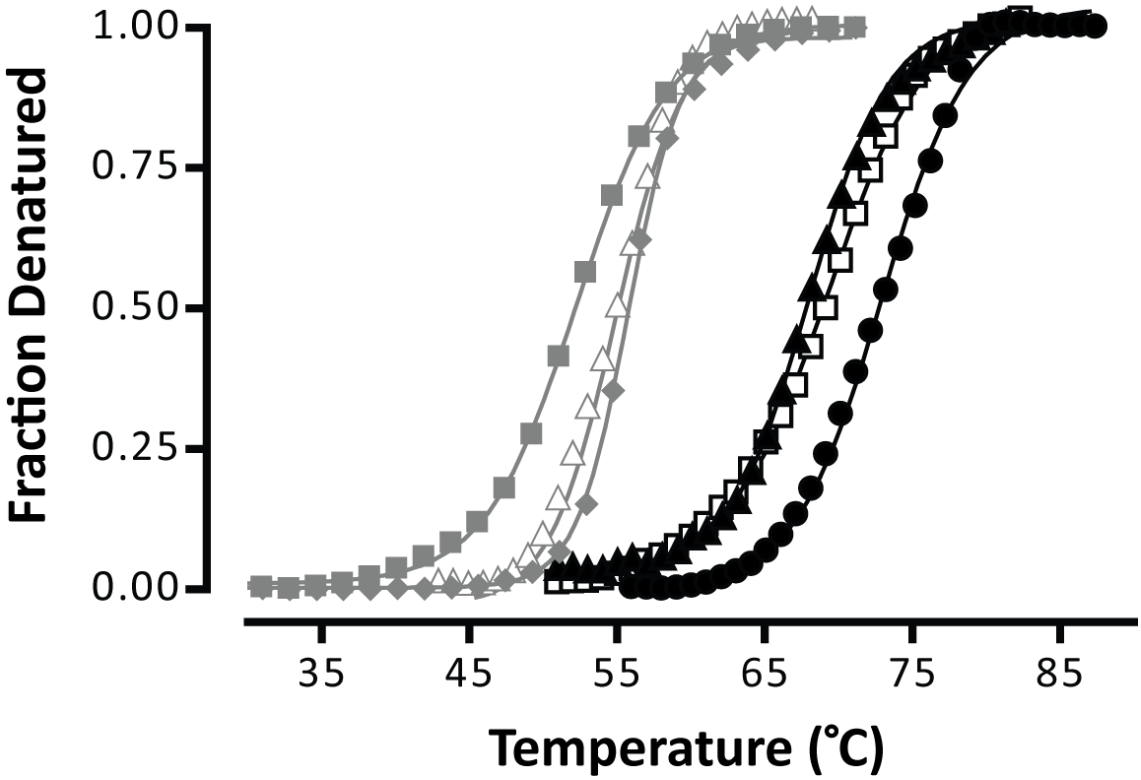
Fraction Denatured
1.00
0.75
0.50
0.25
0.00
35
45
55
65
75
85
Temperature (˚C)

Table 3.1
Thermal stability of GLIC

| Reconstitution | $T_d$ (˚C) | Hill Slope | *N* |
|---|---|---|---|
| aso-GLIC | 68.8±1.5 | 2.44±0.16 | 5 |
| EcoLip-GLIC | 73.7±1.4 | 1.98±0.22 | 5 |
| PC-GLIC | 70.4±0.9 | 2.35±0.20 | 4 |
| aso-nAChR | 55.4±1.0 | 2.25±0.01 | 2 |
| PC/PA/Chol-nAChR[a,b] | 56.4±0.8 | 2.08±0.20 | 6 |
| PC-nAChR[b] | 52.4±0.1 | 3.08±0.12 | 6 |

[a] *the nAChR in membranes composed of PC, phosphatidic acid, and cholesterol*
[b] *from daCosta & Baenziger (40)*

of proton activated currents across the oocyte plasma membranes using a two electrode voltage clamp apparatus (103,111).

The feasibility of the oocyte injection approach for examining the activity of membrane reconstituted pLGICs was first tested using reconstituted nAChR membranes of defined function. Carb-induced currents that decay slowly due to desensitization are observed in oocytes injected with either aso-nAChR or phosphatidyl choline/phosphatidic acid/cholesterol-nAChR (PC/PA/Chol-nAChR) showing that the functional reconstituted nAChR membranes fuse with the oocyte plasma membrane leading to the appearance of functional nAChRs on the oocyte surface (16 fmol 16 fmol binding sites/oocyte, with 0.124 ± 0.061 μA/fmol [$^{125}$I]-α-bungarotoxin binding sites/oocyte; Fig. 3.03). In contrast, weak or negligible Carb-induced currents were observed in oocytes injected with the uncoupled and non-activatable PC-nAChR, even though the reconstituted PC membranes fuse with the plasma membrane leading to the appearance of nAChR agonist sites on the surface of the oocyte (5.5 fmol [$^{125}$I]-α-bungarotoxin binding sites/oocyte, with 0.0034 ± 0.0006 μA current per fmol binding sites/oocyte; Fig. 3.03). The lack of activity of the plasma membrane incorporated PC-nAChR (~40-fold reduction in normalized current levels compared to the injected PC/PA/Chol-nAChRs) has several possible explanations. First, the lack of activity could reflect clustering of the reconstituted membranes within the oocyte plasma membrane and thus the nAChR retaining its "reconstituted membrane" lipid environment. Such clustering of the nAChR on the oocyte surface has been suggested from previous studies of oocytes injected with reconstituted nAChR membranes (111). PC-nAChR may also be locked in an uncoupled conformation because the oocyte plasma membrane lipids

**Figure 3.03** - The Carb-induced response of membrane-reconstituted nAChR after injection into and consequent fusion with the plasma membrane of *Xenopus* oocytes. (A) Currents induced by 500 μM Carb were measured at -20 mV holding potential from oocytes injected with aso-nAChR (left trace) and PC-nAChR (right trace). (B) A bar graph comparing maximal recorded currents, each normalized to the number of [$^{125}$I]-α-Bungarotoxin (BTX) binding sites, induced by 300 μM acetylcholine from individual oocytes microinjected with 125 ng of affinity-purified *Torpedo* nAChR protein reconstituted in either PC/PA/CH (3:1:1 molar ratio; 0.124 ± 0.061 μA/[$^{125}$I]-α-Bungarotoxin binding sites/oocyte; n= 5) or PC lipid vesicles (0.0034 ± 0.0006 μA/[$^{125}$I]-α-Bungarotoxin binding sites/oocyte; *n*= 6).

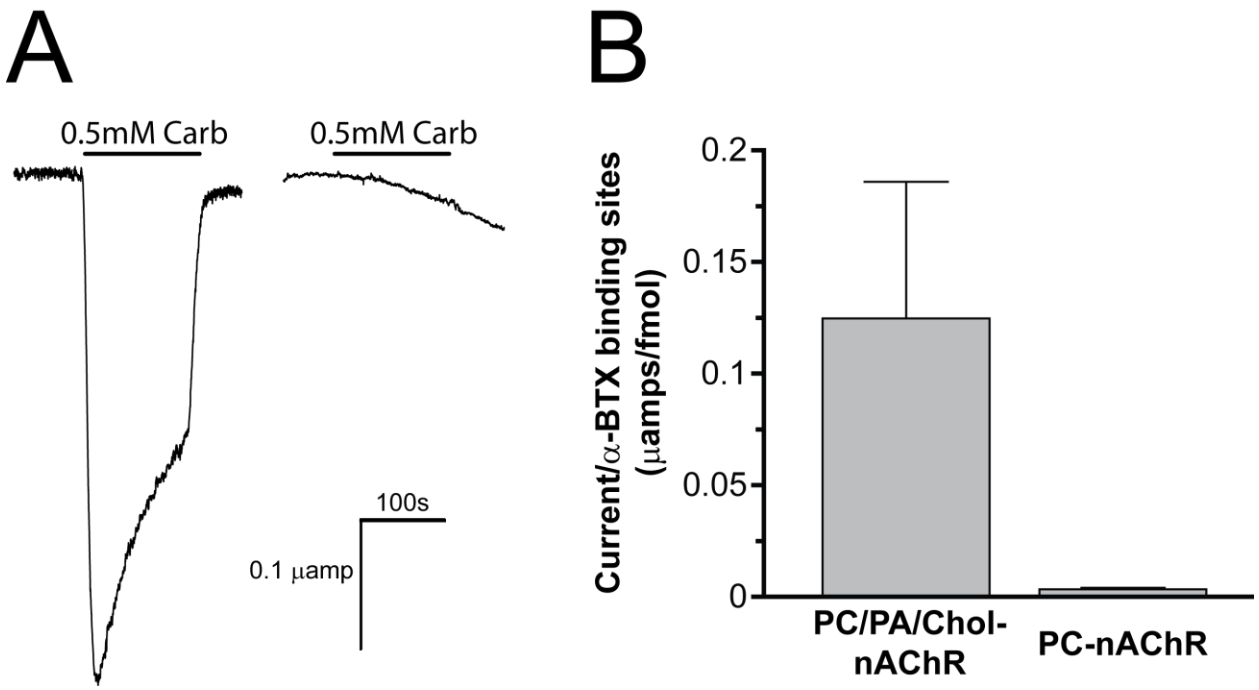
A
0.5mM Carb
0.5mM Carb
100s
0.1 μamp
B
Current/α-BTX binding sites
(μamps/fmol)
0.2
0.15
0.1
0.05
0
PC/PA/Chol-
nAChR
PC-nAChR

do not promote transitions from uncoupled to coupled conformations. Recent studies suggest that the uncoupled nAChR in long chain PC membranes can undergo ligand-induced transitions to coupled conformations (data not shown). Finally, it is possible that detergent solubilization leads to irreversible effects on nAChR structure and function. The latter seems unlikely, however, given that detergent solubilization has no deleterious effects on the nAChR reconstituted into other membranes. In addition, no detectable effects of detergent solubilization and PC reconstitution are observed on nAChR secondary structure. Regardless, these control experiments confirm that the injection of reconstituted nAChR membranes into oocytes can, in principle, be used to indirectly assess the gating activity of reconstituted nAChRs.

We next characterized the response of uninjected, mock injected (membranes alone), and GLIC mRNA injected oocytes to jumps in proton concentration. Both uninjected and mock injected oocytes exhibit weak proton-activated currents due to endogenous acid-sensitive channels (Fig. 3.04). These currents, however, show a roughly linear response to proton concentration at pH values down to 3.5, are insensitive to the GLIC pore-blocker, amantadine, and had maximal currents of 0.069±0.016 μA (n=4) and 0.063±0.021 μA (n=6), respectively, at the maximal utilized proton concentration (pH 3.5). In contrast, oocytes injected with GLIC RNA exhibit robust proton-activated cationic currents (Fig. 3.S04) with relatively large maximal currents typically close to 4 μA. A plot of whole cell currents versus proton concentration for the latter yielded a $pH_{50}$ for activation of 4.82±0.04 (Fig. 3.S04b), consistent with that observed previously for oocyte-expressed GLIC (96). These proton activated currents are sensitive to the pore blocker, amantadine. 150 μM amantadine blocked close to ~50% of the pH activated currents. Oocytes injected with either aso-GLIC or EcoLip-GLIC both exhibit currents that

**Figure 3.04 -** The proton-induced response of membrane-reconstituted GLIC after injection into and consequent fusion with the plasma membrane of *Xenopus* oocytes. (A) Electrophysiology recordings in response to pH jumps from (i) uninjected oocytes and oocytes injected with (ii) aso-GLIC, (iii) EcoLip-GLIC, and (iv) PC-GLIC. The dose-response curves were measured at a relatively low membrane potential of -20 mV, as this seemed to generate more stable baselines. An electrical response to pH 4.0 showing the effect of 150µM amantadine (grey bar) is shown on the right (scaling arbitrary). The latter were performed at a membrane potential of -60 mV. (B) Peak current achieved upon exposure of oocytes injected with the indicated reconstituted membranes at pH 3.5. Reported values are the average±standard deviation from 5 recordings performed on 5 difference oocytes. (C) Comparison of the dose-response curves obtained from oocytes injected with the membrane-reconstituted GLIC or GLIC mRNA. The dose-response curves from oocytes injected with membrane-reconstituted GLIC were normalized assuming a $pH_{50}$ of 2.90 according to Vilissetty *et al.*(69).

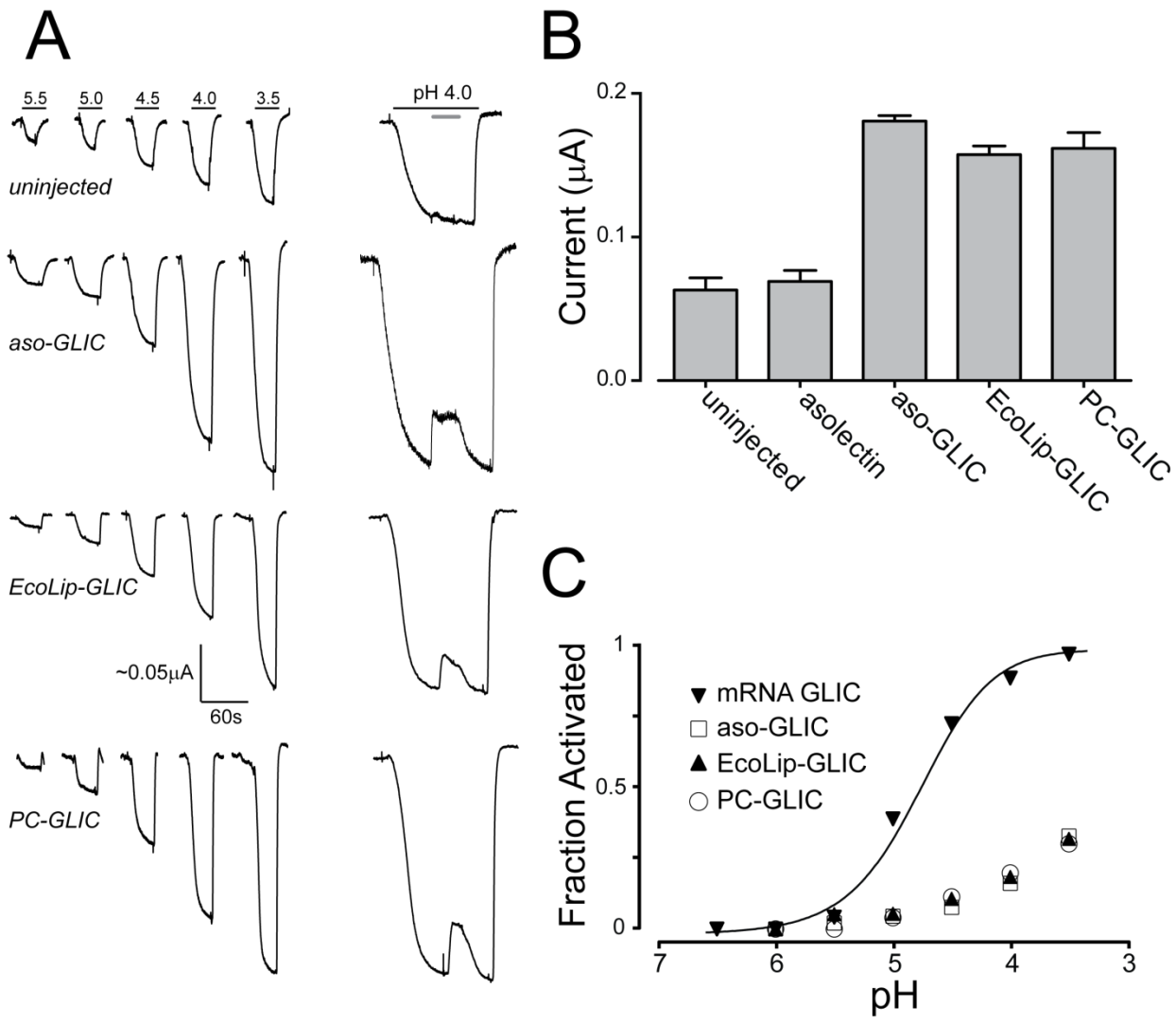
A
5.5
5.0
4.5
4.0
3.5
pH 4.0
uninjected
aso-GLIC
EcoLip-GLIC
~0.05μA
60s
PC-GLIC
B
Current (μA)
0.2
0.1
0.0
uninjected
asolectin
aso-GLIC
EcoLip-GLIC
PC-GLIC
C
Fraction Activated
1
0.5
0
mRNA GLIC
aso-GLIC
EcoLip-GLIC
PC-GLIC
7
6
5
4
3
pH

**Figure 3.S05 -** Current traces of mRNA-GLIC injected oocyted probed by two-electrode voltage clamp. (A) Currents induced by exposure to the pH jumps indicated by the horizontal bars. Cells were held at a membrane potential of -20 mV. (B) mRNA-GLIC injected oocytes were held at a membrane potential of -60mV and exposed to pH 4.0 until steady state was achieved, after which 150μM amantadine (pH 4.0) was introduced into cell profusion chamber (red bar) followed by washout.

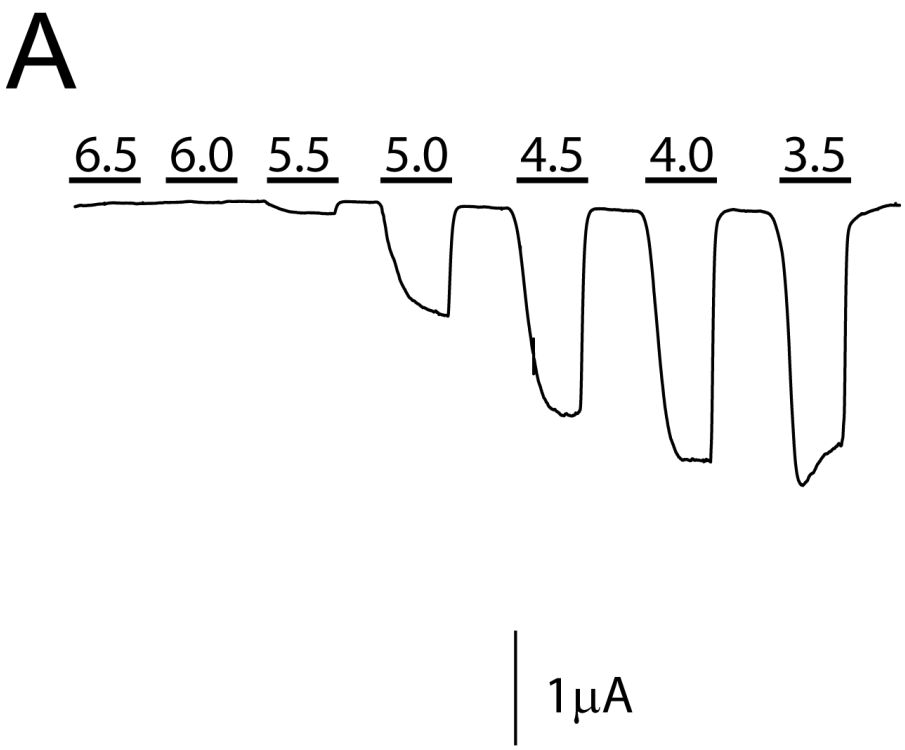
A
6.5
6.0
5.5
5.0
4.5
4.0
3.5
1μA

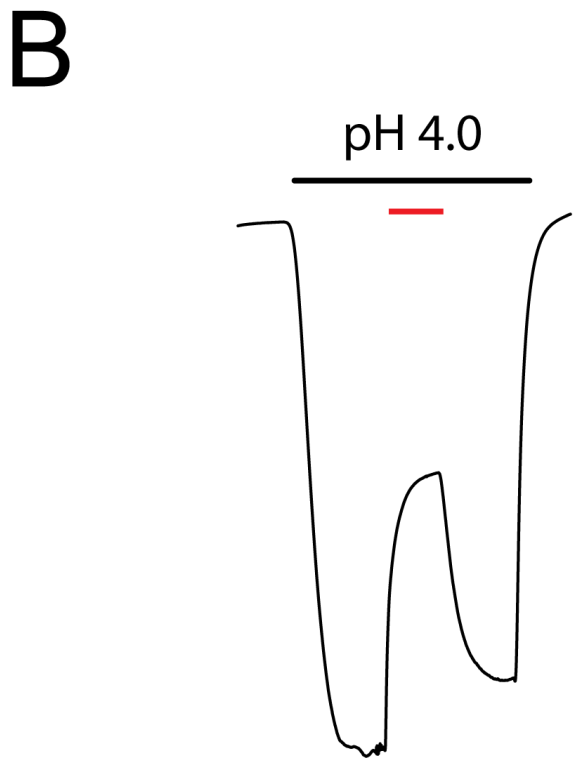
B
pH 4.0

respond to proton concentration in a dose-dependent manner. The maximal responses at pH 3.5 of 0.181±0.008 μA (n=5) and 0.157±0.014 μA (n=5), respectively, are roughly 3-fold larger than the responses observed in mock or uninjected oocytes, yet consistent in magnitude to the Carb-induced currents observed in aso-nAChR injected oocytes. Of particular significance, these proton-induced currents were sensitive to the GLIC channel blocker, amantadine, while the endogenous acid sensitive channels in oocytes are not. These data suggest that the reconstituted GLIC in both membranes retains the ability to gate open in response to proton binding. Interestingly, the proton concentration dependence of GLIC activation is right-shifted relative to the dose response observed with mRNA-injected oocytes, suggesting weaker proton sensitivity. A weaker proton sensitivity has also been observed for GLIC reconstituted into giant unilamellar asolectin liposomes at the high lipid-to-protein ratios required for electrophysiological studies (98). The right shifted dose response supports the possibility that GLIC also clusters within the oocytes plasma membrane thus maintaining its reconstituted lipid environment. The shifted dose response suggests that the gating activity of GLIC is sensitive to its membrane environment.

*Effects of an uncoupling lipid environment on GLIC structure and function.* We next compared the structural and functional properties of aso-GLIC and EcoLip-GLIC to that of GLIC reconstituted into PC membranes (PC-GLIC). The minimal PC environment is of interest because it stabilizes the nAChR in an uncoupled conformation that binds agonist, but does not undergo agonist-induced conformational transitions. A key goal of this work was to ascertain whether GLIC exhibits the same propensity to uncouple as the nAChR in a PC bilayer.

The uncoupled PC-nAChR exhibits biophysical properties that distinguish it from the predominantly resting state aso-nAChR (Figs 3.01 and 3.02). The secondary structure sensitive amide I contour in spectra recorded from PC-nAChR are similar to that of aso-nAChR, but

deconvolution reveals a downshift in amide I component band intensity from 1655 $cm^{-1}$ to near 1645 $cm^{-1}$. This change in amide I band shape occurs as a result of enhanced levels of peptide N-$^{1}$H/N-$^{2}$H exchange in the uncoupled state, as opposed to a change in the global secondary structure. The enhanced peptide N-$^{1}$H/N-$^{2}$H exchange is shown by the reduced residual amide II band intensity in spectra recorded from PC-nAChR versus aso-nAChR. The absence of a change in secondary structure is shown by comparing the amide I bands of PC-nAChR and aso-nAChR at equivalent levels of peptide N-$^{1}$H/N-$^{2}$H exchange (but different exposure times to $^{2}H_2O$). In the latter case, no significant differences in amide I contour were observed (112).

A more detailed analysis of the peptide N-$^{1}$H/N-$^{2}$H exchange kinetics of uncoupled versus resting or desensitized nAChRs shows that regions of the polypeptide backbone that are buried from solvent in the resting conformation become exposed to solvent in the uncoupled state (40). The uncoupled PC-nAChR also undergoes thermal denaturation at temperatures slightly lower than aso-nAChR, and the cooperativity of denaturation is reduced (40). These altered biophysical properties of PC-nAChR have been attributed to weakened interactions leading to an increased physical separation between the agonist-binding and transmembrane domains (40). Weakened interactions could account for the increased solvent exposure, the reduced cooperativity of unfolding, and the lack of coupling of binding and gating (Fig. 3.S06).

Significantly, we detect little if any structural or biophysical difference between PC-GLIC and either aso-GLIC or EcoLip-GLIC (Figs. 3.01 and 3.02). The amide I band shapes of GLIC in all three membranes are similar suggesting a similar global secondary structure (see, however, below). There is no further shift in amide I component band intensity from 1655 $cm^{-1}$ down to near 1645 $cm^{-1}$ after prolonged exposure of PC-GLIC to $^{2}H_2O$. There are no changes in the levels of peptide N-$^{1}$H/N-$^{2}$H exchange, as shown by the similar residual amide II band

**Figure 3.S06** - The M4 lipid-sensor model of uncoupling. The model proposes that interactions between the C-terminus of M4 (orange) forms critical interactions with the Cys-loop (green) of the agonist binding domain. When optimal interactions occur, the Cys-loop adopts a conformation that allows tight interactions with the M2-M3 linker. These tight interactions are essential for coupling binding to gating. In unfavorable lipid environments, the interactions between M4 and the Cys-loop are not optimatal. This leads to an altered conformation of the Cys-loop and weakened interactions between the Cys-loop and M2-M3 linker. Weakened interactions leads to a physical separation between the agonist-binding and transmembrane domains and thus the uncoupling of binding and gating. (daCosta & Baenziger (2009) *J Biol Chem* **284**, 17819-17825)

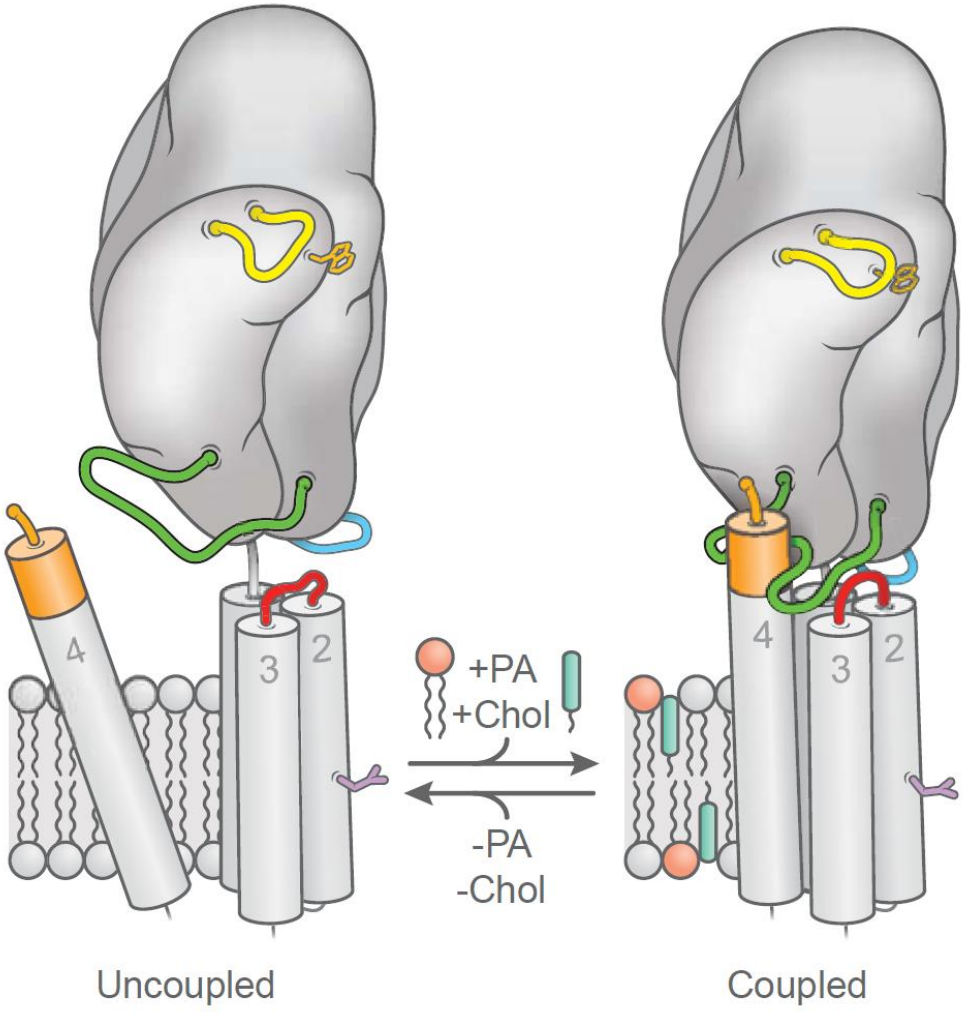
4
3
2
+PA
+Chol
-PA
-Chol
4
3
2
Uncoupled
Coupled

intensities, although both aso-GLIC and PC-GLIC are more exchanged than EcoLip-GLIC. The thermal denaturation temperature of PC-GLIC is also similar to that of both aso-GLIC and EcoLip-GLIC and there are no changes in the cooperativity of unfolding (Table 3.1).

In fact, the only substantial difference observed between spectra recorded from PC-GLIC and either aso-GLIC or EcoLip-GLIC is a slight broadening of the amide I contour, noticeable near 1630 $cm^{-1}$. The degree of this subtle broadening, however, varied between PC-GLIC purifications and reconstitutions. Although the structural basis of this spectral effect remains to be determined, it could reflect variations in GLIC aggregation within the membrane. Previous studies have suggested that the monodispersity of the pentameric GLIC within the membrane is lipid sensitive (98). Monodispersity was found to be ideal in asolectin bilayers. GLIC may tend to aggregate more in PC than in other lipid environments leading to broadening of the amide I band. Regardless, our structural data suggest that GLIC does not adopt an uncoupled conformation in PC membranes similar to that adopted by PC-nAChR.

Finally, we indirectly assessed whether PC-GLIC exhibits the ability to gate open in response to proton binding (Fig. 3.04). As noted, very weak or negligible Carb-induced current are observed in oocytes injected with PC-nAChR even though PC-nAChR fuses with the oocyte plasma membrane. In contrast, oocytes injected with PC-GLIC exhibit currents that both respond to protons in a dose-dependent manner and that are sensitive to amantadine block. The maximal currents obtained upon injection of PC-GLIC are substantially higher than those in mock or uninjected oocytes, and are indistinguishable from those observed in oocytes injected with either aso-GLIC or EcoLip-GLIC. The pH activated currents are also sensitive to amantadine. The electrophysiological recordings suggest that GLIC does not adopt a conformation in PC membranes similar to the uncoupled conformation adopted by the nAChR.

Even the minimal PC membrane environment appears sufficient to stabilize GLIC in a conformation that gates open in response to agonist binding.

### 3.6 - Discussion

The underlying mechanisms by which lipids modulate nAChR function have been the subject of continuous debate for over 30 years (94). There has long been a consensus that both cholesterol and anionic lipids are required in a reconstituted membrane to obtain optimal nAChR function (48-51,75,76,113). It has also been suggested that both lipids influence nAChR function by an allosteric mechanism, whereby lipids alter the functional response to acetylcholine by stabilizing differing proportions of pre-existing resting (activatable) versus desensitized or uncoupled (inactivatable) conformations (75,108). The mechanisms by which these lipids influence function, however, are not clear. It has been suggested that some act by binding to interstitial sites between different α-helices in the transmembrane domain (57,58). Lipids may also interact directly with the lipid-protein interface (40,56,57,114). While the consensus is that lipid chemistry and thus specific lipid sites are likely important, both molecular details and direct experimental evidence for any mechanism of lipid action has yet to be obtained. The lack of mechanistic insight reflects both the complexity of lipid-nAChR interactions and the inability to express site directed mutants of the nAChR, which can be used to test proposed mechanisms of lipid-protein interactions.

Prokaryotic pLGICs provide a new opportunity for probing the molecular details of pLGIC-lipid interactions (3,96). The prokaryotic pLGIC, GLIC, adopts a similar tertiary fold to that of the nAChR. Both GLIC and the nAChR are cation-selective ion channels, although GLIC is gated by protons while the nAChR is gated by acetylcholine. The structural similarities of GLIC and the nAChR, as well as the added advantage that GLIC can be expressed in sufficient

studies for biophysical and crystallographic studies has led the increasing use of GLIC as a model for probing pLGIC structure (26,27,97), basic mechanisms of pLGIC activation (26,27,97), pLGIC-drug interactions (67,115), etc. The ability to express large quantities of site-directed mutants finally opens the door for detailed mechanistic studies lipid-GLIC interactions. Such studies, however, first require a detailed characterization of the effects of lipids on GLIC structure and function.

We report here a simple protocol for reconstituting the prokaryotic pLGIC, GLIC, into defined lipid membranes. Our protocol differs from the standard vesicle detergent-destabilization approach typically used to form high lipid-to-protein ratio membranes for electro-physiological studies (98). One advantage of our approach is the high efficiency incorporation of GLIC into the model membranes (Fig. 3.S01). It is thus easy to accurately adjust the lipid-to-protein ratio of the reconstituted membranes. In addition, this protocol can be used to form relatively low lipid-to-protein ratio proteoliposomes.

Our goal was to reconstitute GLIC into membranes at lipid-to-protein ratios of roughly 2:1 (wt:wt) as the resulting vesicles are ideal for structural studies, such as those used previously to characterize the uncoupled nAChR. These low lipid-to-protein ratio vesicles can be easily separated from both protein-free vesicles and low lipid-protein ratio protein aggregates (see Fig. 3.S01). They are ideal for spectroscopic studies because the scattering of light from the membrane vesicles (per mol of reconstituted protein) is minimized and the spectral overlap between signals from lipid and protein is less of an issue. The higher density low lipid-to-protein ratio proteoliposomes are easier to pellet (particularly in higher density $^{2}H_2O$ buffers) and thus exchange into $^{2}H_20$. Low lipid-to-protein ratio vesicles are also ideal for structural studies using infrared *difference* spectroscopy, a technique that detects residue-specific changes in structure of

the nAChR upon agonist-binding (106,116,117). Application of this approach to prokaryotic pLGICs would be particularly informative given the ability to express mutants and thus assign detected vibrational changes to specific amino acid side chains.

Membrane-reconstituted GLIC and the nAChR exhibit similar structural and biophysical properties. Both proteins exhibit a mixed α-helix/β-sheet secondary structure with both a substantial proportion of the polypeptide backbone exposed to aqueous solvent and a large proportion of α-helical peptides shielded from solvent and likely found in the transmembrane channel pore domain. GLIC exhibits a higher β-sheet content than the nAChR, as expected given that the predominantly β-sheet agonist binding domain in GLIC makes up a larger proportion of the total protein structure (see below). The membrane reconstituted GLIC also undergoes thermal denaturation, albeit at higher temperatures than the nAChR. These observations show that the reconstituted GLIC maintains the expected structural fold.

On the other hand, infrared spectroscopy detects a relatively intense vibration near 1645 $cm^{-1}$ in spectra of the nAChR due to solvent exposed α-helix and/or loop/random secondary structures. This vibration could reflect primarily the solvent exposed α-helix and loop/random secondary structures found in the intracellular domain of the nAChR (Fig. 3.01). The lack of similar intensity in this region in spectra of GLIC is consistent with the lack of an intracellular domain in the GLIC crystal structure.

We used an indirect electrophysiological approach to probe the ability of the reconstituted GLIC to gate open in response to agonist binding. Injection of membrane-reconstituted GLIC into oocytes led to the appearance of proton activated currents across the oocyte plasma membrane. The oocyte membrane incorporated GLIC responds in a dose-dependent manner to protons and the resulting currents were blocked by the GLIC channel

blocker, amantadine. Both our structural and electrophysiological studies thus suggest that the reconstituted GLIC adopts a native structure that gates open in response to agonist binding.

A major goal of this work was to compare the lipid sensitivies of both GLIC and the nAChR. In particular, the nAChR in complex natural lipid membranes, such as those composed of either soybean asolectin lipids or mixtures of defined lipids (PC plus cholesterol and anionic lipids), adopts an activatable resting conformation. In contrast, the nAChR in PC membranes lacking the two "activating lipids" adopts an uncoupled conformation that binds agonist with a resting-state like affinity, but does not typically undergo agonist-induced conformational transitions. We are interested in the uncoupled nAChR because of increasing anecdotal evidence hinting that functionally uncoupled nAChRs may play a role in nicotinic receptor physiology (95). A main goal of this work was to assess whether GLIC exhibits propensity similar to that of the nAChR to adopt an uncoupled conformation in PC bilayers.

Although our data show that GLIC activity is sensitive to lipids (see below), PC-GLIC does not exhibit the structural or functional characteristic of the uncoupled conformation adopted by PC-nAChR. PC-GLIC does not exhibit the substantial increase in solvent accessibility of polypeptide backbone hydrogens, which has been attributed to weakened interactions between the agonist-binding and transmembrane domains. PC-GLIC does not exhibit the reduced cooperativity of thermal denaturation that is observed for PC-nAChR. Finally, unlike PC-nAChR which remains inactive even after fusion with oocyte plasma membranes, fusion of PC-GLIC leads to an active conformation. Although further studies are required to fully characterize the functional properties of GLIC in different membranes, it appears that PC-GLIC is not locked in an uncoupled conformation that is unresponsive to agonist binding.

The finding that GLIC does not exhibit the same propensity as the nAChR to adopt an uncoupled conformation can be interpreted in light of our working model of uncoupling. This model proposes that lipids influence the coupling of binding and gating via the M4 transmembrane α-helices (one per subunit)(40), which are exposed to the surrounding lipid bilayer and thus ideally situated to sense membrane physical and/or chemical properties (Fig. 3.01)(20). Each M4 α-helix extends beyond the bilayer to interact directly with the Cys-loop, a key structure at the interface between the agonist binding (ABD) and transmembrane (TMD) domains. By influencing the conformation of the M4 "lipid-sensor", lipids may modulate interactions between M4 and the Cys-loop (Fig. 3.S06 (40)). Weakened M4/Cys-loop interactions could lead to a Cys-loop conformational change that ultimately reduces contact between the agonist binding and the transmembrane domains, and leads to the uncoupled state.

A dynamic equilibrium may exist between coupled and uncoupled conformations where M4 is bound tightly or tilted away from the Cys-loop, respectively (118,119). In fact, an equilibrium between M4 solvated by lipid and M4 bound tightly to the other transmembrane α-helices, M1+M3, has been demonstrated for the homologous Glycine receptor (120). Significantly, aromatic-aromatic interactions play a key role driving associations between M4 and M1+M3 thus stabilizing a folded structure. In the context of the M4 lipid-sensor model, aromatic-aromatic interactions could play a key role dictating the propensity of M4 to bind tightly to M1+M3 and to thus form a coupled conformation. Aromatic-aromatic interactions could play a role dictating the propensity of a pLGIC to adopt an uncoupled conformation in PC membranes.

In light of this hypothesis, we compared the aromatic-aromatic interactions that exist between M4 and M1+M3 in GLIC versus the nAChR (Fig. 3.05). Consistent with the above

**Figure 3.05 -** Aromatic-aromatic interactions may dictate the propensity of a pLGIC to adopt a lipid-dependent uncoupled conformation. Comparison of the aromatic residues located in M1, M3, and M4 of a single subunit transmembrane domain for (A) GLIC, and (B) the α-subunit of the nAChR. Both a side view of the transmembrane domain of each subunit and a top view looking down at the bilayer surface are shown. Note that the side view orientations of the two transmembrane domains has been rotated $180^{o}$ about the long axis of each molecule relative to the side view orientation shown in the schematic diagram of uncoupling in Fig. 3.S06, as this presents a clearer view of the aromatic-aromatic interactions at the interface between M4 and M1+M3.

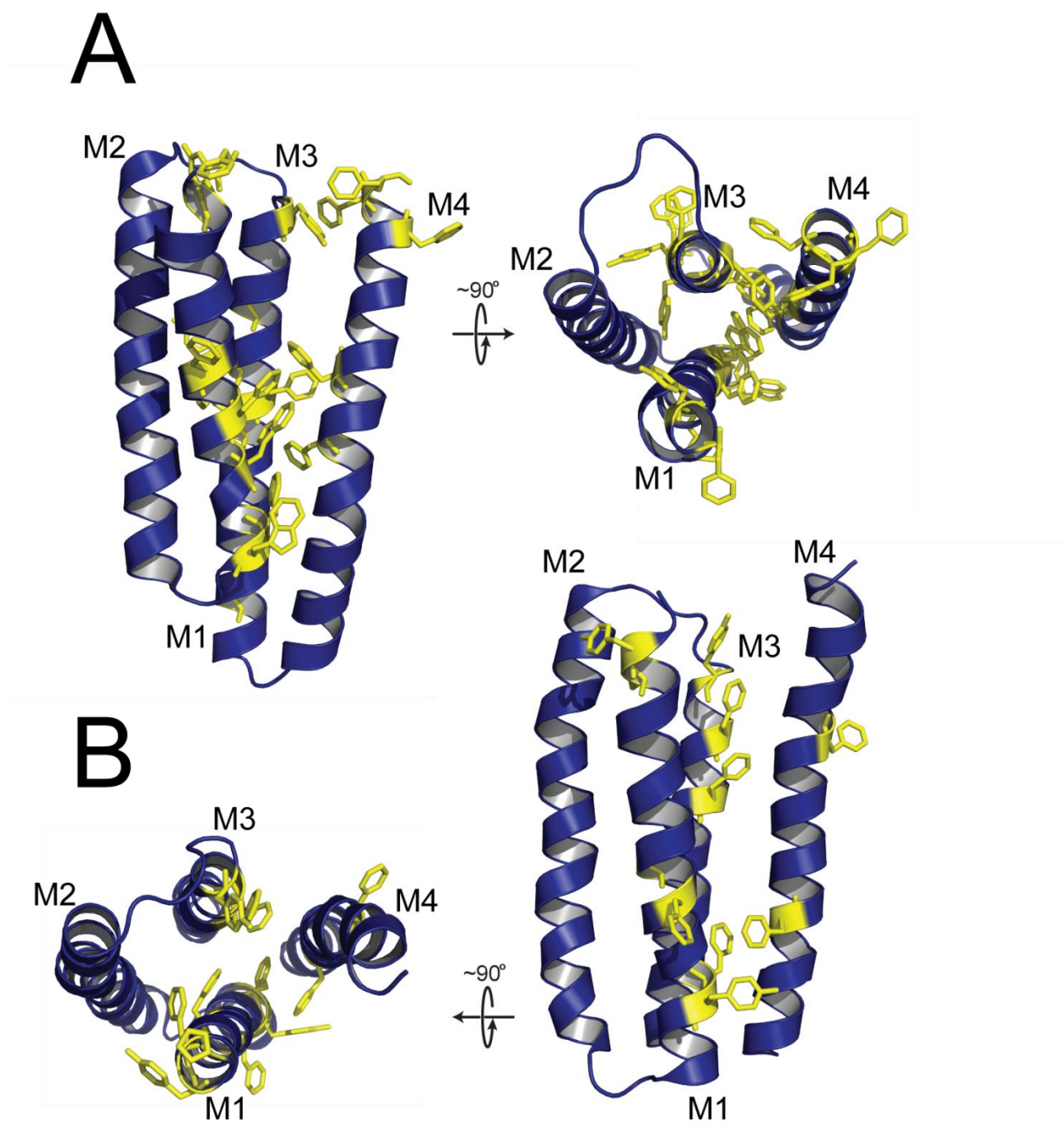
A
M2
M3
M4
M1
~90°
M2
M3
M4
M1
B
M3
M2
M4
M1
~90°
M2
M4
M3
M1

hypothesis, GLIC exhibits a plethora of aromatic-aromatic interactions between M4 and M1+M3, with clusters located in both the cytoplasmic and extracellular leaflets of the lipid bilayer. These aromatics could lead to a highly stable transmembrane domain that is resistant to the formation of an uncoupled conformation. In contrast, while the nAChR exhibits aromatic residues at the interface between M4 and M1+M3, there appear to be few if any direct interactions that could stabilize the nAChR in a coupled conformation where M4 binds tightly to M1+M3, although the lower resolution of the nAChR structure makes this interpretation less definitive. Although other features likely play important roles, the paucity of aromatic-aromatic interactions between M4 and M1+M3 in the nAChR may contribute to weaker M4/M1+M3 interactions and thus to the high propensity of this receptor to adopt an uncoupled conformation. The lack of aromatic-aromatic interactions may also contribute to the lower thermal stability of the nAChR relative to GLIC. Future studies should lead to definitive insight into the molecular basis of lipid sensitivity in pLGICs.

Finally, it is notable that although GLIC does not exhibit the same propensity to uncouple as the nAChR, it still appears to be sensitive to its membrane environment. The dose response of membrane reconstituted GLIC incorporated into oocyte membranes is shifted to higher proton concentrations suggesting a weaker ability of protons to gate open the channel pLGIC. A lower $pH_{50}$ has also been observed in electrophysiology studies of GLIC reconstituted into asolectin membranes at high lipid-protein ratios. In fact, lipid effects may account for the altered $pH_{50}$s observed for GLIC in different heterologous expression systems (121,122). Note that altered sensitivity to protons could reflect altered proton binding and/or altered coupling of binding to

gating. Lipids may still influence the coupling of binding and gating in GLIC, albeit to a lesser extent than with the nAChR.

In addition, we detect both an increased thermal stability and a reduced level of peptide backbone N-$^{1}$H/N-$^{2}$H exchange after prolonged exposure to $^{2}H_2O$ of EcoLip-GLIC relative to both aso-GLIC and PC-GLIC. Both suggest a slightly more rigid structure in the membranes formed from *E. coli* polar lipid extracts. A more detailed characterization of the effects of membranes on GLIC structure should lead to further insight into the molecular coupling of pLGICs with their membrane environment.

# Chapter 4

# General Conclusions

## 4.1 – Conclusions and Future Directions

The focus of this dissertation was to understand lipid-protein interactions within the context of pLGICs and how these interactions affect the structure and function of these proteins. It is also worth noting that lipid protein interactions are implicated in the function of other membrane proteins, one example being the voltage gated K+ channels (123). Thus it appears as though lipid-protein interactions are integral in the function membrane proteins in general. With these considerations and the ones outlined in the introduction in mind, I have made a case that understanding lipid-protein interactions will deepen our understanding of human physiology. Finally, the close link between membrane protein function and the lipid environment implies that understanding the mechanism of these interactions is relevant in conducting studies on pLGICs which require removing these proteins from their native membrane environment.

Within this context, the take home message of Chapter 2 is that the *Torpedo* nAChR is able to modify its surrounding lipid environment through a tightly associated PA-specific phospholipase C activity which converts PA to DAG. DAG, in turn, is able to stabilise functional nAChRs in a PC environment, where nAChR would normally be uncoupled. Therefore, PA-specific phospholipase activity presents a mechanism wherein nAChR may modulate its own function. Future work on this project should be aimed at identifying the region on nAChR, or the tightly associated compound, that is responsible for the phospholipase activity. One way that this may be achieved is through the use of activity based probes, which are chemicals able to covalently attach themselves to the active site of enzymes, including phospholipases. These probes are connected via linkers to moieties that make them suitable for

pulldown assays which, coupled with tryptic digest and mass spectrometry, will allow mapping of the phospholipase active site. Once the active site or species is identified, functional, biophysical, and biochemical analysis of mutants which disrupt this activity will lead to elucidation of the role of phospholipase activity in the structure and function on nAChRs.

In chapter 3 the development of a reconstitution protocol for the prokaryotic pLGIC GLIC and a characterization of its lipid sensitivity is presented. The purpose of this study is to serve as a basis for understanding the mechanism of lipid protein interactions in pLGICs, for which GLIC will serve as an excellent model as discussed in the introduction. The extensive aromatic interactions between the M4 and M3+M1 helices of GLIC may play a role in dictating lipid sensitivity of pLGICs, as predicted by the M4 lipid sensor model. Future studies will be aimed at investigating the lipid sensitivity of GLIC mutants which abolish these interactions. It is predicted that manipulating aromatic interactions between M4 and M3+M1 in GLIC, and pLGICs generally, will allow tuning of their lipid sensitivity.

Although aromatic interactions between M4 and M3+M1 is a plausible factor which dictates pLGIC lipid sensitivity, there are others. For example, in GLIC crystal structures well ordered electron density is observed between post M4 and the Cys-loop. This electron density is modelled as a lipid molecule, which suggests lipids bind tightly to this location. This lipid molecule may be capable of remaining bound to GLIC throughout solubilisation and purification. Thus a possible reason that GLIC appears insensitive to its lipid environment is that it is able to tightly bind lipid molecules which are required for stabilization of its structure and function. Therefore, future studies should also be aimed at determining if lipids are bound to solubilised GLIC samples, through extensive washing followed by lipid extraction and analysis by thin layer chromatography or even a more sensitive technique such as mass spectrometry. If

lipid is detected, residues which are potentially responsibly for binding, as predicted by crystal structures, should be investigated by mutagenesis.

# Appendix I

## AI.01 - Expression and purification of GLIC

Initially, there were problems obtaining pure GLIC in sufficient quantities for reconstitution and subsequent structural and functional studies. Studies conducted by Dr. Baenziger during his sabbatical at the Institut Pasteur (Paris, France) indicated that yields of pure GLIC should be in the range of 3mg from 8L of bacterial culture. Initial purifications performed in Ottawa, however, produced only ~500µg of protein from 8L of culture. To conduct the experiments outlined in the introduction of this dissertation required milligram amounts of protein. Therefore, the sub-milligram amount of protein obtained in preliminary expression trials was not sufficient. As a result, the initial part of this project involved extensive characterization of the expression system and purification toward the end of optimizing these protocols to obtain the highest yield of pure GLIC possible.

## AI.02 - Characterization of MBP-GLIC expression and purification in C43 cells

The GLIC cDNA sequence was obtained from Dr. Corringer (Pasteur institute, France) cloned into a pET20+b expression vector covalently linked to maltose binding protein (MBP) through a thrombin sensitive peptide linker (Figure AI.01A). MBP acts as both an affinity tag to aid in purification as well as increasing solubility of typically insoluble proteins (124).

**Figure AI.01** – Characterization of MBP-GLIC expression and purification in *E. Coli.* C43 cells. (A) Cartoon of the MBP-GLIC DNA construct. cDNA encoding a GLIC subunit was covalently linked to MBP via a thrombin sensitive peptide linker. (B) Gel-filtration analysis of eluants from solubilised C43 cell membranes expressing MBP-GLIC which were bound to and eluted from amylose resin. The top panel shows traces of proteins eluted from the resin with maltose; black trace – maltose eluants, red trace – isolated 12.8mL peak which is the MBP-GLIC construct, blue trace – isolated 14.5mL peak which is the unknown protein. The bottom panel shows traces of proteins eluted after thrombin cleavage, red trace – isolated 14.8mL peak which is natively folded GLIC. (C) SDS-PAGE analysis on a 10% gel of amylose resin eluted proteins and gel filtration peaks. The top gel is an analysis of the gel-filtration peaks from maltose eluted protein. Lane 1 – 14.5mL peak, 2 – 12.8mL peak, 3 – 10mL region, 4 – 7mL peak. The bottom gel is an analysis of thrombin treatment. Lane 1 – protein eluted from amylose resin by 20mM maltose, lane 2 – maltose eluted protein after gel-filtration 12-15mL region collected, lane 3 – after treatment of lane 2 proteins with thrombin, lane 4 – specifically eluted with maltose after incubation of lane 3 with amylose resin, lane 5 – flow through from lane 3 protein incubated with amylose resin, lane 6 – isolated unknown protein.

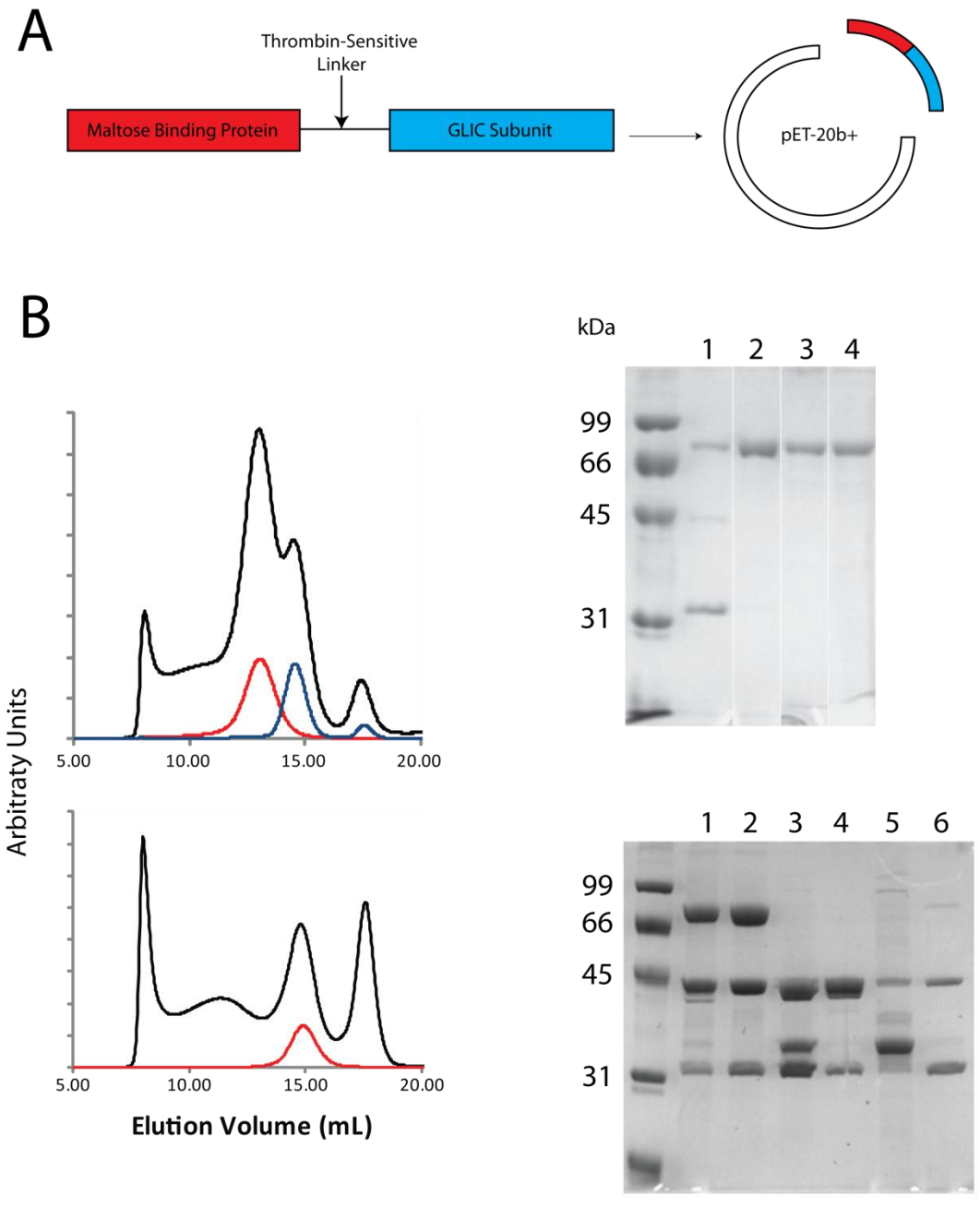
A
Thrombin-Sensitive Linker
Maltose Binding Protein
GLIC Subunit
pET-20b+
B
Arbitraty Units
5.00
10.00
15.00
20.00
Elution Volume (mL)
kDa
1 2 3 4
99
66
45
31
1 2 3 4 5 6
99
66
45
31

We chose to express this construct in C43 *E. coli.* which are derived from BL21 expression cells and contain all the same expression machinery but are resistant to the effects of overexpression of toxic proteins such as integral membrane proteins (125).

Preliminary experiments were performed wherein cells expressing this construct were lysed, the membrane fraction collected and solubilised with the detergent n-dodecyl-β-D-maltopyranoside (DDM), and the solubilised material subsequently purified with amylose resin (Figure AI.01B). Specifically bound protein was eluted with 20mM maltose and applied to a gel-filtration column. The elution profile revealed several peaks, suggesting multiple proteins bound to the amylose resin (Figure AI.01B), with monodisperse MBP-GLIC eluting around 12.8mLs. SDS-PAGE shows the void volume (~8mL) and the 9 – 11.5mL peaks corresponds to MBP-GLIC aggregates (Figure AI.01C), while the peak at 17.5mL is due to endogenous MBP. The peak eluting at 14.5mL corresponds to two separate peptide chains, one at ~44kDa and the other at ~32kDa (Figure AI.01C) which bind specifically to the amylose resin and are endogenously expressed in C43 cells (data not shown).

**AI.03 - Optimization of MBP-GLIC expression**

Many factors known to affect protein expression levels in this type of system were investigated in order to optimize the overall yield of purified GLIC. First, we tested overexpression of constructs under control of a T7 promoter by our C43 cell line using a Set7/9 c construct provided by Dr. Jean-Francois Couture (University of Ottawa). These experiments showed robust expression of the construct (data not shown).

A typical practice for heterologous protein expression is to make glycerol stocks of a well expressing culture and keep it at -80˚C for all subsequent expressions. To determine whether this would affect protein expression levels, gel-filtration profiles of protein purified from a

freshly picked colony and the same colony after it was used to make a 10% glycerol stock were compared. I found that using cells from a glycerol stock resulted in a decreased MBP-GLIC expression relative to that of the unknown protein as shown by the gel-filtration elution profiles. Since the source of the unknown protein is from the C43 cells themselves I assumed that expression of this unknown protein was consistent from culture to culture. With this assumption, the relative expression of MBP-GLIC can be roughly assessed by comparing its intensity with that of the unknown protein peak. Figure AI.02A shows that the relative expression of MBP-GLIC drops drastically when cultures are inoculated from a glycerol stock.

Other factors that can influence protein expression levels in these systems include the amount of IPTG used to induce expression, the amount of time the protein is expressed for, and the temperature at which the protein is expressed. The first two factors were investigated by western blots. Figure AI.04B shows western blots of whole C43 cells expressing MBP-GLIC under various conditions. The antibody used in this experiment was raised against MBP. Note that the band around 42kDa is due to endogenously expressed MBP. The expression protocol used in France suggested that 100μM IPTG was ideal for the induction of MBP-GLIC expression. Figure AI.02B shows that varying the concentration of IPTG used to induce cells from the same colony had little effect on the amount of MBP-GLIC that was expressed. Moreover, this observation was temperature independent. Analysis by gel-filtration confirmed this result (data not shown). Next, the time of expression was examined. I observed that expression increased over 3 hours, and then significantly from 3 hours to overnight (Figure AI.02B). Consequently, overnight expression was used in the final protocol.

**Figure AI.02** - Characterization of factors known to effect protein expression levels in heterologous expression systems. (A) Gel-filtration profile of purified MBP-GLIC from a colony freshly picked from and LB-AMP plate (red trace) and the same culture made into a glycerol stock (blue trace). (B) Western blot analysis of whole cell cultures expression MBP-GLIC under various conditions. Proteins were detected through a monoclonal anti-MBP antibody. (C) Gel-filtration profiles of purified MBP-GLIC from cultures under different overnight expression temperatures.

A

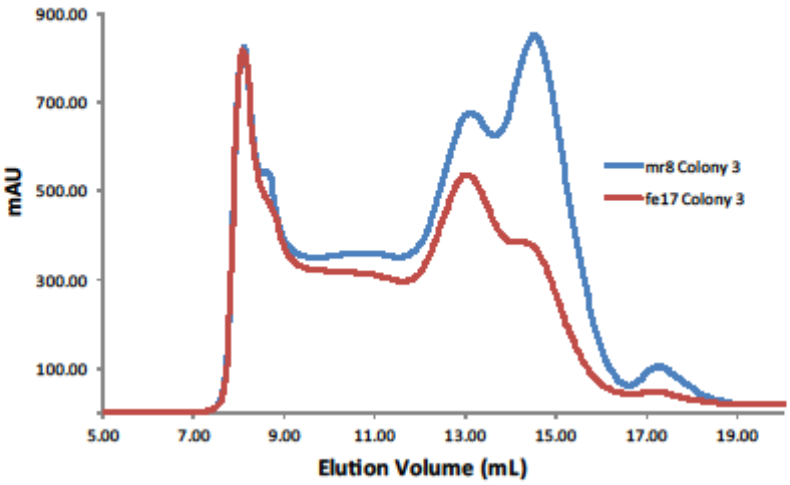
900.00
700.00
500.00
300.00
100.00
mAU
5.00
7.00
9.00
11.00
13.00
15.00
17.00
19.00
Elution Volume (mL)
mr8 Colony 3
fe17 Colony 3

B

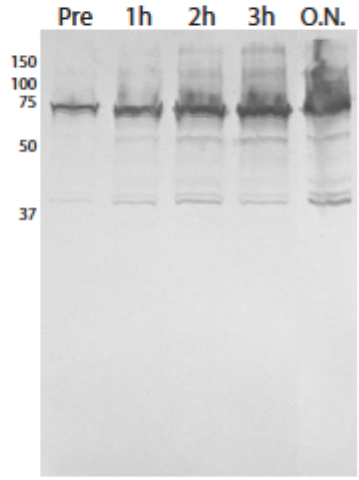
Pre
1h
2h
3h
O.N.
150
100
75
50
37

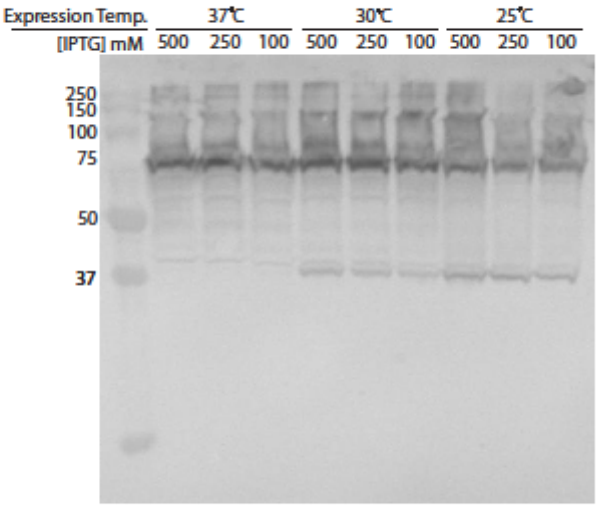
Expression Temp.
37℃
30℃
25℃
[IPTG] mM
500
250
100
500
250
100
500
250
100
250
150
100
75
50
37

C

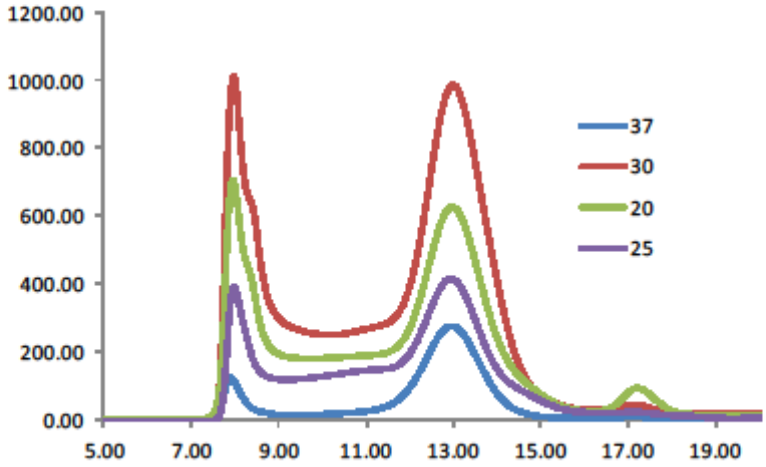
1200.00
1000.00
800.00
600.00
400.00
200.00
0.00
5.00
7.00
9.00
11.00
13.00
15.00
17.00
19.00
37
30
20
25

I also examined at the effect of temperature on protein expression. Typically, expression of toxic proteins is induced at lower temperatures in order to curb rapid overexpression of the target protein and subsequent toxic effects. Accordingly, the protocol from the Corringer lab suggested an expression temperature of 20˚C. I picked a colony from a freshly transformed plate to inoculate a starter culture. This starter culture was used to inoculate 3 expression cultures. These cultures were grown at 37˚C and subsequently placed at 3 different temperatures, 37˚C, 30˚C, and 20˚C, for overnight expression. Purification and gel-filtration analysis revealed that expression at 30˚C produced the highest yield of MBP-GLIC (Figure AI.02C).

The final factor I investigated was the amount of DNA used to transform the competent C43 cells. 50μL of C43 cells were transformed with varying amounts of plasmid DNA, each from the same preparation. I analysed the amount of protein expressed from each transformation conditions by gel-filtration. Again, assuming the relative MBP-GLIC expression can be determined by comparing to that of the unknown protein there is a clear effect on the final yield of MBP-GLIC (Figure AI.03). In this experiment the least amount of DNA used in transformation (100ng) yielded the most protein relative to the unknown protein peak. Consequently, I sought to determine whether using less than 100ng of DNA for transformation resulted in even higher yields of MBP-GLIC. The results of these experiments showed less correlation, however 100ng of DNA was still optimal. Subsequently, using cells freshly transformed with 100ng of plasmid DNA in subsequent large scale purifications yielded suitable quantities of protein for the proposed biophysical experiments.

**Figure AI.03** – Total amount of vector DNA used for transformation effects yield of soluble MBP-GLIC. C43 competent cells from the same stock were transformed with varying amounts of DNA from the same sample and plated on different LB-100μg/mL ampicillin plates. One colony from each plate was used to express and purify the MBP-GLIC construct as described in materials and methods. Each trace is the total protein purified from 500mL of culture from each DNA condition using 1mL of amylose resin eluted with 20mM maltose. There is a slight correlation between DNA amount and MBP-GLIC expression level. In the inset each trace is normalized to the level of the unknown protein, demonstrating that that the ratio of MBP-GLIC to unknown protein levels is negatively correlated with DNA level.

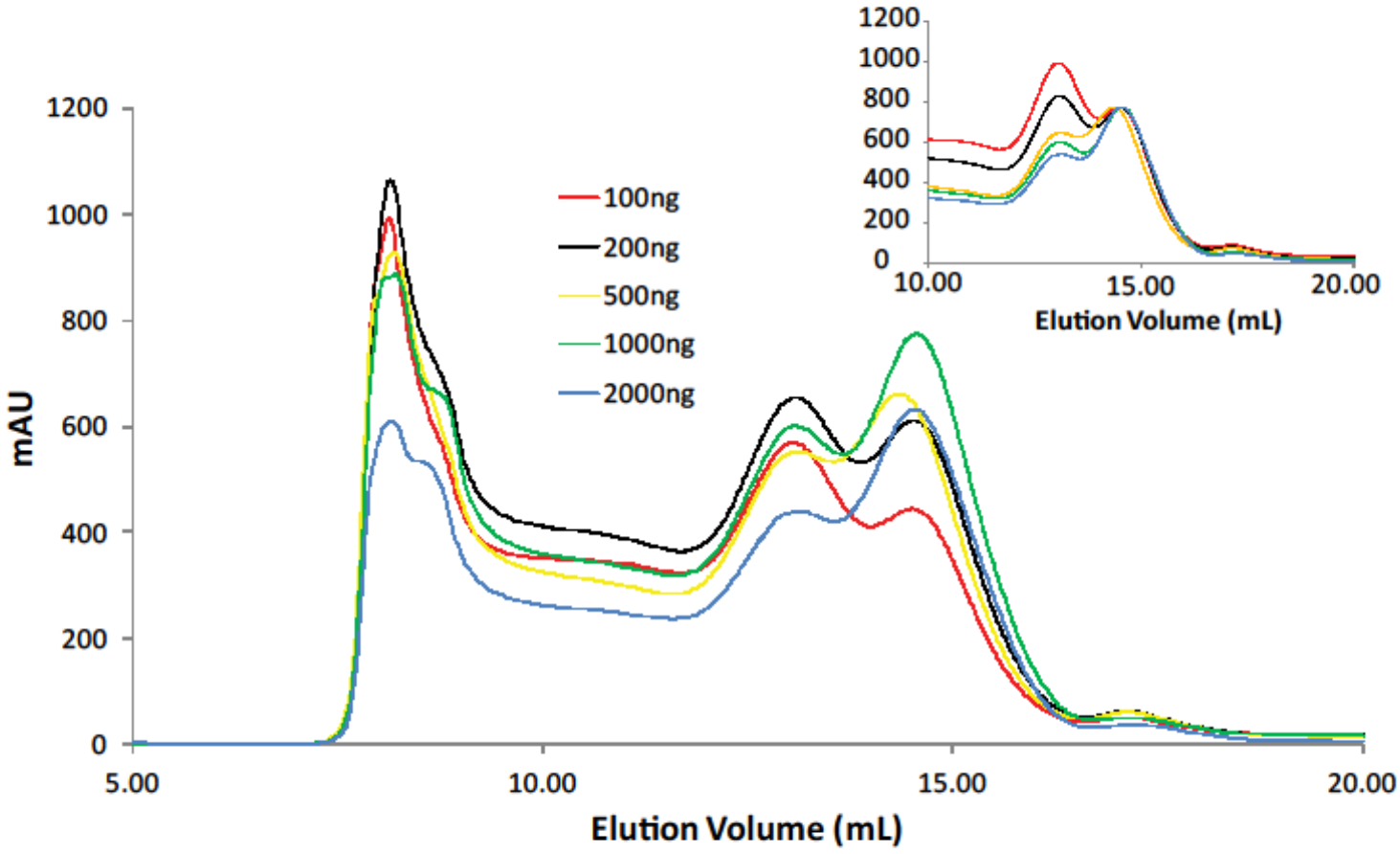
1200
1000
800
600
400
200
0
mAU
5.00
10.00
15.00
20.00
Elution Volume (mL)
100ng
200ng
500ng
1000ng
2000ng
1200
1000
800
600
400
200
0
10.00
15.00
20.00
Elution Volume (mL)

**AI.04 – Analysis of Raw Reconstituted GLIC Thermal Denaturation Curves**

The thermal stability of each membrane-reconstituted GLIC sample was measured using infrared spectroscopy. Infrared temperature recorded as a function of increasing temperature reveal changes in the shape of the Amide I region of the IR spectra stemming from changes in secondary structure that occur as protein thermally denatures. To characterize the thermal stability of GLIC in various membrane environments I plotted the intensity of the underlying Amide I band component at 1683cm$^{-1}$ in deconvolved spectra (see Chapter 3 materials and methods for details on spectra processing) versus temperature. Surprisingly, I found that this plot yielded a two component sigmoidal curve (Figure AI.04), suggesting two distinct unfolding events.

In order to determine if GLIC is undergoing two separate unfolding events the spectral changes that occur as the sample is heated were examined in more detail (Figure AI.04). Note that after the first unfolding event the amide I component bands at 1655cm$^{-1}$ and 1640cm$^{-1}$ due to α-helices and β-sheets, respectively, have essentially disappeared and are replaced by a prominent peak at 1620cm$^{-1}$ and a broad band around 1680cm$^{-1}$, which are characteristic of denatured protein. This observation suggests a complete loss of secondary structure and therefore complete unfolding of the protein after the first component. Note that during the second component the amide I bandshape is essentially unchanged, although the intensity at 1620cm$^{-1}$ and 1680cm$^{-1}$ increases slightly. One possible explanation for the second component in the denaturation curve is that heating causes loss of hydration in the sample cell and thus increasing intermolecular bonds between the unfolded peptide backbone. Further experiments are needed to test this interpretation.

To process the data, the second response was removed by the following strategy. The plot was fit to a modified Boltzmann sigmoid with two exponential elements,

$$F(x) = \left[\frac{Top}{1+ e^{\left(\frac{Td1-x}{m1}\right)}}\right] + \left[\frac{Top}{1+e^{\frac{(Td2-x)}{m2}}}\right]$$

where *F(x)* describes the fraction of denatured receptors as a function of temperature (*x*), *Top* is the plateau value of each response which is normalized to 1, $T_{d1}$ and $T_{d2}$ is the temperature at half the maximum for response *1* and *2*, respectively, and $m_1$ and $m_2$ are the Hill slopes of response *1* and *2*, respectively. In order to calculate $T_{d1}$, taken as the temperature at half maximal denaturation of the entire sample (see Chapter 3), more accurately and for presentation purposes the second response was subtracted out of the entire curve which was then refit to a normal Boltzmann equation (see Figure AI.05). I found that this procedure did not significantly alter the temperature calculated for $T_{d1}$, however all values reported in Table 2 were calculated in this manner. Curves that are presented in Figure 3.6 were also modified in this way.

**Figure AI.04.** Analysis of raw thermal denaturation spectra from reconstituted GLIC. (A) The intensity at 1683cm$^{-1}$ from spectra collected at various temperatures (see figure 3.S04) was plotted verse temperature (white squares). This yielded a sigmoidal curve with two responses. The curve was subsequently fit to a double dose-response curve (see text). The curve was plotted using the parameters for the second response only (black squares). The second response curve was subtracted from the total curve to give the processed curve (grey squares) from which all final parameters were calculated. (B) Comparison of raw FTIR spectra before the first response element (solid line), after first response (long dash), and at the middle of the second response (short dash).

A

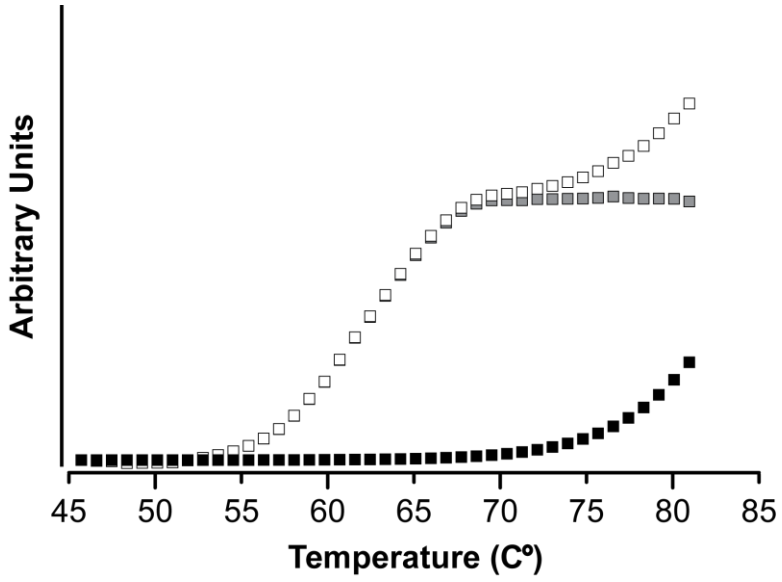
Arbitrary Units
45
50
55
60
65
70
75
80
85
Temperature (Cº)

B

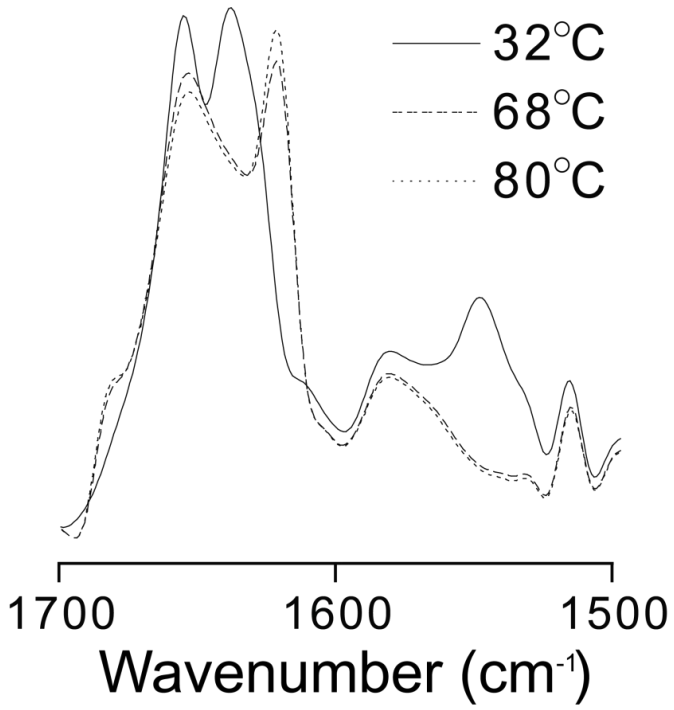
32°C
68°C
80°C
1700
1600
1500
Wavenumber (cm-1)

1. Ohno, K., Hutchinson, D. O., Milone, M., Brengman, J. M., Bouzat, C., Sine, S. M., and Engel, A. G. (1995) *Proceedings of the National Academy of Sciences of the United States of America* **92**, 758-762
2. Sine, S. M., and Engel, A. G. (2006) *Nature* **440**, 448-455
3. Tasneem, A., Iyer, L. M., Jakobsson, E., and Aravind, L. (2005) *Genome biology* **6**, R4
4. Changeux, J. P., Podleski, T. R., and Wofsy, L. (1967) *Proceedings of the National Academy of Sciences of the United States of America* **58**, 2063-2070
5. Schofield, P. R., Darlison, M. G., Fujita, N., Burt, D. R., Stephenson, F. A., Rodriguez, H., Rhee, L. M., Ramachandran, J., Reale, V., Glencorse, T. A., and et al. (1987) *Nature* **328**, 221-227
6. Grenningloh, G., Rienitz, A., Schmitt, B., Methfessel, C., Zensen, M., Beyreuther, K., Gundelfinger, E. D., and Betz, H. (1987) *Nature* **328**, 215-220
7. Changeux, J. P., Kasai, M., and Lee, C. Y. (1970) *Proceedings of the National Academy of Sciences of the United States of America* **67**, 1241-1247
8. Baenziger, J. E., and Corringer, P. J. (2011) *Neuropharmacology* **60**, 116-125
9. Brejc, K., van Dijk, W. J., Klaassen, R. V., Schuurmans, M., van Der Oost, J., Smit, A. B., and Sixma, T. K. (2001) *Nature* **411**, 269-276
10. Smit, A. B., Syed, N. I., Schaap, D., van Minnen, J., Klumperman, J., Kits, K. S., Lodder, H., van der Schors, R. C., van Elk, R., Sorgedrager, B., Brejc, K., Sixma, T. K., and Geraerts, W. P. (2001) *Nature* **411**, 261-268
11. Celie, P. H., van Rossum-Fikkert, S. E., van Dijk, W. J., Brejc, K., Smit, A. B., and Sixma, T. K. (2004) *Neuron* **41**, 907-914
12. Lummis, S. C., McGonigle, I., Ashby, J. A., and Dougherty, D. A. (2011) *The Journal of neuroscience : the official journal of the Society for Neuroscience* **31**, 12371-12376
13. Carpenter, T. S., Lau, E. Y., and Lightstone, F. C. (2012) *Journal of molecular biology*
14. Changeux, J. P., Devillers-Thiery, A., and Chemouilli, P. (1984) *Science* **225**, 1335-1345
15. Dellisanti, C. D., Yao, Y., Stroud, J. C., Wang, Z. Z., and Chen, L. (2007) *Nature neuroscience* **10**, 953-962
16. Li, S. X., Huang, S., Bren, N., Noridomi, K., Dellisanti, C. D., Sine, S. M., and Chen, L. (2011) *Nature neuroscience* **14**, 1253-1259
17. Karlin, A., and Akabas, M. H. (1995) *Neuron* **15**, 1231-1244
18. Spurny, R., Ramerstorfer, J., Price, K., Brams, M., Ernst, M., Nury, H., Verheij, M., Legrand, P., Bertrand, D., Bertrand, S., Dougherty, D. A., de Esch, I. J., Corringer, P. J., Sieghart, W., Lummis, S. C., and Ulens, C. (2012) *Proceedings of the National Academy of Sciences of the United States of America* **109**, E3028-3034
19. Pless, S. A., Hanek, A. P., Price, K. L., Lynch, J. W., Lester, H. A., Dougherty, D. A., and Lummis, S. C. (2011) *Molecular pharmacology* **79**, 742-748
20. Unwin, N. (2005) *Journal of molecular biology* **346**, 967-989
21. Unwin, N., Toyoshima, C., and Kubalek, E. (1988) *The Journal of cell biology* **107**, 1123-1138
22. Unwin, N., and Fujiyoshi, Y. (2012) *Journal of molecular biology*
23. Unwin, N. (1993) *Journal of molecular biology* **229**, 1101-1124
24. Toyoshima, C., and Unwin, N. (1990) *The Journal of cell biology* **111**, 2623-2635
25. Brisson, A., and Unwin, P. N. (1984) *The Journal of cell biology* **99**, 1202-1211
26. Hilf, R. J., and Dutzler, R. (2008) *Nature* **452**, 375-379
27. Bocquet, N., Nury, H., Baaden, M., Le Poupon, C., Changeux, J. P., Delarue, M., and Corringer, P. J. (2009) *Nature* **457**, 111-114
28. Hibbs, R. E., and Gouaux, E. (2011) *Nature* **474**, 54-60
29. Labriola, J. M., Pandhare, A., Jansen, M., Blanton, M. P., Corringer, P. J., and Baenziger, J. E. (2013) *The Journal of biological chemistry* **288**, 11294-11303
30. Miyazawa, A., Fujiyoshi, Y., and Unwin, N. (2003) *Nature* **423**, 949-955
31. Chang, Y., Wang, R., Barot, S., and Weiss, D. S. (1996) *The Journal of neuroscience : the official journal of the Society for Neuroscience* **16**, 5415-5424

32. Revah, F., Bertrand, D., Galzi, J. L., Devillers-Thiery, A., Mulle, C., Hussy, N., Bertrand, S., Ballivet, M., and Changeux, J. P. (1991) *Nature* **353**, 846-849
33. Labarca, C., Nowak, M. W., Zhang, H., Tang, L., Deshpande, P., and Lester, H. A. (1995) *Nature* **376**, 514-516
34. Unwin, N. (1995) *Nature* **373**, 37-43
35. Wilson, G. G., and Karlin, A. (1998) *Neuron* **20**, 1269-1281
36. Panicker, S., Cruz, H., Arrabit, C., and Slesinger, P. A. (2002) *The Journal of neuroscience : the official journal of the Society for Neuroscience* **22**, 1629-1639
37. Akabas, M. H. (2004) *International review of neurobiology* **62**, 1-43
38. Lee, W. Y., and Sine, S. M. (2005) *Nature* **438**, 243-247
39. Jha, A., Cadugan, D. J., Purohit, P., and Auerbach, A. (2007) *The Journal of general physiology* **130**, 547-558
40. daCosta, C. J., and Baenziger, J. E. (2009) *J Biol Chem* **284**, 17819-17825
41. Tobimatsu, T., Fujita, Y., Fukuda, K., Tanaka, K., Mori, Y., Konno, T., Mishina, M., and Numa, S. (1987) *FEBS letters* **222**, 56-62
42. Paradiso, K., Zhang, J., and Steinbach, J. H. (2001) *The Journal of neuroscience : the official journal of the Society for Neuroscience* **21**, 6561-6568
43. Boyd, N. D., and Cohen, J. B. (1980) *Biochemistry* **19**, 5353-5358
44. Boyd, N. D., and Cohen, J. B. (1980) *Biochemistry* **19**, 5344-5353
45. Epstein, M., and Racker, E. (1978) *The Journal of biological chemistry* **253**, 6660-6662
46. Gonzalez-Ros, J. M., Llanillo, M., Paraschos, A., and Martinez-Carrion, M. (1982) *Biochemistry* **21**, 3467-3474
47. Barrantes, F. J. (1993) *FASEB journal : official publication of the Federation of American Societies for Experimental Biology* **7**, 1460-1467
48. Criado, M., Eibl, H., and Barrantes, F. J. (1984) *The Journal of biological chemistry* **259**, 9188-9198
49. Criado, M., Eibl, H., and Barrantes, F. J. (1982) *Biochemistry* **21**, 3622-3629
50. Ryan, S. E., Demers, C. N., Chew, J. P., and Baenziger, J. E. (1996) *The Journal of biological chemistry* **271**, 24590-24597
51. Fong, T. M., and McNamee, M. G. (1986) *Biochemistry* **25**, 830-840
52. Ochoa, E. L., Dalziel, A. W., and McNamee, M. G. (1983) *Biochimica et biophysica acta* **727**, 151-162
53. Dalziel, A. W., Rollins, E. S., and McNamee, M. G. (1980) *FEBS letters* **122**, 193-196
54. daCosta, C. J., Wagg, I. D., McKay, M. E., and Baenziger, J. E. (2004) *J Biol Chem* **279**, 14967-14974
55. daCosta, C. J., Ogrel, A. A., McCardy, E. A., Blanton, M. P., and Baenziger, J. E. (2002) *J Biol Chem* **277**, 201-208
56. Ellena, J. F., Blazing, M. A., and McNamee, M. G. (1983) *Biochemistry* **22**, 5523-5535
57. Jones, O. T., and McNamee, M. G. (1988) *Biochemistry* **27**, 2364-2374
58. Brannigan, G., Henin, J., Law, R., Eckenhoff, R., and Klein, M. L. (2008) *Proceedings of the National Academy of Sciences of the United States of America* **105**, 14418-14423
59. Li, P., and Steinbach, J. H. (2010) *British journal of pharmacology* **160**, 1906-1915
60. Vallejo, Y. F., Buisson, B., Bertrand, D., and Green, W. N. (2005) *The Journal of neuroscience : the official journal of the Society for Neuroscience* **25**, 5563-5572
61. Baier, C. J., and Barrantes, F. J. (2007) *Journal of neurochemistry* **101**, 1072-1084
62. Bruses, J. L., Chauvet, N., and Rutishauser, U. (2001) *The Journal of neuroscience : the official journal of the Society for Neuroscience* **21**, 504-512
63. Sanes, J. R., and Lichtman, J. W. (2001) *Nature reviews. Neuroscience* **2**, 791-805
64. Sturgeon, R. M., and Baenziger, J. E. (2010) *Biophysical journal* **98**, 989-998
65. Labriola, J. M., daCosta, C. J., Wang, S., Figeys, D., Smith, J. C., Sturgeon, R. M., and Baenziger, J. E. (2010) *The Journal of biological chemistry* **285**, 10337-10343

66. Pons, S., Sallette, J., Bourgeois, J. P., Taly, A., Changeux, J. P., and Devillers-Thiery, A. (2004) *The European journal of neuroscience* **20**, 2022-2030
67. Nury, H., Van Renterghem, C., Weng, Y., Tran, A., Baaden, M., Dufresne, V., Changeux, J. P., Sonner, J. M., Delarue, M., and Corringer, P. J. (2011) *Nature* **469**, 428-431
68. Gonzalez-Gutierrez, G., Lukk, T., Agarwal, V., Papke, D., Nair, S. K., and Grosman, C. (2012) *Proceedings of the National Academy of Sciences of the United States of America* **109**, 6331-6336
69. Velisetty, P., and Chakrapani, S. (2012) *The Journal of biological chemistry* **287**, 18467-18477
70. Dougherty, D. A. (2008) *Chem Rev* **108**, 1642-1653
71. Goetz, T., Arslan, A., Wisden, W., and Wulff, P. (2007) *Prog Brain Res* **160**, 21-41
72. Thompson, A. J., and Lummis, S. C. (2006) *Curr Pharm Des* **12**, 3615-3630
73. Shen, X. M., Deymeer, F., Sine, S. M., and Engel, A. G. (2006) *Ann Neurol* **60**, 128-136
74. Karlin, A. (2002) *Nat Rev Neurosci* **3**, 102-114
75. Baenziger, J. E., Morris, M. L., Darsaut, T. E., and Ryan, S. E. (2000) *The Journal of biological chemistry* **275**, 777-784
76. Hamouda, A. K., Sanghvi, M., Sauls, D., Machu, T. K., and Blanton, M. P. (2006) *Biochemistry* **45**, 4327-4337
77. daCosta, C. J. B., Medaglia, S. A., Lavigne, N., Wang, S., Carswell, C. L., and Baenziger, J. E. (2009) *submitted to Journal of Biological Chemistry*
78. Kihara, T., Shimohama, S., Sawada, H., Honda, K., Nakamizo, T., Shibasaki, H., Kume, T., and Akaike, A. (2001) *J Biol Chem* **276**, 13541-13546
79. de Jonge, W. J., and Ulloa, L. (2007) *Br J Pharmacol* **151**, 915-929
80. Sharma, G., and Vijayaraghavan, S. (2002) *J Neurobiol* **53**, 524-534
81. Suzuki, T., Hide, I., Matsubara, A., Hama, C., Harada, K., Miyano, K., Andra, M., Matsubayashi, H., Sakai, N., Kohsaka, S., Inoue, K., and Nakata, Y. (2006) *J Neurosci Res* **83**, 1461-1470
82. Blanchet, M. R., Israel-Assayag, E., Daleau, P., Beaulieu, M. J., and Cormier, Y. (2006) *Am J Physiol Lung Cell Mol Physiol* **291**, L757-763
83. daCosta, C. J., and Baenziger, J. E. (2003) *Acta Crystallogr D Biol Crystallogr* **59**, 77-83
84. Bligh, E. G., and Dyer, W. J. (1959) *Can J Biochem Physiol* **37**, 911-917
85. McCarthy, M. P., and Moore, M. A. (1992) *J Biol Chem* **267**, 7655-7663
86. Reue, K., and Brindley, D. N. (2008) *J Lipid Res* **49**, 2493-2503
87. Simon, M. F., Rey, A., Castan-Laurel, I., Gres, S., Sibrac, D., Valet, P., and Saulnier-Blache, J. S. (2002) *J Biol Chem* **277**, 23131-23136
88. Brindley, D. N., and Waggoner, D. W. (1998) *J Biol Chem* **273**, 24281-24284
89. Herz, J. M., Johnson, D. A., and Taylor, P. (1987) *J Biol Chem* **262**, 7238-7247
90. Bleasdale, J. E., Hawthorne, J. N., Widlund, L., and Heilbronn, E. (1976) *Biochem J* **158**, 557-565
91. Taly, A., Corringer, P. J., Guedin, D., Lestage, P., and Changeux, J. P. (2009) *Nat Rev Drug Discov* **8**, 733-750
92. Sine, S. M. (2012) *Physiological reviews* **92**, 1189-1234
93. Changeux, J. P. (2012) *Current opinion in anaesthesiology* **25**, 397-404
94. Heidmann, T., Sobel, A., Popot, J. L., and Changeux, J. P. (1980) *European journal of biochemistry / FEBS* **110**, 35-55
95. Baenziger, J. E., and daCosta, C. J. B. (2012) *Biophysical Reviews DOI: DOI 10.1007/s12551-012-0078-7*
96. Bocquet, N., Prado de Carvalho, L., Cartaud, J., Neyton, J., Le Poupon, C., Taly, A., Grutter, T., Changeux, J. P., and Corringer, P. J. (2007) *Nature* **445**, 116-119
97. Hilf, R. J., and Dutzler, R. (2009) *Nature* **457**, 115-118
98. Velisetty, P., Chalamalasetti, S. V., and Chakrapani, S. (2012) *J Biol Chem*
99. Carswell, C. L., Rigden, M. D., and Baenziger, J. E. (2008) *Journal of bacteriology* **190**, 5650-5662
100. Sayeed, W. M., and Baenziger, J. E. (2009) *Biochimica et biophysica acta* **1788**, 1108-1115

101. Hamouda, A. K., Chiara, D. C., Sauls, D., Cohen, J. B., and Blanton, M. P. (2006) *Biochemistry* **45**, 976-986
102. Reid, S. E., Moffat, D. J., and Baenziger, J. E. (1996) *Spectrochimica Acta, Part A* **52**, 1347-1356
103. Pandhare, A., Hamouda, A. K., Staggs, B., Aggarwal, S., Duddempudi, P. K., Lever, J. R., Lapinsky, D. J., Jansen, M., Cohen, J. B., and Blanton, M. P. (2012) *Biochemistry* **51**, 2425-2435
104. Methot, N., Ritchie, B. D., Blanton, M. P., and Baenziger, J. E. (2001) *The Journal of biological chemistry* **276**, 23726-23732
105. Baenziger, J. E., and Chew, J. P. (1997) *Biochemistry* **36**, 3617-3624
106. daCosta, C. J., Michel Sturgeon, R., Hamouda, A. K., Blanton, M. P., and Baenziger, J. E. (2011) *Biochem Biophys Res Commun* **407**, 456-460
107. Baenziger, J. E., and Methot, N. (1995) *J Biol Chem* **270**, 29129-29137
108. daCosta, C. J., Medaglia, S. A., Lavigne, N., Wang, S., Carswell, C. L., and Baenziger, J. E. (2009) *J Biol Chem* **284**, 33841-33849
109. Unwin, N., and Fujiyoshi, Y. (2012) *J Mol Biol* **422**, 617-634
110. Alexandrov, A. I., Mileni, M., Chien, E. Y., Hanson, M. A., and Stevens, R. C. (2008) *Structure* **16**, 351-359
111. Morales, A., Aleu, J., Ivorra, I., Ferragut, J. A., Gonzalez-Ros, J. M., and Miledi, R. (1995) *Proceedings of the National Academy of Sciences of the United States of America* **92**, 8468-8472
112. Methot, N., Demers, C. N., and Baenziger, J. E. (1995) *Biochemistry* **34**, 15142-15149
113. Rankin, S. E., Addona, G. H., Kloczewiak, M. A., Bugge, B., and Miller, K. W. (1997) *Biophys J* **73**, 2446-2455
114. Marsh, D., Watts, A., and Barrantes, F. J. (1981) *Biochim Biophys Acta* **645**, 97-101
115. Weng, Y., Yang, L., Corringer, P. J., and Sonner, J. M. (2010) *Anesthesia and analgesia* **110**, 59-63
116. Ryan, S. E., Hill, D. G., and Baenziger, J. E. (2002) *The Journal of biological chemistry* **277**, 10420-10426
117. Baenziger, J. E., Ryan, S. E., Goodreid, M. M., Vuong, N. Q., Sturgeon, R. M., and daCosta, C. J. (2008) *Mol Pharmacol* **73**, 880-890
118. De Almeida, R. F., Loura, L. M., Prieto, M., Watts, A., Fedorov, A., and Barrantes, F. J. (2006) *Molecular membrane biology* **23**, 305-315
119. Xu, Y., Barrantes, F. J., Luo, X., Chen, K., Shen, J., and Jiang, H. (2005) *J Am Chem Soc* **127**, 1291-1299
120. Haeger, S., Kuzmin, D., Detro-Dassen, S., Lang, N., Kilb, M., Tsetlin, V., Betz, H., Laube, B., and Schmalzing, G. (2010) *Nature structural & molecular biology* **17**, 90-98
121. Wang, H. L., Cheng, X., and Sine, S. M. (2011) *J Biol Chem*
122. Goyal, R., Salahudeen, A. A., and Jansen, M. (2011) *J Biol Chem* **286**, 34635-34642
123. Xu, Y., Ramu, Y., and Lu, Z. (2008) *Nature* **451**, 826-829
124. Korepanova, A., Moore, J. D., Nguyen, H. B., Hua, Y., Cross, T. A., and Gao, F. (2007) *Protein expression and purification* **53**, 24-30
125. Miroux, B., and Walker, J. E. (1996) *Journal of molecular biology* **260**, 289-298